

Measuring gravitational waves from binary black hole coalescences: I. Signal to noise for inspiral, merger, and ringdown.

Éanna É. Flanagan

Newman Laboratory, Cornell University, Ithaca, NY 14853-5001.

Scott A. Hughes

Theoretical Astrophysics, California Institute of Technology, Pasadena, California 91125.

We estimate the signal-to-noise ratios (SNRs) that one would expect to measure from coalescing binary black hole (BBH) systems for the following three broadband gravitational-wave observatories: initial and advanced ground-based interferometers (LIGO/VIRGO) and space-based interferometers (LISA). We focus particularly on the highly relativistic and nonlinear *merger* portion of the gravitational-wave signal, which comes after the adiabatic *inspiral* portion and before the *ringdown* portion due to the quasinormal ringing of the final Kerr black hole.

Ground-based interferometers can do moderate SNR (a few tens), moderate accuracy studies of the dynamics of merging black holes in the mass range (a few) M_{\odot} to $\sim 2000M_{\odot}$. LISA, by contrast, can do high SNR (a few $\times 10^4$), high-accuracy studies of BBH systems in the mass range $10^5 M_{\odot} \lesssim (1+z)M \lesssim 10^8 M_{\odot}$, where z is the binaries' cosmological redshift.

Our estimated SNRs suggest that coalescing black holes might well be the first sources detected by the LIGO/VIRGO network of ground-based interferometers. Because of their larger masses, they can be seen out to much greater distances (up to ~ 250 Mpc for $M \lesssim 50M_{\odot}$ for the initial LIGO interferometers) than coalescing neutron star binaries (heretofore regarded as the “bread and butter” workhorse source for LIGO/VIRGO, visible to ~ 30 Mpc by the initial LIGO interferometers).

Low-mass BBHs ($M \lesssim 30M_{\odot}$ for the first LIGO interferometers; $M \lesssim 80M_{\odot}$ for the advanced; $(1+z)M \lesssim 3 \times 10^6 M_{\odot}$ for LISA) are best searched for via their well-understood inspiral waves; more massive BBHs must be searched for via their more poorly understood merger waves and/or their well-understood ringdown waves. A search for low-mass BBHs based on the inspiral waves, at a sensitivity level roughly half way between the first LIGO interferometers and the advanced LIGO interferometers, should be capable of finding BBHs out to ~ 1 Gpc. A search for massive BBHs based on the ringdown waves can be performed using the method of matched filters. If one wants the reduction in the event rate due to the discreteness of the template family to be no more than 10%, then the number of independent templates needed in the search will only be about 6000 or less. Such a search with the first LIGO interferometers should be capable of finding BBHs in the mass range from about $100M_{\odot}$ to about $700M_{\odot}$ out to ~ 200 Mpc; with advanced LIGO interferometers, from about $200M_{\odot}$ to about $3000M_{\odot}$ out to $z \sim 1$; and with LISA, BBHs with $10^6 M_{\odot} \lesssim (1+z)M \lesssim 3 \times 10^8 M_{\odot}$ should be visible out to $z \gtrsim 100$. The effectiveness of a search based on the merger waves will depend on how much one has learned about the merger waveforms from numerical relativity simulations. With only a knowledge of the merger waves' range of frequency bands and range of temporal durations, a search based on merger waves can be performed using a nonlinear filtering search algorithm. Such a search should increase the number of discovered BBHs by a factor of roughly 10 over those found from the inspiral and ringdown waves. On the other hand, a full set of merger templates based on numerical relativity simulations could further increase the number of discovered BBHs by an additional factor of up to about 4.

PACS numbers: 04.80.Nn, 04.25.Dm, 04.30.Db, 95.55.Ym

I. INTRODUCTION AND SUMMARY

A. Coalescences of black hole binaries

It has long been recognized that coalescences of binary systems of two black holes could be an important source of gravitational waves [1,2], both for the ground based interferometric detectors LIGO [3] and VIRGO [4] currently under construction, and also for the possible future space-based interferometer LISA [5,6,7]. The orbits of binary black holes (BBHs) gradually decay from energy and angular momentum loss to gravitational radiation. Eventually, the holes coalesce to form a final black hole. For gravitational radiation reaction to successfully drive the binary to merge in less than a Hubble time, the initial orbital period must be $\lesssim 0.3$ days $(M/M_\odot)^{5/8}$, where M is the total mass of the binary; thus the critical orbital period is of order days for solar mass black holes, and of order years to hundreds of years for supermassive black holes ($10^6 M_\odot \lesssim M \lesssim 10^9 M_\odot$).

The process of coalescence can be divided up into three more or less distinct phases:

- An adiabatic *inspiral*, during which the gravitational radiation reaction timescale is much longer than the orbital period. The inspiral ends when the binary orbit becomes relativistically dynamically unstable at an orbital separation of $r \sim 6M$ (in units where $G = c = 1$) [8,9]. The gravitational waves from the inspiral carry encoded within them the masses and spins of the two black holes, some of the orbital elements of the binary and the distance to the binary [1,10].
- Towards the end of the inspiral, the black holes encounter the dynamical instability and make a gradual transition from a radiation-reaction driven inspiral to a freely-falling plunge [8,11,12], after which, even if the radiation reaction could be turned off, the black holes would still merge. We will call the subsequent plunge and violent collision the *merger* phase. Gravitational waves from the merger could be rich with information about the dynamics of relativistic gravity in a highly nonlinear, highly dynamic regime about which we have a poor theoretical understanding today.
- As the final black hole settles down to a stationary Kerr state, the nonlinear dynamics of the merger gradually become more and more describable as oscillations of this final black hole's quasinormal modes [13,14]. The corresponding emitted gravitational waves consist of a superposition of exponentially damped sinusoids. We will call the phase of the coalescence for which the emitted gravitational-wave signal is dominated by the strongest $l = m = 2$ quasinormal mode signal the *ringdown* phase. The waves from the ringdown carry information

about the mass and spin of the final black hole [15,16]. (Note that, for want of a better terminology, throughout this paper we consistently use *coalescence* to refer to the entire process of inspiral, merger and ringdown, and reserve the word merger for the phase intermediate between inspiral and ringdown.)

In this paper we focus primarily on BBHs in which the masses of the two black holes are approximately the same, although we do also consider sources where one BH is much smaller than the other. We consider three different classes of BBHs:

(i) *Solar mass* black hole binaries, *i.e.*, binaries that are formed from massive main-sequence progenitor binary stellar systems. Such BBHs are expected to have total masses in the range $10M_\odot \lesssim M \lesssim 50M_\odot$, but not much larger than this. The rate of coalescence of solar-mass BBHs in the Universe is not very well known. However, theory suggests that most of the BBH progenitor systems may not disrupt during the stellar collapses that produce the black holes, so that their coalescence rate could be about the same as the birth rate for their progenitors, about 1/100,000 years in our Galaxy, or several per year within a distance of 200 Mpc [17,18,19,20,21]. Note that this coalescence rate is roughly the same as the expected event rate for what has traditionally been regarded as the most promising source for ground based interferometers, coalescences of neutron star—neutron star (NS-NS) binaries [3,10]. The expected rate of NS-NS coalescences is more firmly known, however, since it is based on extrapolations from detected progenitor NS-NS systems [17,18,19].

(ii) *Intermediate mass* black hole binaries, with total masses in the range $50M_\odot \lesssim M \lesssim (\text{a few}) \times 10^3 M_\odot$. In contrast to the cases of solar mass black holes and supermassive black holes (discussed below), there is little direct observational evidence for the existence of black holes in this mass range. Although there have been suggestions that the globular cluster M15 harbors a black hole of mass $\sim 10^3 M_\odot$ [22], theoretical modeling combined with the most recent HST observations neither confirm nor rule out this possibility [23]. Despite the lack of observational evidence, it is plausible that black holes in this mass range are formed in the cores of globular clusters, or in galactic nuclei in the process of formation of a supermassive black hole [26]. Simulations by Quinlan and Shapiro suggest that black holes with $M \sim 100M_\odot - 1000M_\odot$ could be formed in the evolution of dense stellar clusters of main sequence stars in galactic nuclei [24], and that coalescences of binaries of such black holes could be possible en route to the formation of a supermassive black hole.

We are prompted to consider these intermediate mass BBHs by the following consideration: even if the coalescence rate of intermediate mass BBHs is $\sim 10^{-4}$ that of NS-NS binaries (which is thought to be $\sim 10^{-5} \text{ yr}^{-1}$

in our Galaxy as discussed above), these sources would still be seen more often than NS-NS binaries by LIGO’s initial and advanced interferometers, and thus could be the first detected type of source. (See Sec. IE for further details.)

(iii) *Supermassive* black holes binaries: There is a variety of strong circumstantial evidence that supermassive black holes (SMBHs) in the mass range $10^6 - 10^9 M_\odot$ are present in quasars and active galactic nuclei, and also that $\sim 25\% - 50\%$ of nearby massive spiral and elliptical galaxies harbor quiescent SMBHs [7,25]. See Ref. [26] for a review of this evidence. One of the main scientific goals of the LISA project is to detect and monitor various processes involving SMBHs, such as the capture of compact stars [2,7,10,27,28], and their formation [2,7]. In particular, the coalescences of SMBH binaries that are formed in Galaxy mergers, in which the individual SMBHs are driven together by dynamical friction and gas accretion until gravitational radiation reaction takes over [29], have often been suggested as a promising source for space-based interferometers [1,2,7,10,30,31]. Such coalescences would be detectable throughout the observable universe with large signal to noise ratios [7,10]. There is also observational evidence for SMBH binaries: wiggles in the radio jet of QSO 1928+738 have been attributed to the orbital motion of a SMBH binary [32], as have time variations in quasar luminosities [33] and in emission line redshifts [34]. The overall event rate is uncertain, but could be large ($\gtrsim 1/\text{yr}$), especially if the hierarchical scenario for structure formation is correct [31].

B. Status of theoretical calculations of the gravitational-wave signal

Detailed theoretical understanding and predictions of the gravitational waveforms $h_+(t)$ and $h_\times(t)$ produced in BBH coalescences will facilitate both the detection of the gravitational-wave signal, and the extraction of its useful information. In situations where a complete family of theoretical template waveforms is available, it will be possible to use the procedure of Wiener optimal filtering to search the interferometer data streams and to detect the gravitational-wave signal [1,35]. The resulting signal-to-noise ratios (SNRs) can be larger than those obtainable without theoretical templates by a substantial factor; see Sec. II. Thus, while it is possible to detect the various phases of BBH coalescences without theoretical templates, such templates can greatly increase the effective range of the interferometers and the event detection rate. (Accurate theoretical templates are also essential for extracting the maximum amount of information from detected signals [36].)

Such theoretical template waveforms are available for the inspiral and ringdown phases of the coalescence, but not yet for the merger phase, as we now discuss.

For the inspiral phase of the coalescence, the gravitational waves and orbital evolution can be described reasonably well using the post-Newtonian approximation to general relativity. To date, inspiral waveforms have been calculated up to post-2.5-Newtonian order [37], and the prospects look good for obtaining waveforms up to post-3.5-Newtonian order [38,39]. Post-Newtonian templates will be fairly accurate over most of the inspiral, the most important error being a cumulative phase lag [40,41]. This cumulative phase lag will not be important for searches for inspiral waves; template phasing error will be largely compensated for by systematic errors in best-fit values of the binary’s parameters, and the signals will still be found [40,42,43,44]. By contrast, template inaccuracies will be significant when one attempts to extract from the data the binary’s parameters. In particular, post-Newtonian templates’ errors start to become very significant around an orbital separation of $r \sim 12M$ [45], well before the end of the inspiral at the dynamical orbital instability ($r \sim 6M$). Templates for the phase of the inspiral between roughly $12M$ and $6M$ will most likely have to be calculated using methods other than the post-Newtonian approximation. Moreover, the methods of full blown numerical relativity cannot be applied to this “Intermediate Binary Black Hole” (IBBH) phase, since the total time taken to evolve from $12M$ to $6M$ is about $1500M$, too long for supercomputer simulations to even contemplate evolving. Alternative analytic and numerical methods for calculating gravitational waveforms from the IBBH portion of BBH inspirals, based on the adiabatic approximation, are under development [46]; it is likely that such alternative methods will be successfully developed and implemented before the gravitational-wave detectors begin their measurements [47].

Waveforms from the dynamic, complicated merger phase of the coalescence can only be obtained from numerical relativity. Unlike mergers of neutron star binaries, BBH mergers are particularly clean in the sense that there is no microphysics or hydrodynamics to complicate simulations of the evolution, and external perturbations are negligible: the entire merger can be described as a solution to the vacuum Einstein equation [49]. Finding that solution is not a particularly easy task: a major computational effort to evolve the vacuum Einstein equation for BBH mergers using massive computational resources is currently underway, funded by the National Science Foundation’s Grand Challenge program [50,51].

The ringdown phase of the coalescence can be accurately described using perturbation theory on the Kerr spacetime background [52]. The gravitational waveforms from this phase are well understood, being just exponentially damped sinusoids. Thus, Wiener optimal filtering is feasible for searches for ringdown waves.

C. Purpose of this paper

The principal purpose of this paper is to estimate, in more detail than has been done previously, the prospects for measuring gravitational waves from the three different phases of coalescence events (inspiral, merger and ringdown), for various different detectors, and for a wide range of BBH masses. We estimate in each case the distances to which the different types of source can be seen by calculating expected SNRs. In particular, we determine for each BBH mass and each detector whether a coalescence event is most effectively detected by searching for the inspiral portion of the signal, or the merger portion, or the ringdown portion. We also determine how much the availability of theoretical template waveforms for the merger phase could increase the event detection rate.

Previous estimates of SNRs for ground-based interferometers have focused on the inspiral [1,40] and ringdown [15,16] phases, and also focused on solar-mass BBHs. For space-based interferometers, previous estimates of SNRs from the merger phase [7,10] were restricted to specific mass values and did not consider the ringdown portion of the signal.

In a companion paper, we discuss in detail the useful information carried by the three phases of the gravitational-wave signal, and methods and prospects for extracting this information both with and without templates for the merger phase [36].

In the following subsection we describe our calculations and summarize the assumptions underlying our estimated signal-to-noise ratios. In Sec. I E we summarize our main results and conclusions, and an outline of the paper is given in Sec. I F.

D. Estimating the signal-to-noise ratios: method and assumptions

We calculate SNRs for three different types of interferometer: initial and advanced ground-based interferometers (LIGO/VIRGO), and the proposed space-based interferometer LISA. The noise spectra of the initial and advanced ground-based interferometers we took from Ref. [3], and that for LISA we obtained from Ref. [7]. Our approximate versions of these noise spectra are given in Eqs. (4.1) – (4.4), and are illustrated in Figs. 1 – 3 in Sec. V A.

We consider the following three different signal-detection methods:

(i) *Matched filtering searches*: For those phases of the coalescence for which a complete set of theoretical templates will be available (the inspiral, the ringdown, and possibly the merger), the method of matched filtering or optimal filtering can be used to search for the waves [1,35,53,54,55]. The theory of matched filtering is briefly sketched in Sec. II A. For any source of waves, the SNR,

ρ , obtained from matched filtering is related to the gravitational waveform $h(t)$ measured by the interferometer and to the spectral density $S_h(f)$ of the strain noise in the interferometer via [56]

$$\rho^2 = 4 \int_0^\infty \frac{|\tilde{h}(f)|^2}{S_h(f)} df, \quad (1.1)$$

where $\tilde{h}(f)$ is the Fourier transform of $h(t)$ defined by Eq. (2.3). The SNR (1.1) depends, through the waveform $h(t)$, on the orientation and position of the source relative to the interferometer. In Sec. II C we show that if we perform an rms average over source orientations and positions (at a fixed distance), the rms SNR thus obtained depends only on the energy spectrum dE/df carried off from the source by the gravitational waves. The resulting relationship between the waves' energy spectrum and the rms angle-averaged SNR forms the basis for most of our calculations. It is given by [cf. Eq. (2.34)]

$$\langle \rho^2 \rangle = \frac{2(1+z)^2}{5\pi^2 D(z)^2} \int_0^\infty df \frac{1}{f^2 S_h(f)} \frac{dE}{df} [(1+z)f], \quad (1.2)$$

where z is the source's cosmological redshift and $D(z)$ is the luminosity distance from the source.

In order for a signal to be detected, the waves' measured SNR must be larger than the detection threshold

$$\rho_{\text{threshold}} \approx \sqrt{2 \ln(\mathcal{N}_{\text{start-times}}) + 2 \ln(\mathcal{N}_{\text{shapes}})}; \quad (1.3)$$

see, for example, Ref. [40] and also Sec. II B. Here $\mathcal{N}_{\text{start-times}}$ is the number of independent starting times of the gravitational wave signal that are searched for in the data set, determined by the total duration of the data set (of order one year) and the sampling time. The quantity $\mathcal{N}_{\text{shapes}}$ is the total number of statistically independent waveform shapes in the set of signals that one is searching for [57].

(ii) *Band-pass filtering searches*: For the merger phase, a complete set of theoretical templates may not be available. It therefore may not be possible to use matched filtering, and other search methods will need to be employed. Band-pass filtering, followed by setting a detection threshold in the time domain, is a simple method of searching an interferometer data stream for bursts of unknown form [35]. In Sec. II A we derive an approximate relation between the SNR obtainable from band-pass filtering, and the SNR (1.1) obtainable from matched filtering, for any burst of waves, namely

$$\left(\frac{S}{N}\right)_{\text{band-pass}} \approx \frac{1}{\sqrt{2T\Delta f}} \left(\frac{S}{N}\right)_{\text{optimal}}. \quad (1.4)$$

Here T is the duration of the burst and Δf is the bandwidth of the band-pass filter [cf. Eq. (2.14)]. The quantity $2T\Delta f$ is the dimension of the linear space of signals being searched for, which is roughly the same as

the “number of cycles” of the gravitational waveform. We use this formula in Sec. VIB to estimate band-pass-filter search SNRs for the merger waves from BBH coalescences, by inserting on the right hand side the rms angle-averaged matched-filter search SNR (1.2), and by making estimates of T and Δf .

(iii) *Noise-monitoring, nonlinear filtering searches:* The traditional view has been that the SNR (1.4) is about the best that can be achieved in the absence of theoretical templates; that is, that the gain in SNR obtainable from matched filtering is approximately the square root of the number of cycles in the gravitational wave signal. This view is based on the the assumption that the search method used in the absence of templates is band-pass filtering or something very similar. However, we suggest in Sec. IIB an alternative search method, motivated by Bayesian analyses and incorporating nonlinear filtering, which performs much better than band-pass filtering and in some cases almost as well as matched filtering. In essence, one monitors the noise level in the interferometer in a certain frequency band, over short timescales, and looks for statistically significant changes. The noise level is estimated by calculating the quantity

$$\frac{1}{T} \int_{-T/2}^{T/2} d\tau s(t + \tau)^2, \quad (1.5)$$

where T is the maximum expected duration of the signal, and $s(t)$ is a suitably pre-filtered version of the interferometer data stream.

The efficiency of this noise-monitoring search method cannot usefully be described in terms of a signal-to-noise ratio, since the detection statistic is very non-Gaussian. Instead, its efficiency can be described in the following way. Let ρ denote the SNR that would be obtained if matched filtering were possible [Eq. (1.1)]. We use ρ as a convenient parameterization of the signal strength; as such, it is meaningful even in situations where matched filtering cannot be carried out. Then, a signal will be detected with high confidence using the noise-monitoring technique whenever ρ is larger than the threshold ρ_* , where to a good approximation ρ_* satisfies

$$\rho_*^2 = 2 \ln(\mathcal{N}_{\text{start-times}}) + \mathcal{N}_{\text{bins}} \ln(1 + \rho_*^2/\mathcal{N}_{\text{bins}}). \quad (1.6)$$

Here $\mathcal{N}_{\text{bins}} = 2T\Delta f$ is the dimension of the signal space discussed above (or the number of independent frequency bins in the Fourier domain). The derivation of Eq. (1.6) is given in Sec. IIB.

The relation (1.2) forms the basis of our SNR calculations. We use the SNR thresholds (1.3) and (1.6) to deduce from the SNR values the detectability of the various parts of the gravitational-wave signal. To calculate the SNRs, we also need to specify the waves’ energy spectra for the three different phases of the coalescence. As we now outline, for the inspiral and ringdown phases the waves’ energy spectrum is essentially known, while for

the merger phase we make an educated guess of dE/df . Sec. III gives more details.

Inspirational energy spectrum: We use the leading order expression for dE/df obtained using Newtonian gravity supplemented with the quadrupole formula [59] [Eq. (3.20)]. Strictly speaking, this spectrum describes the SNR that would be achieved by searching for Newtonian, quadrupole waves using Newtonian, quadrupole templates. The actual SNR obtained when searching for a real, general-relativistic inspiral waveform using post-Newtonian templates should deviate from this by only a few tens of percent [60]. We terminate the spectrum at the frequency $f_{\text{merge}} = 0.02/M$ which is (roughly) the frequency of quadrupole waves emitted at the orbital dynamical instability at $r \sim 6M$ [8]. For LISA, we assume that the measurement process lasts at most one year, and choose the frequency at which the inspiral spectrum starts accordingly.

Ringdown energy spectrum: The spectrum that we use [Eq. (3.24)] is determined (up to its overall amplitude) by the characteristics of the $l = m = 2$ quasi-normal ringing (QNR) mode of the final Kerr black hole. This mode is the most slowly damped of all QNR modes, so we expect it to dominate the last stages of the gravitational-wave emission. The QNR spectrum depends on three parameters: the quasi-normal modes’ frequency f_{qnr} and damping time τ , and the overall amplitude of the quasinormal mode signal. Equivalently, the three parameters can be taken to be the mass M and dimensionless spin parameter a of the final black hole (which determine f_{qnr} and τ) and the total amount of energy radiated in the ringdown (which determines the overall amplitude). The spectrum is peaked at $f = f_{\text{qnr}}$ with width $\Delta f \sim 1/\tau$.

In our analyses, we (somewhat arbitrarily) assume that $a = 0.98$. It seems likely that in many coalescences the spin of the final black hole will be close to maximal, since the total angular momentum of the binary at the end of the inspiral is $\sim 0.9M^2$ when the individual black holes are non-spinning [62], and the individual black hole spins can add to this. Exactly how close to maximally spinning the final black hole will be is a matter that probably will not be decided until supercomputer simulations—or observations—settle the issue. In any case, the ringdown SNR values that we obtain depend only weakly on our assumed value of a [*cf.* Eq. (A14)], for fixed total energy radiated in the ringdown.

The overall amplitude of the ringdown signal depends upon one’s delineation of where “merger” ends and “ringdown” begins, which is somewhat arbitrary. For equal-mass BBHs, we assume a value of the overall amplitude that corresponds to a total radiated energy in the ringdown of $0.03M$ —a radiation efficiency of 3%. This number is based on a back-of-the-envelope, quadrupole-formula-based estimate of the QNR mode’s amplitude when the distortion of the horizon of the black hole is of order unity (*cf.* Sec. IIID). Although this radiation efficiency seems rather high, there have been numerical

simulations of the evolution of distorted, spinning black holes in which the ringdown waves carry away $\gtrsim 3\%$ of the black hole’s total mass energy [63].

For non equal-mass black holes, we assume that the total energy radiated is $F(\mu/M)0.03M$, where $F(\mu/M) = (4\mu/M)^2$ and μ is the reduced mass of the binary. This function gives the correct results for the equal-mass case and also gives the correct scaling law in the regime $\mu \ll M$; for general mass ratios the scaling law is probably a good approximation.

Merger energy spectrum: Realistic merger energy spectra will vary substantially from event to event (depending on the initial spins of the inspiraling black holes). Currently, we have very little concrete information about such spectra, pending supercomputer simulations of BBH mergers. In Sec. IIIB we describe various circumstantial pieces of evidence, culled from the literature, relevant to merger spectrum. Based on that evidence, we adopt the following crude model for equal-mass BBHs: we assume a flat spectrum $dE/df = \text{const}$ extending from the frequency $f_{\text{merge}} = 0.02/M$ of quadrupole waves at the end of inspiral to the quasinormal ringing frequency $f_{\text{qnr}} = 0.13/M$, with amplitude such that the total radiated energy in the merger is 10% of the total mass energy of the spacetime [Eq. (3.14)]. We outline in Sec. IIIB two different “handwaving” arguments which suggest that in favorable cases the merger radiation efficiency may be as high as our assumed value of $\sim 10\%$. One of these arguments, due originally to Smarr [64] and explored by Detweiler [65], is based on extrapolation of perturbation theory results; the other argument is based on angular momentum conservation.

Our assumed radiation efficiencies of 3% and 10% for the ringdown and merger phases should perhaps be interpreted as reasonable upper bounds that could be achieved in favorable cases, rather than as best-guess estimates. We note that numerical simulations that have been performed to date (which are restricted to axisymmetric situations) generally yield lower radiation efficiencies than we have assumed [66]; moreover, these axisymmetric simulations generally find that ringdown waves carry most of the radiated energy. In Sec. IIIB we argue that the radiated energy in the merger phase could be boosted by the lack of symmetry in generic black hole mergers, and especially by the individual black holes’ spins (if these spins are large).

For non-equal mass BBHs, we again simply reduce the energy spectrum by the factor $F(\mu/M) = (4\mu/M)^2$, while the upper and lower frequencies f_{merge} and f_{qnr} are taken to be independent of μ .

E. Signal-to-noise ratios: results and implications

By inserting our assumed energy spectra (3.20), (3.14) and (3.24) into Eq. (1.2), we obtain optimal-filtering SNRs for the three different phases of BBH coalescences

as a function of the redshifted total mass $(1+z)M$ of the binary. The results are shown in Figs. 4, 5 and 6 and formulae summarizing the results are given in Appendix A. Also in Sec. IIIE we estimate that, for the merger waves, the number of independent frequency bins $\mathcal{N}_{\text{bins}}$ which characterize the signal falls roughly in the range $10 \lesssim \mathcal{N}_{\text{bins}} \lesssim 30$, and that a conservative upper-bound is ~ 60 . We use this upper bound in Sec. VIB to estimate the SNR threshold (1.6) for merger waves using noise-monitoring searches when templates are unavailable. We discuss the implications of these SNRs and SNR thresholds in Sec. VI; here we summarize our main conclusions:

- Ground-based interferometers can study black-hole mergers in the mass range (a few) M_{\odot} to $\sim 2000M_{\odot}$; LISA, by contrast can study mergers in the mass range $10^5M_{\odot} \lesssim (1+z)M \lesssim 10^8M_{\odot}$.
- Ground-based interferometers can do moderate SNR (a few tens), moderate accuracy studies of the dynamics of merging black holes. LISA, by contrast, can do high SNR (a few $\times 10^4$), high-accuracy studies.
- Coalescing black holes are fairly likely to be the first sources detected by the LIGO/VIRGO network of ground-based interferometers: because of their larger masses, they can be seen out to much greater distances than coalescing neutron star binaries. (With the initial LIGO interferometers, binary black holes with $M \lesssim 50M_{\odot}$ can be seen out to ~ 250 Mpc, whereas binary neutron stars can be seen out to ~ 30 Mpc [67]). Estimates of the number of BBH coalescences per NS-NS coalescence by experts in binary evolution range from 1/10 [68] to 1/300 [20]; the distance gain factor for BBHs could easily compensate for the reduced birth rate.
- Low-mass BBHs [$M \lesssim 30M_{\odot}$ for the first LIGO interferometers; $M \lesssim 80M_{\odot}$ for the advanced; $(1+z)M \lesssim 3 \times 10^6M_{\odot}$ for LISA] are best searched for via their well-understood inspiral waves; while more massive BBHs must be searched for via their more poorly understood merger waves and/or their well-understood ringdown waves.
- When the interferometers’ sensitivities has reached a level roughly half way between the first LIGO interferometers and the advanced LIGO interferometers [67], a search based on the inspiral waves should be capable of finding low-mass BBHs out to about 1 Gpc.
- A search for massive BBHs based on the ringdown waves can be performed using matched filtering. We show in Sec. VIA that the number of independent templates needed for such a search is about 6000 or less, assuming that one wants the event rate reduction due to discreteness of the template family to be no more than 10%. With the

first LIGO interferometers, such a search should be capable of finding equal-mass BBHs in the mass range $100M_{\odot}$ to $700M_{\odot}$ out to about 200 Mpc; with advanced LIGO interferometers, BBHs with $200M_{\odot} \lesssim M(1+z) \lesssim 3000M_{\odot}$ should be detectable out to $z \sim 1$; and with LISA, BBHs with $10^6M_{\odot} \lesssim (1+z)M \lesssim 3 \times 10^8M_{\odot}$ should be visible out to $z \gtrsim 100$. These distances are reduced by a factor $\sim (4\mu/M)$ for non-equal-mass BBHs.

- The effectiveness of a search based on the merger waves will depend on how much one has learned about the merger waveforms from numerical relativity simulations. With only a knowledge of the merger waves' range of frequency bands and range of temporal durations, a search based on merger waves can be performed using the noise-monitoring search algorithm discussed above. Such a search should increase the number of discovered BBHs by a factor ~ 10 over those found from the inspiral and ringdown waves. On the other hand, a full set of merger templates based on numerical relativity simulations could further increase the number of discovered BBHs by an additional factor of up to ~ 4 .

F. Organization of this paper

The organization of this paper is as follows. In Sec. II we discuss in detail the three methods of searching for gravitational wave signals referred to above. In Sec. IIC we derive the general formula [Eq. (2.34)] discussed above for the optimally-filtered SNR of a gravitational-wave source at a cosmological distance, in terms of the source's emitted spectrum, redshift and luminosity distance, and the detector's noise spectrum. This formula is one underpinning for the BBH SNR computations of Appendix A and Sec. V. In Sec. IIA we derive the approximate formula [Eq. (2.14)] discussed above for the SNR obtainable by band-pass filtering in the absence of theoretical templates. In Sec. IIB we describe our suggested noise-monitoring search, and derive the relevant detection threshold [Eqs. (2.30) and (2.31)].

In Sec. IIIA we split the waveform from a coalescing equal-mass black hole binary into three successive epochs: inspiral, merger and coalescence. Then we estimate the frequency bands and spectra for each of these epochs: the merger phase in Sec. IIIB [Eqs. (3.4), (3.5), (3.14)]; the inspiral phase in Sec. IIIC [Eq. (3.20)]; and the ringdown phase in Sec. IIID [Eqs. (3.24) – (3.26)]. We have already summarized, above, the assumptions that underlie our assumed merger and ringdown spectra, and the uncertainties in those assumptions; we give a more detailed description in Secs. IIIB – IIID. A subtlety in the derivation of the ringdown energy spectrum is explained in Appendix B. In Sec. IIIE we make rough estimates of

the range of the bandwidths and temporal durations of merger waveforms.

In Sec. IV we devise a simple piece-wise power-law analytic fit [Eq. (4.1)] to the noise spectra of an initial LIGO interferometer, an advanced LIGO interferometer, and a space-based LISA interferometer. This single formula, by adjustment of its parameters, can describe all three interferometer types.

In Appendix A, we insert the interferometer noise spectra from Sec. IV, and the estimated BBH inspiral, merger, and ringdown spectra from Secs. IIIB, IIIC and IIID, into the general SNR formula (2.34). That formula's frequency integral is then performed to compute the angle-averaged, optimal-filtering SNR for each type of interferometer and each phase of BBH coalescence. The resulting SNRs for an initial LIGO interferometer, an advanced LIGO interferometer, and a LISA interferometer, are expressed in terms of the binary's total mass M , cosmological redshift z , and luminosity distance D .

In Sec. VB, we graph the SNR formulae derived in Appendix A (Fig. 4 for an initial LIGO interferometer; Fig. 5 for an advanced LIGO interferometer; Fig. 6 for LISA). We give intuitive insight into these SNRs in Sec. VA by re-expressing the power SNR for a source as

$$\rho^2 = \int d(\ln f) [h_{\text{char}}(f)/h_n(f)]^2, \quad (1.7)$$

where $h_{\text{char}}(f)$ is the source's "characteristic amplitude" as a function of frequency, and $h_n(f)$ is the detector's rms noise in a bandwidth equal to frequency for sources with random orientations. We give plots of $h_{\text{char}}(f)$ and $h_n(f)$ for five specific examples of binaries — a $10M_{\odot} - 10M_{\odot}$ binary at distance $D = 200$ Mpc and a $15M_{\odot} - 15M_{\odot}$ binary at cosmological redshift $z = 1$ (Fig. 1); a $50M_{\odot} - 50M_{\odot}$ binary at cosmological redshift $z = 0.5$ (Fig. 2); a $5 \times 10^6M_{\odot} - 5 \times 10^6M_{\odot}$ binary at $z = 5$ and a $2.5 \times 10^4M_{\odot} - 2.5 \times 10^4M_{\odot}$ binary at $z = 1$ observed by LISA (Fig. 3). For each example, we explain, in terms of the plots, why the inspiral, merger, and ringdown SNRs have the values shown in Figs. 4, 5 or 6.

The SNR graphs in Figs. 4, 5 and 6 are the foundation for our conclusions, summarized above, about what features of which binaries should be observable with which interferometers. A detailed discussion of these conclusions is given in Sec. VI. In Sec. VIA, we estimate the number of templates required for a search for ringdown waves based on matched filtering, estimate the SNR detection thresholds, and hence the range of the various interferometers for ringdown waves. In Sec. VIB we examine the prospects for searches for BBHs via their merger waves, both with and without templates.

II. DERIVATION OF GENERAL FORMULAE FOR SIGNAL-TO-NOISE RATIOS AND DETECTION THRESHOLDS

In this section we discuss in detail the various signal-search methods which were briefly described in the Introduction. We start in Sec. II A by deriving the approximate relation (1.4) between the SNR achievable using matched filtering searches for signals and the SNR obtainable via band-pass filtering searches. This approximate relation is closely related to the standard lore that the gain factor due to matched filtering is the square root of the number of cycles in the waveform [1,35], which strictly speaking is applicable only to waveforms that are almost monochromatic. For completeness, we discuss in Sec. II A both the standard lore relation [Eq. (2.9)] and the approximate more general relation [Eq. (2.14)].

In Sec. II B we describe our proposed noise-monitoring search method, and derive the detection threshold (1.6) discussed in Sec. I E. Finally, in Sec. II C we derive the general formula [Eq. (2.34)] for the angle-averaged, optimal-filtering SNR for a gravitational-wave source, which was discussed in the Introduction.

A. Searches for gravitational-wave bursts: band-pass filtering and matched filtering

Consider the situation where some arbitrary gravitational-wave burst $h(t)$ is present in the data stream $s(t)$, so that

$$s(t) = h(t) + n(t), \quad (2.1)$$

where $n(t)$ is the noise. If one integrates a filter $K(t)$ against the data stream $s(t)$ to produce a number, $Y = \int K(t)s(t) dt$, then the standard definition of the signal to noise ratio is [56]

$$\begin{aligned} \frac{S}{N} &= \frac{\text{expected value of } Y \text{ when signal present}}{\text{rms value of } Y \text{ when no signal present}} \\ &= \frac{\langle Y \rangle}{\sqrt{\langle Y^2 \rangle_{s=0}}} \\ &= \frac{4 \int_0^\infty df \Re [\tilde{h}(f)^* \tilde{K}(f)]}{\sqrt{4 \int_0^\infty df |\tilde{K}(f)|^2 S_h(f)}}; \end{aligned} \quad (2.2)$$

see, *e.g.*, Refs. [53,54]. Here tildes denote Fourier transforms according to the convention

$$\tilde{h}(f) = \int_{-\infty}^{\infty} e^{2\pi i f t} h(t) dt, \quad (2.3)$$

and $S_h(f)$ is the power spectral density of strain noise in the detector [56].

Now, consider searching for a signal $h(t)$ when the only information about it that one has is its approximate bandwidth in the frequency domain. Perhaps the

simplest search algorithm one could use to search for the signal is to choose for $K(t)$ the following band-pass filter:

$$\tilde{K}(f) = e^{2\pi i f t_{\text{start}}} \Theta(\Delta f/2 - |f - f_{\text{char}}|). \quad (2.4)$$

Here Θ is the step function and t_{start} is the starting time of the filter. This filter chops out all the data in the frequency domain except that in a bandwidth Δf about a characteristic central frequency f_{char} [69]. Suppose that the frequency interval has been chosen wisely, so that the signal $h(t)$ has negligible power outside the interval. Then $\tilde{h}(f)$ can be taken to vanish outside the chosen bandwidth, and Eqs. (2.2) and (2.4) yield

$$\begin{aligned} \left(\frac{S}{N}\right)_{\text{band-pass filter}} &= \frac{h(t_{\text{start}})}{\sqrt{\int_{\Delta f} df S_h(f)}} \\ &\approx \sqrt{\frac{f_{\text{char}}}{\Delta f}} \frac{h(t_{\text{start}})}{h_{\text{rms}}(f_{\text{char}})}, \end{aligned} \quad (2.5)$$

where $h_{\text{rms}}(f) \equiv \sqrt{f S_h(f)}$ is the rms fluctuation in the noise at frequency f in a bandwidth equal to f . The starting time of the filter t_{start} is then varied to give the maximum filter output Y , which is achieved at some value t_{best} of t_{start} . At this maximum overlap time, the SNR is given by Eq. (2.5) with t_{start} replaced by t_{best} . In particular, for broadband signals for which $\Delta f \sim f_{\text{char}}$ (as opposed to $\Delta f \ll f_{\text{char}}$), Eq. (2.5) simplifies to the standard result [35]

$$\left(\frac{S}{N}\right)_{\text{band-pass filter}} \approx \frac{h(t_{\text{best}})}{h_{\text{rms}}(f_{\text{char}})}. \quad (2.6)$$

By contrast, if the shape of the signal is known one can use the well known optimal filter $\tilde{K}(f) = \tilde{h}(f)/S_h(f)$, for which the SNR squared is, from Eq. (2.2) [53,54,56]

$$\rho^2 = \left(\frac{S}{N}\right)_{\text{optimal filter}}^2 = 4 \int_0^\infty \frac{|\tilde{h}(f)|^2}{S_h(f)} df. \quad (2.7)$$

A crucial element of both optimal filtering searches and most especially band-pass filtering searches with ground-based interferometers is the use of coinciding between different interferometers to circumvent the effects of non-Gaussian noise bursts [35]. Coinciding between the 4 interferometers in the LIGO/VIRGO network (the Hanford 2 km, Hanford 4 km, Livingston 4 km and Pisa 3 km interferometers) should be sufficient to achieve this. To be conservative, our assumed detection thresholds for the SNR values (which we discuss in Sec. VI) are based on combining just the two LIGO 4 km interferometers, albeit with assumed Gaussian statistics.

The standard lore approximate relationship between the optimal-filtering SNR (2.7) and the band-pass filtering SNR (2.6) can be obtained as follows. Consider the special case of a waveform that is quasi-monochromatic, *i.e.*, of the form

$$h(t) = h_{\text{amp}}(t) \cos[\Phi(t)], \quad (2.8)$$

where the amplitude $h_{\text{amp}}(t)$ and instantaneous frequency [given by $2\pi f(t) = d\Phi/dt$] are slowly evolving. Using Eq. (2.7) and the stationary phase approximation to the Fourier transform of the signal (2.8) yields

$$\rho^2 = \int d(\ln f) n_{\text{cyc}}(f) \frac{h_{\text{amp}}[t(f)]^2}{h_{\text{rms}}(f)^2}, \quad (2.9)$$

where $n_{\text{cyc}}(f) \equiv f^2/\dot{f}$ is the number of cycles spent within a bandwidth $\Delta f \sim f$ centered on f , and $t(f)$ is the time at which the gravitational-wave frequency is f . By comparing Eqs. (2.6) and (2.9) it can be seen that $n_{\text{cyc}}(f)$ is the gain factor in SNR squared for optimal filtering over band-pass filtering, per logarithmic interval in frequency [1].

For general signals $h(t)$ which are not quasi-monochromatic, Eq. (2.8) does not apply. However, we can derive an approximate formula for the SNR (2.6) for general signals as follows. Approximating $S_h(f)$ to be constant in Eq. (2.7) gives [35]

$$\begin{aligned} \left(\frac{S}{N}\right)_{\text{optimal filter}}^2 &\approx \frac{2}{S_h(f_{\text{char}})} \int_{-\infty}^{\infty} dt [h(t)]^2 \\ &\approx 2f_{\text{char}}T \frac{\bar{h}^2}{h_{\text{rms}}(f_{\text{char}})^2} \end{aligned} \quad (2.10)$$

where \bar{h} is a rms average of $h(t)$ and T is the effective duration of the signal. Comparing Eqs. (2.10) and (2.5) we find that

$$\frac{(S/N)_{\text{band-pass filter}}}{(S/N)_{\text{optimal filter}}} \approx \frac{h(t_{\text{best}})}{\bar{h}} \frac{1}{\sqrt{\mathcal{N}_{\text{bins}}}}, \quad (2.11)$$

where the ‘‘number of *a priori* frequency bins’’ is

$$\mathcal{N}_{\text{bins}} = 2T\Delta f. \quad (2.12)$$

The reason for this terminology is as follows. Suppose that we are trying to detect a signal whose total duration we know to be less than or equal to T , and whose spectrum we know to lie in some frequency interval of bandwidth Δf . When we discard the measured data outside of these time and frequency intervals, the remaining relevant data is described by $\mathcal{N}_{\text{bins}} = 2T\Delta f$ real Fourier coefficients (or equivalently, $\mathcal{N}_{\text{bins}}$ frequency bins). The quantity $\mathcal{N}_{\text{bins}}$ is the number of independent real variables that parameterize the space of signals for which we will search.

This notion of number of *a priori* frequency bins is closely related to the notion of number of cycles in the waveform. The number of waveform cycles will be approximately $\mathcal{N}_{\text{cyc}} \sim T f_{\text{char}}$, and so for a broadband burst for which $\Delta f \approx f_{\text{char}}$ we have $\mathcal{N}_{\text{cyc}} \approx \mathcal{N}_{\text{bins}}$. There is a distinction between the two concepts, however: the number of cycles is intrinsic to the signal, whereas the number of frequency bins in part characterizes our *a priori*

information or assumptions about the signal and not the signal itself. This is because for band-pass filtering we must choose at the start some bandwidth Δf . Since the true bandwidth of the signal will vary from one signal to another and will not be known in advance, the true bandwidth of the signal will in general be somewhat less than Δf if we have chosen Δf wisely. The quantity $\mathcal{N}_{\text{bins}}$ depends not on the true bandwidth of the signal but on our assumed bandwidth Δf .

The first factor on the right hand side of Eq. (2.11) is the ratio between the peak strain amplitude $h(t_{\text{best}})$ in the time domain and an rms value \bar{h} of this strain amplitude. By defining the effective duration T of the signal to be given by

$$\int dt [h(t)]^2 = T h(t_{\text{best}})^2, \quad (2.13)$$

this factor reduces to unity. With this interpretation of T in Eq. (2.12), Eq. (2.11) reduces to the formula

$$\frac{(S/N)_{\text{band-pass filter}}}{(S/N)_{\text{optimal filter}}} \approx \frac{1}{\sqrt{\mathcal{N}_{\text{bins}}}} \quad (2.14)$$

discussed in the Introduction. We use this formula in Sec. VI B.

The SNR threshold $\rho_{\text{threshold}}$ appropriate for matched filtering is approximately given by [40]

$$\text{erfc}(\rho_{\text{threshold}}/\sqrt{2}) = \frac{\epsilon}{\mathcal{N}_{\text{start-times}} \mathcal{N}_{\text{shapes}}} \quad (2.15)$$

which to a good approximation reduces to

$$\rho_{\text{threshold}} \approx \sqrt{2 \ln(\mathcal{N}_{\text{start-times}}/\epsilon) + 2 \ln(\mathcal{N}_{\text{shapes}})}; \quad (2.16)$$

[*cf.* Eq. (1.3) where the factor of ϵ , which does not have a large effect, was omitted]. Here the number $\mathcal{N}_{\text{shapes}} = \mathcal{N}_{\text{shapes}}(\rho_{\text{threshold}})$ is the number of statistically independent waveforms with $\text{SNR} \leq \rho_{\text{threshold}}$ in the set of signals to be searched for [57]; Eq. (2.16) must be solved self-consistently to determine $\rho_{\text{threshold}}$.

B. Searches for gravitational-wave bursts: noise monitoring

In this section we describe our suggested noise-monitoring method for searching for gravitational wave bursts of unknown form; more details can be found in Ref. [58]. In essence, the method consists of monitoring over short timescales the total rms noise in the detector output in the frequency band in which the signal is expected, and waiting for statistically significant changes in one’s estimate of the noise power.

Suppose that the maximum expected signal duration is T , and that the interferometer output is $s(t)$. We construct a quantity $Q(t)$ in the following way. First, focus

attention on the data stream $s(\tau)$ in the time interval $t - T/2 \leq \tau \leq t + T/2$. Because the data stream is in fact discrete and not continuous, this interval of data can be represented by the numbers

$$s_j = s(t - T/2 + j\Delta t) \quad (2.17)$$

for $0 \leq j \leq N_{\text{total}} = T/\Delta t$, where Δt is the sampling time. From Eq. (2.1) we have

$$s_j = h_j + n_j, \quad (2.18)$$

where h_j is the gravitational wave signal and n_j is the noise. Now because the interferometer noise is colored, the noise matrix

$$\Sigma_{ij} \equiv \langle n_i n_j \rangle \quad (2.19)$$

will not be diagonal. Here, angle brackets denote ensemble averaging over realizations of the noise. If one performs an FFT just of this finite stretch of data, the noise matrix on the new basis will not be diagonal either because of aliasing effects. However, it is possible to diagonalize the matrix (2.19) and change to a basis on which the noise is diagonal. We will denote this new basis by capital Roman letters I, J, K . The data points s_I on this new basis can be chosen to correspond approximately to frequencies $f_I = I/T$, $I = 1, -1, 2, -2, \dots$ [58]. Equation (2.19) can now be replaced by

$$\langle n_I n_J \rangle = \delta_{IJ} \sigma_I^2. \quad (2.20)$$

The data s_I extend up to some high frequency (of order several kHz) determined by the sampling time. We next discard all data above some upper cutoff frequency. (Note that we have effectively performed band-pass filtering of the data, since the restriction to a segment of length T in the time domain removes frequency components at $f \lesssim 1/T$.) Let us denote by $\mathcal{N}_{\text{bins}}$ the total number of data points remaining, which will be approximately given by

$$\mathcal{N}_{\text{bins}} = 2T\Delta f \quad (2.21)$$

where Δf is the bandwidth of our effective band-pass filter.

In terms of this basis, matched filtering consists of calculating, for each trial waveform shape h_J , the quantity

$$\frac{\sum_J s_J h_J / \sigma_J^2}{\sqrt{\sum_J h_J^2 / \sigma_J^2}} \quad (2.22)$$

(We are assuming here that all the trial waveform shapes have duration less than T and in the frequency domain have most of their power within the bandwidth Δf). We introduce the notation $\rho_I = h_I / \sigma_I$; then the optimal filtering SNR (1.1) is given by

$$\rho^2 = \sum_I \rho_I^2 = \sum_I \frac{h_I^2}{\sigma_I^2}. \quad (2.23)$$

Thus, the quantity ρ_I^2 is the optimal filtering signal-to-noise squared per data bin. Note that throughout this subsection, we use ρ as a convenient parameterization of the signal strength, which is meaningful even in situations where templates are not available and where optimal filtering cannot be carried out. Band-pass filtering (of a pre-whitened data stream) approximately corresponds in this language to calculating the statistic

$$\hat{\rho}_{\text{BP}} \equiv \max_J \frac{s_J}{\sigma_J}. \quad (2.24)$$

This will have an expected value of roughly $\rho / \sqrt{\mathcal{N}_{\text{bins}}}$ [cf. Eq. (2.14)] if the signal is not sharply peaked in frequency but instead is spread out over the bandwidth Δf .

The statistic used to diagnose the presence of a signal is

$$Q(t) = -\mathcal{N}_{\text{bins}} + \sum_{J=-\mathcal{N}_{\text{bins}}/2}^{J=\mathcal{N}_{\text{bins}}/2} \frac{s_J^2}{\sigma_J^2}. \quad (2.25)$$

This statistic is essentially an estimate of the apparent rms noise power in the given bandwidth over the given time interval, up to an additive constant. The additive constant, $-\mathcal{N}_{\text{bins}}$, is chosen so that when no signal is present, $\langle Q(t) \rangle = 0$ and thus $Q(t)$ random walks over positive and negative values. When a signal is present, $Q(t)$ will with high probability be large and positive. One monitors $Q(t)$ as a function of time and sets a detection threshold such that when $Q(t)$ exceeds the threshold, the probability that the data stream contains no signal is very low (see below). Note that this search method constitutes a type of nonlinear filtering.

The technique of monitoring the statistic (2.25) is closely related to two commonly used techniques in radio astronomy. In the first such technique, observers sum the power from frequency bins which are expected to contain harmonics of the signal they are trying to detect. This procedure is not quite as good as coherently combining the signal from all the frequency bins but is much easier, computationally. The second technique [70] is useful when one is looking for periodic signals in a data train that is too long to Fourier transform. One splits the data train into some number N of shorter data segments, takes the FFT of each shorter segment, and adds the FFTs incoherently (*i.e.*, adds the individual power spectra). Again, this is not the optimal search method, but it is often a useful thing to do given finite computational resources. One difference between our suggested noise-monitoring search method and the radio astronomy techniques is the following: One adds the frequency bins incoherently in the statistic (2.25) because the phase relationships are unknown; in the radio astronomy contexts, one adds the frequency bins incoherently to save on computation time. But the techniques themselves are conceptually very similar.

We now turn to a derivation of the efficiency and performance of our suggested noise-monitoring search

method. It is straightforward to show that when a signal is present

$$\langle Q(t) \rangle = \rho^2 \quad (2.26)$$

and that

$$\langle [Q(t) - \langle Q(t) \rangle]^2 \rangle = 4\rho^2 + 2\mathcal{N}_{\text{bins}}. \quad (2.27)$$

When no signal is present, Eqs. (2.26) and (2.27) continue to hold with $\rho = 0$. These equations show that a signal should be detectable in the regime

$$\mathcal{N}_{\text{bins}}^{1/4} \ll \rho \lesssim \mathcal{N}_{\text{bins}}^{1/2}, \quad (2.28)$$

as well as at larger ρ , since in the regime (2.28) the expected value (2.26) of Q is large compared to its rms value in the absence of a signal. By contrast, a signal is detectable using band-pass filtering only in the regime $\rho \gtrsim \mathcal{N}_{\text{bins}}^{1/2}$, from Eq. (2.24) and associated discussion. The noise-monitoring method thus extends the domain of detectable signals to include the regime (2.28).

The approximate SNR threshold predicted by Eq. (2.27) is correct in order of magnitude, but to obtain an accurate SNR threshold it is necessary to calculate the full probability distribution for the statistic Q , since its statistical properties are very non-Gaussian. This probability distribution is given by, from Eqs. (2.18), (2.20) and (2.25),

$$P[Q(t) \geq Q_0] = \frac{\Gamma[\mathcal{N}_{\text{bins}}/2, (Q_0 + \mathcal{N}_{\text{bins}})/2]}{\Gamma(\mathcal{N}_{\text{bins}}/2)} \quad (2.29)$$

where $\Gamma(\dots, \dots)$ is the incomplete Gamma function and $\Gamma(\dots)$ is the usual Gamma function. Suppose now that we examine a number $\mathcal{N}_{\text{start-times}}$ of different starting times t , and that we wish to find the number Q_0 such that the probability (2.29) of $Q(t)$ exceeding Q_0 for any t , in the absence of a signal, is some small number $\epsilon \sim 10^{-4}$. This threshold Q_0 is obtained by solving

$$\frac{\Gamma[\mathcal{N}_{\text{bins}}/2, (Q_0 + \mathcal{N}_{\text{bins}})/2]}{\Gamma(\mathcal{N}_{\text{bins}}/2)} = \frac{\epsilon}{\mathcal{N}_{\text{start-times}}}. \quad (2.30)$$

From Eq. (2.26), this threshold will be exceeded by a signal whenever the signal strength (2.23) satisfies

$$\rho \geq \rho_* = \sqrt{Q_0}. \quad (2.31)$$

Equations (2.30) and (2.31) determine the threshold ρ_* as a function of the parameters ϵ , $\mathcal{N}_{\text{start-times}}$, and $\mathcal{N}_{\text{bins}}$; we use these formulae in Sec. VI B.

We now discuss an approximate formulae for the threshold ρ_* which gives an insight into the nature of the nonlinear filtering algorithm. It can be shown [58] that for $\mathcal{N}_{\text{bins}} \gg 1$, ρ_* can be obtained to a good approximation by solving the equation

$$\rho_*^2 = 2 \ln(\mathcal{N}_{\text{start-times}}/\epsilon) + \mathcal{N}_{\text{bins}} \ln(1 + \rho_*^2/\mathcal{N}_{\text{bins}}), \quad (2.32)$$

[cf. Eq. (1.6) discussed in the Introduction]. It is possible to understand the origin of Eq. (2.32) in the following simple way.

The total number $\mathcal{N}_{\text{shapes,max}}$ of waveform shapes of duration less than or equal to T , with bandwidth Δf and with $\text{SNR} \leq \rho$ which are distinguishable in the interferometer noise is approximately given by [36]

$$\ln(\mathcal{N}_{\text{shapes,max}}) \approx \frac{1}{2} \mathcal{N}_{\text{bins}} \ln(1 + \rho^2/\mathcal{N}_{\text{bins}}). \quad (2.33)$$

Let us denote by \mathcal{M} the manifold of all possible waveforms satisfying these criteria — duration less than or equal to T , bandwidth Δf and $\text{SNR} \leq \rho$. Not all of the waveforms in this manifold correspond to physically interesting BBH merger waveforms; the set $\mathcal{M}_{\text{merge}}$ of BBH merger waveforms will form a sub-manifold of \mathcal{M} . Consider now the hypothetical limit in which the sub-manifold $\mathcal{M}_{\text{merge}}$ becomes so large (perhaps curving back and intersecting itself) that, when smeared out by the interferometer noise, it effectively fills the entire manifold \mathcal{M} . In this limit, the number $\mathcal{N}_{\text{shapes}}$ of BBH merger waveform shapes for which we are searching approaches $\mathcal{N}_{\text{shapes,max}}$. It is clear that in this limit, knowledge of the waveform shapes is not useful in searching for the waves, and that a search method which simply seeks the maximum overlap between the measured signal and all possible waveform shapes (thus not requiring templates) would perform just as well as matched filtering. This is essentially what the nonlinear search method does. Using this insight, the threshold (2.32) can be obtained simply by combining Eqs. (2.16) and (2.33).

The above derivation is based on frequentist statistics. In Ref. [58] a Bayesian analysis is outlined of the detection of gravitational wave signals of unknown form which automatically identifies the statistic $Q(t)$ as optimal, and which also approximately reproduces the detection threshold ρ_* .

In practice, this search method would be combined with coincidenting between interferometers to achieve high detection reliability and to reduce the effects of non-Gaussian noise, as is the case with band-pass filtering as discussed in Sec. II A. Matched filtering could be more efficient than the noise-monitoring method at combating non-Gaussian noise via coincidenting, for the following reason. When coincidenting with templates, one can demand that the SNR in each interferometer be above the appropriate threshold, *and* that the signal-parameter values deduced in each interferometer be consistent with each other. For the noise-monitoring searches, one can only demand that the SNR in each interferometer be above the appropriate threshold. Hence, matched filtering has more discriminating power against situations in which all the interferometers have moderately large non-Gaussian noise spikes somewhere in the relevant time window. Non-Gaussian noise may therefore make the less-discriminating noise-monitoring search perform somewhat worse in practice, relative to matched filtering searches, than is indicated by the threshold (2.32).

C. Signal-to-noise ratio for matched filtering in terms of waves' energy spectrum

In this section we derive the relation [Eq. (2.34)] between the expected value of the optimal-filtering SNR (2.7), and the energy spectrum of gravitational waves emitted by the source. In general, the SNR (2.7) for a burst of waves depends on the details of the gravitational waveform, on the orientation of the source with respect to the interferometer, and on the direction to the source. By contrast, the quantity $\langle \rho^2 \rangle$, the average of the squared SNR over all orientations of and directions to the source, depends only on the total energy per unit frequency dE/df carried off from the source by the waves. Specifically, consider a gravitational-wave source located at a cosmological redshift z and corresponding luminosity distance $D(z)$. Let the locally measured frequency of the waves near the source be f_e , related to the frequency f measured at the interferometer by $f = f_e/(1+z)$. Let the locally measured energy spectrum of the waves be $dE_e/df_e(f_e)$. Then the orientation-averaged SNR squared measured at the interferometer is given by

$$\langle \rho^2 \rangle = \frac{2(1+z)^2}{5\pi^2 D(z)^2} \int_0^\infty df \frac{1}{f^2 S_h(f)} \frac{dE_e}{df_e} [(1+z)f]. \quad (2.34)$$

Note that the relation (2.34) refers to an angle-averaged SNR obtained from an *rms average* of signal amplitudes over different possible orientations of the source and interferometer. This averaging convention differs from that adopted in Refs. [1,10]. There, the angle-averaged SNR is defined to be a cube root of an average of cubed signal amplitudes, rather than an rms average. That ‘‘cube root of a mean cube’’ averaging method is the appropriate method for calculating the expected event detection rate [1]. As a result, the SNR formulae used in Refs. [1,10] are a factor of $\sqrt{3/2}$ larger than the formulae used in this paper, the factor of $\sqrt{3/2}$ being an approximation to the effect of the different angle-averaging methods.

We now turn to the derivation of Eq. (2.34). Consider first the case where the source of gravitational waves is sufficiently close that cosmological effects can be neglected. Let the source be at a distance r from the detector and at a location (θ, φ) on the sky. Let (ι, β) denote the direction towards the detector (spherical polar angles) with respect to a set of Cartesian axes centered at and determined by the source. Let the two independent polarizations of the strain amplitude at the interferometer be $h_+(t, r, \iota, \beta)$ and $h_\times(t, r, \iota, \beta)$, and let the polarization angle be ψ . Then the response of the interferometer will be $h(t) + n(t)$, where $n(t)$ is the interferometer noise, and

$$h(t) = F_+(\theta, \varphi, \psi) h_+(t, r, \iota, \beta) + F_\times(\theta, \varphi, \psi) h_\times(t, r, \iota, \beta). \quad (2.35)$$

Here F_+ and F_\times are the interferometer beam pattern functions, given in, *e.g.*, Ref. [1]. The dependence of the Fourier transformed waveform \tilde{h}_+ on r is clearly of the form

$$\tilde{h}_+(f, r, \iota, \beta) = H_+(f, \iota, \beta)/r \quad (2.36)$$

for some function H_+ ; we define $H_\times(f, \iota, \beta)$ similarly. Combining Eqs. (2.7), (2.35) and (2.36) gives

$$\rho^2(r, \theta, \varphi, \psi, \iota, \beta) = \frac{4}{r^2} \int_0^\infty \frac{|F_+ H_+ + F_\times H_\times|^2}{S_h(f)} df. \quad (2.37)$$

We now average over all of the angles $\theta, \varphi, \psi, \iota$ and β . The average over polarizations and over the sky location gives $\langle F_+^2 \rangle = \langle F_\times^2 \rangle = 1/5$, $\langle F_+ F_\times \rangle = 0$ [1], where the meaning of the angular brackets is given by, for example,

$$\langle F_+^2 \rangle \equiv \frac{1}{4\pi} \int d\Omega_{\theta, \varphi} \int_0^\pi \frac{d\psi}{\pi} F_+(\theta, \varphi, \psi)^2. \quad (2.38)$$

From Eq. (2.37) this gives

$$\langle \rho^2 \rangle = \frac{4}{5r^2} \int_0^\infty \frac{H(f)^2}{S_h(f)} df, \quad (2.39)$$

where

$$H(f)^2 \equiv \frac{1}{4\pi} \int d\Omega_{\iota, \beta} (|H_+(\iota, \beta)|^2 + |H_\times(\iota, \beta)|^2). \quad (2.40)$$

We now express the energy spectrum dE/df of the waves in terms of the quantity $H(f)^2$. The local energy flux is

$$\frac{dE}{dA dt} = \frac{1}{16\pi} \overline{\left[\left(\frac{\partial h_+}{\partial t} \right)^2 + \left(\frac{\partial h_\times}{\partial t} \right)^2 \right]}, \quad (2.41)$$

where the overbar means an average over several cycles of the wave. Switching to the frequency domain using Parseval's theorem, inserting a factor of two to account for the folding of negative frequencies into positive, and using $|\tilde{h}_{+, \times}(f)|^2 dA = |\tilde{H}_{+, \times}(f)|^2 d\Omega$ gives

$$\frac{dE}{d\Omega df} = \frac{\pi f^2}{2} (|\tilde{H}_+(\iota, \beta)|^2 + |\tilde{H}_\times(\iota, \beta)|^2). \quad (2.42)$$

Combining Eqs. (2.39), (2.40) and (2.42) now yields

$$\langle \rho^2 \rangle = \frac{2}{5\pi^2 r^2} \int_0^\infty df \int d\Omega \frac{1}{f^2 S_h(f)} \frac{dE}{d\Omega df} [f]. \quad (2.43)$$

This is essentially Eq. (2.34) with $z = 0$ and $D(z) = r$, the limiting form that applies when cosmological effects are neglected.

Consider now sources at cosmological distances. We can generalize Eq. (2.43) to incorporate redshift effects as follows: (i) Observe that Eq. (2.43) is valid for arbitrary

bursts of gravitational waves provided that we interpret the quantity

$$\frac{1}{r^2} \frac{dE}{d\Omega df}$$

as the locally measured energy flux $dE/dAdf$. (ii) Use the fact that the number of gravitons per unit solid angle per unit frequency is conserved for propagation in a Friedmann-Robertson-Walker background in the geometric optics limit:

$$\frac{dE}{d\Omega df}(f) = \frac{dE_e}{d\Omega df_e}[(1+z)f]. \quad (2.44)$$

Here f_e is the frequency at the source and $f = f_e/(1+z)$ is the frequency at the detector. (iii) The conversion factor at the detector from energy per unit solid angle to energy per unit area is just $(1+z)^2/D(z)^2$, where $D(z)$ is the luminosity distance [71]. Hence

$$\frac{dE}{dAdf} = \frac{(1+z)^2}{D(z)^2} \frac{dE_e}{d\Omega df_e}[(1+z)f]. \quad (2.45)$$

Combining this with Eq. (2.43) now yields Eq. (2.34).

An alternative derivation of the cosmological modifications to Eq. (2.43), which yields a useful rule of thumb for understanding redshift effects, is the following. Suppose that an arbitrary source of waves is specified by parameters θ_i for $1 \leq i \leq n$. In the local wave zone the gravitational waveform is of the form

$$h(t) = \frac{H(t; \theta_i)}{r}, \quad (2.46)$$

for some function H , where r is the distance to the source. After propagating through a FRW background the waveform becomes

$$h(t) = \frac{H(t; \theta_{i, \text{redshifted}})}{D(z)}, \quad (2.47)$$

where if θ_i has dimension (length) ^{p} or (mass) ^{p} , then $\theta_{i, \text{redshifted}}$ is just $(1+z)^p \theta_i$. Equation (2.47) can be derived from the general solution for wave propagation in FRW backgrounds in the geometric optics limit given in Ref. [72]. The fact that the waveform must depend on and reveal the ‘‘redshifted’’ source parameters is clear: all source parameters with dimension that we can measure from the waves must essentially come from timescales in the waveform, since the wave amplitude is dimensionless. All these timescales will be redshifted.

There is a corresponding simple rule for how the SNR is affected by cosmological effects. Suppose that when cosmological effects are neglected, the SNR is of the form

$$\rho = \frac{F(\theta_i)}{r}, \quad (2.48)$$

for some function F . Then the correct SNR is just

$$\rho = \frac{F(\theta_{i, \text{redshifted}})}{D(z)}. \quad (2.49)$$

Applying this rule to Eq. (2.43) yields Eq. (2.34).

III. THE GRAVITATIONAL-WAVE SIGNAL FROM COALESCING BLACK HOLES

In this section we describe our assumptions concerning the gravitational-wave signal from BBH mergers, and the evidence that underlies those assumptions. We start in subsection III A by discussing the approximate splitting of the total waveform into the inspiral, merger, and ringdown epochs. In Sec. III B we discuss the various circumstantial pieces of evidence, culled from the literature, about the energy spectrum and the total energy radiated during the nonlinear merger phase. Our assumed merger energy spectrum is given by Eq. (3.14), with parameters given by Eqs. (3.4), (3.5) and (3.13). The inspiral energy spectrum is discussed in Sec. III C and specified in Eq. (3.20). Section III D discusses the spectrum and likely overall amplitude of the ringdown signal; the spectral shape is given in Eq. (3.24) and our assumption about the overall energy radiated in Eq. (3.28). In Sec. III E we estimate the SNR obtainable in band-pass filtering searches for waves from the merger phase.

A. The three phases of the gravitational-wave signal

As discussed in the Introduction, the coalescence and its associated gravitational-wave signal can be divided into three successive epochs in the time domain: inspiral, merger, and ringdown. Physically, the inspiral consists of the portion of the coalescence in which the black holes are separated bodies that gradually lose energy and angular momentum, slowly spiraling towards one another. By contrast, the merger consists of that portion of the coalescence in which the dynamics are highly nonlinear and must be treated by numerical relativity. With this in mind, it is useful to define the end of inspiral as the time and frequency [73] at which numerically generated templates start to be needed. Up to this time, post-Newtonian templates, possibly supplemented with IBBH templates, will be used (*cf.* Sec. IB).

After inspiral, we expect there to be a lot of complicated merger dynamics that at present are not well understood. The system will gradually settle down to a Kerr black hole; the last gravitational waves we expect to see are those produced by the quasi-normal ringing modes of this merged black hole. It is clear that there will be a smooth transition in the gravitational waveform from the merger portion to the ringdown portion, as the effects of nonlinearities become less and less important with time. As this happens, the signal should become increasingly well approximated by a linear combination of exponentially decaying sine waves. This is the behavior that has been seen in numerical simulations of, for example, head-on collisions [74,75]. At late times, the $l = m = 2$ mode will dominate over other quasi-normal modes, for two reasons which are of comparable importance: (i) The $l = m = 2$ mode is the most slowly

damped of all the QNR modes [14], and (ii) during coalescence, the binary will have a rotating shape roughly corresponding to spheroidal harmonic indices $l = m = 2$, and thus this mode will be preferentially excited [76]. We define the ringdown as beginning when the waveform becomes dominated by the $l = m = 2$ QNR mode; the merger thus contains those portions of the waveform where other modes and/or non-linear mode-mode couplings are important. Clearly there is some arbitrariness in the exact time at which the ringdown starts, related to the accuracy we require of the fit of the waveform to the ringdown signal.

Note that, by definition, the three phases of the signal are disjoint in the time domain. It does not follow, though, that they should be disjoint in the frequency domain: their energy spectra might overlap. However, it is at least approximately true that the inspiral and merger and disjoint in both time and frequency. Let t_{merge} be the time at which inspiral is said to end and merger to begin. Then, since the inspiral waves chirp monotonically and since the adiabatic approximation is just beginning to break down at the end of the inspiral, the inspiral spectrum is confined, to good approximation, to the frequency region $f < f_{\text{merge}}$. Here, f_{merge} is the frequency of the inspiral waves at $t = t_{\text{merge}}$. We shall further assume that the merger waves' spectrum is confined to the frequency regime $f > f_{\text{merge}}$; this assumption should be valid to a moderately good approximation. (We discuss below estimates of the value of f_{merge} .)

One particular component of the gravitational-wave signal, the Christodoulou memory [77], will violate this assumption. The memory component of the gravitational-wave signal has most of its power below f_{merge} in the frequency domain, but accumulates gradually during the inspiral, merger and ringdown in the time domain. The memory waves from BBH coalescences will probably not be detectable with ground based interferometers, but very probably will be detectable with LISA [78]. We will neglect the memory component of the waves in our analysis, since it will not be as easy to detect as the components we do discuss.

B. Energy spectrum of the emitted gravitational radiation from the merger phase

The total amount of energy radiated in BBH mergers, and its distribution in frequency, is highly uncertain because detailed numerical calculations of these mergers have not yet been made. In this subsection, we discuss what little evidence there is about the energy radiated, and describe our crude model of the spectrum. We assume a uniform distribution in frequency from the lower frequency f_{merge} mentioned above and some upper frequency f_{high} .

The total amount of energy radiated during a BBH coalescence will be some fraction ϵ of the total mass $M = m_1 + m_2$ of the system:

$$E_{\text{radiated}} = \epsilon M. \quad (3.1)$$

The fraction ϵ will depend only on the mass ratio m_1/m_2 , on the initial spins \mathbf{S}_1 and \mathbf{S}_2 of the two black holes, and on the initial direction $\hat{\mathbf{L}}$ of the orbital angular momentum [79]:

$$\epsilon = \epsilon \left(\frac{m_1}{m_2}, \frac{\mathbf{S}_1}{M^2}, \frac{\mathbf{S}_2}{M^2}, \hat{\mathbf{L}} \right). \quad (3.2)$$

We can very roughly divide up this fraction as

$$\epsilon = \epsilon_{\text{inspiral}} + \epsilon_{\text{merger}} + \epsilon_{\text{ringdown}}, \quad (3.3)$$

according to the amounts of energy radiated in the three different epochs of the waveform. There is clearly some arbitrariness in this division of the radiated energy into three pieces, which is related to the choice of the frequency f_{merge} at which the inspiral is said to end and the merger to begin [73], and also to the choice of the time t_{qnr} at which the merger is said to end and the ringdown to begin.

We now discuss methods of estimating f_{merge} , ϵ_{merger} , and $\epsilon_{\text{ringdown}}$. Roughly speaking, we want to choose the interface between “inspiral” and “merger” to be at that point where post-Newtonian templates cease to be useful and where numerically generated templates will need to be used. Numerically generated initial data sets of two orbiting black holes provide some guidance about this interface. Cook [9] compares the properties of such initial data sets to the predictions of post-Newtonian theory at second post-Newtonian order. He finds, for example, that the discrepancy in the binding energy will be $\sim 5\%$ when the gravitational-wave frequency (twice the orbital frequency) is $f \sim 0.02/M$, where M is the total mass of the system, and will be $\sim 15\%$ at $f \sim 0.05/M$ [9].

Towards the end of the inspiral, the black holes make a gradual transition from a radiation-reaction driven inspiral to a freely-falling plunge [8,11,12], after which, even if the radiation reaction could be turned off, the black holes would still merge. This will occur roughly at the last stable circular orbit (LSCO). It would seem to make sense to choose $f_{\text{merge}} = f_{\text{LSCO}}$, the frequency at which this occurs. Strictly speaking, the concept of an LSCO makes sense only in the test particle limit ($m_1/m_2 \ll 1$). Various somewhat *ad hoc* methods have been used to estimate f_{LSCO} outside this regime, but the results differ by factors $\gtrsim 2$. Cook’s initial data set analysis together with the calculation of an “effective potential” yields the estimate $f_{\text{LSCO}} \sim 0.055/M$ for equal mass black holes [9]. In post-Newtonian theory, the LSCO can be defined by artificially turning off the radiation reaction terms in the equations of motion. Using this method, Kidder, Will and Wiseman estimate that $f_{\text{LSCO}} \sim 0.02/M$ [8]. They use hybrid equations of motion which are accurate to post-2-Newtonian order for comparable mass ratios, and which are exact in the test particle limit. The value they obtain varies by less than $\sim 20\%$ as the mass ratio is varied. Note that the frequency $0.02/M$ is close

to the value $6^{-3/2}/(\pi M)$ obtained from the usual LSCO at $r = 6M$ in the test particle limit (here r is the usual Schwarzschild radial coordinate). Finally, earlier analyses by Blackburn and Detweiler used a variational principle together with the assumption of periodic solutions to Einstein's equations to obtain the approximate lower bound $f_{\text{LSCO}} \gtrsim 0.06/M$ [80].

Note that all of these estimates are for equal mass, non spinning black holes; the value of the frequency f_{LSCO} can also vary by factors $\gtrsim 2$ if the black holes are spinning or have different masses.

In light of this uncertainty, we somewhat arbitrarily adopt the conservative value of

$$\begin{aligned} f_{\text{merge}} &= \frac{0.02}{M} \\ &= 205 \text{ Hz} \left(\frac{20M_{\odot}}{M} \right) \end{aligned} \quad (3.4)$$

as the lower cutoff frequency for the energy spectrum. This (low) value of f_{merge} is conservative in the sense that we can be reasonably sure that numerically generated templates will not be needed before $f = f_{\text{merge}}$. On the other hand, it may optimistically overestimate the merger SNR by increasing the number of cycles in what we define as our merger waveform at the expense of the number of cycles in the inspiral.

We next discuss our choice of upper frequency shut-off for the merger energy spectrum. As discussed above, we define the end of the merger to occur at that time t_{qnr} after which the waveform can be fit fairly accurately by the $l = m = 2$ QNR mode signal. The merger and the ringdown will therefore be disjoint in the time domain, but not necessarily in the frequency domain. It seems likely, however, that an approximate upper bound for the frequencies carrying appreciable power during the merger is the quasinormal ringing frequency itself. This is supported to some extent by calculations of the energy spectrum of waves produced in the test particle limit—see Fig. 2 of Ref. [65]. The energy spectrum dE/df in that case is peaked near the quasinormal mode frequency $.06/M$ of a non-rotating black hole, and has fallen by 2 orders of magnitude at $.14/M$. Although this analysis does not incorporate any nonlinear effects, there is some evidence that the energy spectrum in the equal mass case will be qualitatively similar—namely, the head-on collision of black holes in full numerical relativity *has* been computed, and the resulting waveforms are qualitatively similar to those predicted from perturbation theory [74,75]. It is not clear how relevant the head-on collision case is to the gradual inspiral; but on the other hand, there is no other guidance available at the present time. We will therefore use as our upper shutoff frequency for the merger spectrum the frequency f_{qnr} of the $l = m = 2$ quasinormal mode. This frequency will depend on the unknown dimensionless spin parameter a of the final Kerr black hole (its spin angular momentum divided by M^2). We choose to use the value of a for

which the frequency is highest: in the limit $a \rightarrow 1$, the QNR frequency becomes $0.9/(2\pi M)$ (more than twice the value for a Schwarzschild black hole) [52]. Thus, our upper cutoff frequency is

$$\begin{aligned} f_{\text{high}} = f_{\text{qnr}} &= \frac{0.13}{M} \\ &= 1430 \text{ Hz} \left(\frac{20M_{\odot}}{M} \right). \end{aligned} \quad (3.5)$$

Our reasons for assuming a high value of a are discussed in Sec. III D below.

Finally, consider the total amount of energy

$$E_{\text{rad}} = (\epsilon_{\text{merger}} + \epsilon_{\text{ringdown}})M \quad (3.6)$$

radiated during the final merger and ringdown. To estimate this we consider first an extrapolation due to Smarr [64,74]. The idea is to calculate the energy radiated in the test particle approximation using black-hole perturbation theory. The result will be of the form $E_{\text{rad}} = k\mu^2/M$, where k is a dimensionless constant, μ is the mass of the test particle, and M is the total mass. Now simply replace μ by the reduced mass $m_1 m_2 / (m_1 + m_2)$ of the two black holes. This extrapolation works exactly in Newtonian gravity supplemented by the quadrupole formula, in the sense that the dynamics of two bodies of comparable masses can be deduced from the corresponding dynamics in the extreme mass ratio limit. Surprisingly, it also works to within $\sim 20\%$ to predict the total energy radiated in the head-on collision of two equal-mass black holes [65,74,75,81]. Thus, one might consider applying this extrapolation to inspiral-preceded mergers. Such a calculation would require a determination of the radiated energy from the final plunge of a test particle, *i.e.*, the solution of a coupled radiation reaction/radiation generation problem outside of the adiabatic regime (although the coupling is important only in a brief transitional phase and essentially sets the initial conditions for an approximately geodesic plunge [11]). This calculation has not yet been done. However, there is an alternative approximate method to estimate the amount of energy radiated in the test particle limit. The innermost, marginally bound (unstable) circular orbits should be a fair approximation to the motion during the final plunge. Detweiler [65] showed that the amount of energy radiated per orbit by a test particle in such an orbit is of the form $E_{\text{rad}} = k\mu^2/M$, where k varies from 0.65 at $a = 0$ to 2.8 at $a = 0.95$, where a is the spin parameter of the black hole. Assuming that there will be $\gtrsim 1$ effective orbit during the final plunge, Detweiler estimated that [65]

$$0.03M F(\mu/M) \lesssim E_{\text{rad}} \lesssim 0.2M F(\mu/M), \quad (3.7)$$

where

$$F(\mu/M) = \left(\frac{4\mu}{M} \right)^2 \quad (3.8)$$

which is unity in the equal-mass case $\mu = M/4$.

Arguments based on conservation of angular momentum also suggest an approximate lower bound on the radiated energy of about $0.1M$ for equal-mass BBHs in the most favorable cases, as we now outline. Roughly speaking, the system’s angular momentum divides up as

$$\mathbf{S}_1 + \mathbf{S}_2 + \mathbf{L}_{\text{orb}} = \mathbf{L}_{\text{rad}} + \mathbf{S}_{\text{final}}, \quad (3.9)$$

where \mathbf{S}_1 and \mathbf{S}_2 are the spins of the two black holes just before the final plunge, \mathbf{L}_{orb} is the orbital angular momentum just before the plunge, \mathbf{L}_{rad} is the angular momentum carried off by the gravitational waves, and $\mathbf{S}_{\text{final}}$ is the spin of the final Kerr black hole. This splitting of the total angular momentum of the spacetime into various pieces is really only well defined only in a post-Newtonian type of limit; however, the effects of this ambiguity are presumably not important for the purposes of our crude, approximate argument. We now specialize to the most favorable case in which \mathbf{S}_1 , \mathbf{S}_2 and \mathbf{L}_{orb} are all aligned. We take the orbital angular momentum at the beginning of merger to be $|\mathbf{L}_{\text{orb}}| \approx 0.9M^2$, the value predicted by Cook’s initial data sets at $f = 0.02/M$ [9]. We also assume that both inspiraling black holes are rapidly spinning, so that $|\mathbf{S}_1| \approx |\mathbf{S}_2| \approx (M/2)^2$. Equation (3.9) then yields

$$|\mathbf{L}_{\text{rad}}| \gtrsim 0.4M^2, \quad (3.10)$$

since $|\mathbf{S}_{\text{final}}| \leq M^2$.

Next, we use that fact that the energy E_{rad} and the angular momentum L_{rad} carried off by gravitons of frequency f and azimuthal multipole order m are related by [82]

$$E_{\text{rad}} = 2\pi f L_{\text{rad}}/m. \quad (3.11)$$

If we estimate f as $(f_{\text{merge}} + f_{\text{qnr}})/2$, and make the admittedly optimistic assumption that most of the radiation is quadrupolar, we obtain from Eqs. (3.10) and (3.11) the crude estimate for the total radiated energy [83]

$$E_{\text{rad}} \gtrsim 0.1M. \quad (3.12)$$

This estimate includes both merger and ringdown radiated energies; we need to subtract out the ringdown portion to obtain the energy contained in the merger portion of the waveform. Below we estimate $\sim 0.03M$ to be an approximate upper bound for the ringdown energy, and hence most of the energy (3.12) should be radiated in the merger waves.

There is an additional, separate argument one can make which indicates that most of the energy (3.12) should be radiated as merger waves and not as ringdown waves. As noted by Eardley and Hirschmann [84], any system with $J > M^2$ cannot evolve to $J < M^2$ by radiating quadrupolar waves at the ringing frequency $f_{\text{qnr}} \sim 1/(2\pi M)$ of a near-extremal Kerr black hole. This is because at this high frequency, too much mass-energy is radiated per unit angular momentum radiated; Eq. (3.11)

with $m = 2$ and with $f = f_{\text{qnr}}$ yields $\Delta J = \Delta(M^2)$. Hence, since the final black hole must have $J < M^2$, a substantial amount of the radiation must be emitted at lower frequencies.

Based on the estimates (3.7) and (3.12), and on the estimated upper bound $\sim 0.03M$ mentioned above for the ringdown radiated energy, we perhaps optimistically take $0.1M$ to be the energy radiated during merger in the equal-mass case (which corresponds to about $0.13M$ total radiated energy in the merger and ringdown). For non equal-mass BBHs we assume that the radiated energy is reduced by the factor (3.8), so that

$$E_{\text{merger}} = \epsilon_{\text{merger}} F(\mu/M) M = 0.1F(\mu/M)M. \quad (3.13)$$

The rather high radiation efficiency of 0.1 that we are assuming is probably most plausible in the context of rapidly spinning coalescing black holes. In particular, if the spins and the orbital angular momentum are somewhat misaligned, the coalescence will be something like “two tornados with orientations skewed to each other, embedded in a third, larger tornado with a third orientation” [10]. Intuitively one would expect that such systems have more “settling down” to do to get to the final Kerr black hole, and that correspondingly the non-linear, highly dynamical phase should last longer and/or produce more radiation. Also, the potential barrier that surrounds the final black hole (which normally tends to reflect back into the black hole the dominant waves of frequency $f \sim 1/a$ few times M) presumably will effectively not be present during the violent phase of a merger in which the spins and orbital angular momentum are of comparable magnitude and are misaligned.

We note that coalescences which radiate as much energy as the estimate (3.13) will also likely radiate a substantial amount of linear momentum, and the consequent recoil of the final black hole could correspond to a kick velocity that is a moderate fraction of the speed of light.

Finally, consider the shape of the energy spectrum dE/df between f_{merge} and f_{qnr} . For simplicity, and for lack of evidence in favor of anything more specific, we choose a flat spectrum:

$$\begin{aligned} \frac{dE}{df} &= \frac{\epsilon_m M F(\mu/M)}{f_{\text{qnr}} - f_{\text{merge}}} \Theta(f - f_{\text{merge}})\Theta(f_{\text{qnr}} - f) \\ &= 0.91M^2 F(\mu/M) \Theta(f - f_{\text{merge}})\Theta(f_{\text{qnr}} - f), \end{aligned} \quad (3.14)$$

where $\epsilon_m = \epsilon_{\text{merger}} = 0.1$ and Θ is the step function.

Our assumed merger spectrum has the desirable feature that it is reasonably consistent with the inspiral energy spectrum at $f = f_{\text{merge}}$. This can be seen as follows. We do not expect a very large change in dE/df at the interface between inspiral and merger, for the following reason: throughout the inspiral, the energy spectrum can be written [1]

$$\frac{dE}{df}(f) \propto n_{\text{cyc}}(f) h[t(f)]^2, \quad (3.15)$$

where $n_{\text{cyc}}(f)$ is the number of cycles spent near frequency f , and $h[t(f)]$ is the wave amplitude at the time $t(f)$ when the waves' frequency is f [see also Eqs. (2.9) and (5.2)]. In the transition from inspiral to plunge, the amplitude $h[t(f)]$ should change only moderately, but $n_{\text{cyc}}(f)$ could conceivably change by a large amount: from its pre-plunge value to ~ 1 . It turns out that the number of cycles does not change very drastically: at the interface between inspiral and merger,

$$n_{\text{cyc}}(f) = \frac{f^2}{\dot{f}} \approx \frac{5}{96\pi} (\pi \mathcal{M} f)^{-5/3} \sim 6.7 \left[\frac{f}{f_{\text{merge}}} \right]^{-5/3}. \quad (3.16)$$

(Here, $\mathcal{M} = \mu^{3/5} M^{2/5}$ is the so-called chirp mass.) Hence, we do not expect dE/df to change too much.

We now show that our assumed values of dE/df from the end of the inspiral and from the beginning of the merger are reasonably close to one another, in agreement with the above expectation. Using the approximation that the motion is an adiabatic evolution from one circular orbit to another, the energy radiated during inspiral can be written

$$\left(\frac{dE}{df} \right)_{\text{radiated}} = \frac{d}{df} E_{\text{circ}}(f) [1 + O(1/n_{\text{cyc}}(f))], \quad (3.17)$$

where $E_{\text{circ}}(f)$ is the binding energy of a particle in a circular orbit at orbital frequency $f/2$ (recall that the gravitational-wave frequency is twice the orbital frequency). At our estimated plunge frequency $f_{\text{merge}} = 0.02/M$, the hybrid equations of motion of Kidder, Will and Wiseman [8] predict in the equal mass case that

$$\frac{dE_{\text{circ}}}{df}(f = 0.02/M) = 0.88M^2, \quad (3.18)$$

while Cook's initial data sets predict that [9]

$$\frac{dE_{\text{circ}}}{df}(f = 0.02/M) = 0.41M^2. \quad (3.19)$$

The true value of dE_{circ}/df is presumably somewhere between these two values. We would expect the value of $(dE/df)_{\text{radiated}}$ to be smaller than this, because the approximation (3.17) is breaking down at this point—some of the gravitational binding energy is being converted to inward radial kinetic energy instead of being radiated. This picture is roughly consistent with our assumption of $dE/df = 0.91M^2$ for $f \geq 0.02/M$, given that Eqs. (3.18) and (3.19) apply to the non-spinning case, and we are interested in the rapidly spinning case for which dE/df could be a few times larger.

C. Energy spectrum of the radiation from the inspiral phase

The standard quadrupole formula prediction for the inspiral energy spectrum is (see, *e.g.*, Ref. [85])

$$\frac{dE}{df} = \frac{1}{3} \pi^{2/3} \mu M^{2/3} f^{-1/3}. \quad (3.20)$$

This approximate formula is adequate to estimate the SNR obtained from optimal filtering of the inspiral waveform. The formula will be accurate to within a few tens of percent up to $f = f_{\text{merge}}$ [60]. Using Eq. (3.20) to estimate the SNR effectively assumes that both the gravitational-wave signal and the theoretical templates used to cross-correlate with the data stream are given by the quadrupole approximation (3.20). The SNR we calculate using this lowest order formula will be approximately the same as that found by cross-correlating real signals [which incorporate higher order corrections to Eq. (3.20)] against sufficiently accurate theoretical templates. As outlined in Sec. IB, the required template accuracy should be achievable by post-Newtonian expansions [44,86], perhaps supplemented with alternative techniques for the latter, high frequency part of the signal at $0.01/M \lesssim f \lesssim 0.02/M$ (the IBBH regime). We assume that the inspiral energy spectrum shuts off at $f = f_{\text{merge}} = 0.02/M$, as discussed in Sec. III B.

D. Energy spectrum of the radiation from the ringdown phase

As we have discussed, the ringdown portion of the gravitational-wave signal is that portion in the time domain that can be fit fairly accurately by an exponentially decaying sinusoid corresponding to the most slowly damped $l = m = 2$ quasinormal mode of the final black hole. The shape of the corresponding energy spectrum is well understood: it is just a resonance curve (although see Appendix B for discussion of a subtlety in the applicability of the concept of the waves' energy spectrum for calculating ringdown SNRs). The overall amplitude of the energy spectrum, however, is not well understood. In this section we discuss our estimate of the overall amplitude for the ringdown signal.

The QNR gravitational waveforms $h_+(t, \iota, \beta)$ and $h_\times(t, \iota, \beta)$ are given by [15]

$$h_+ - ih_\times = \frac{\mathcal{A}M}{r} {}_2S_2^2(\iota, \beta, a) \times \exp[-2i\pi f_{\text{qnr}} t - t/\tau + i\varphi_0], \quad (3.21)$$

for $t > 0$. Here we have chosen $t = 0$ to be the time of the start of the ringdown, M is the mass of the black hole, aM^2 is its spin, and φ_0 is a constant phase. The quantities ι and β are spherical polar coordinates centered on the black hole [*cf.* Sec. II C], ${}_2S_2^2(\iota, \beta, a)$ is a spin weighted spheroidal harmonic whose angle averaged rms value is

$$\left(\frac{1}{4\pi} \int d\Omega |{}_2S_2^2(\iota, \beta, a)|^2 \right)^{1/2} = \frac{1}{\sqrt{4\pi}}, \quad (3.22)$$

and \mathcal{A} is a dimensionless coefficient that describes the magnitude of the perturbation when the ringdown begins. The quantities f_{qnr} and τ are the frequency and

damping time, respectively, of the QNR mode of the black hole. The quality factor Q of the mode is given by $Q = \pi\tau f_{\text{qnr}}$.

As mentioned in the Introduction, there is a mapping between the values of M and a , and of f_{qnr} and τ . This mapping has been explored by Leaver [87] and Echeverria [15]. Leaver studied in depth the damping times and ringing frequencies of various QNR modes for various Kerr black hole masses and spins. By numerically solving the Teukolsky equation, he produced extensive catalogs of the variation of τ and f_{qnr} with black hole mass M and dimensionless spin a [87]. From that data for the $l = m = 2$ mode, Echeverria [15] produced the following analytic fits, which are good to within roughly 5%:

$$\begin{aligned} f_{\text{qnr}} &\approx \left[1 - 0.63(1-a)^{3/10}\right] \frac{1}{2\pi M} \\ &= \left[1 - 0.63(1-a)^{3/10}\right] \left(\frac{37 M_{\odot}}{M}\right) 865 \text{ Hz} \\ Q &\approx 2(1-a)^{-9/20}. \end{aligned} \quad (3.23)$$

Note that Q diverges as $a \rightarrow 1$ but that f_{qnr} tends towards a constant.

The energy spectrum for the QNR waveform (3.21) is derived in Appendix B and is given by

$$\frac{dE}{df} = \frac{\mathcal{A}^2 M^2 f^2}{32\pi^3 \tau^2} \left\{ \frac{1}{[(f - f_{\text{qnr}})^2 + (2\pi\tau)^{-2}]^2} + \frac{1}{[(f + f_{\text{qnr}})^2 + (2\pi\tau)^{-2}]^2} \right\} \quad (3.24)$$

$$\approx \frac{1}{8} \mathcal{A}^2 Q M^2 f_{\text{qnr}} \delta(f - f_{\text{qnr}}) [1 + O(1/Q)]. \quad (3.25)$$

Approximating the energy spectrum by a delta function as in Eq. (3.25) will often (but not always) provide a fairly good approximation to the SNR; see Appendix B for more details.

The values of the spin a of the final black hole (and correspondingly, Q) and also of the amplitude \mathcal{A} will depend on the initial parameters of the system as in Eq. (3.2). This dependence is very poorly understood at present. We expect the final black hole to be rapidly spinning since, as explained in Sec. III B, the total angular momentum of the binary at the end of the inspiral is $\sim 0.9M^2$ when even the individual black holes are non-spinning [62], and the individual black hole spins can add to this. Moreover, the individual black holes in the binary may typically have been spun up to near maximal rotation by an accretion disk [88]. For definiteness, we somewhat arbitrarily take $a = 0.98$, which corresponds from Eq. (3.23) to $Q = 12$ and $f_{\text{qnr}} = 0.13/M$. The final ringdown SNR values we obtain vary only weakly with our assumed value of a [*cf.* Eq. (A14)], for fixed total energy radiated in the ringdown.

Although the value of the overall amplitude \mathcal{A} is uncertain, we can estimate an upper bound on \mathcal{A} for equal

mass BBHs in the following way. When the $l = m = 2$ quasinormal mode becomes the dominant mode present, the merged body will be a distorted Kerr black hole. The horizon's cross section, seen looking down on this black hole from above, will be a rotating oval rather than a circle. We can quantify the distortion by the ratio of the polar circumference about the long axis of this oval to the polar circumference about the short axis. Let \mathcal{A}_2 denote the perturbation amplitude such that the ratio of circumferences is, say, $2 : 1$. It is fairly clear that non-linear couplings between the $l = m = 2$ mode and other modes will be important for $\mathcal{A} \gtrsim \mathcal{A}_2$; thus, at this $2 : 1$ distortion ratio, the signal will not be well approximated by just the $l = m = 2$ mode. Hence, \mathcal{A}_2 is a reasonable upper bound for the true amplitude \mathcal{A} .

We could in principle calculate the upper bound \mathcal{A}_2 by writing the spacetime metric as

$$g_{ab} = g_{ab}^{\text{KERR}} + \mathcal{A}_2 h_{ab}^{\text{QNR}}$$

where g_{ab}^{KERR} is the Kerr metric and h_{ab}^{QNR} is the $l = m = 2$ quasinormal mode whose asymptotic form at large r is given by Eq. (3.21), and by calculating from this metric the ratio of circumferences [89]. For this paper, we used a much less sophisticated method to estimate \mathcal{A}_2 . Using the quadrupole formula, we examined the radiation produced by a solid body that is distorted with the same $2 : 1$ circumference ratio as the merged black hole, and obtained the estimate $\mathcal{A}_2 \sim 0.4$ [90]. Setting our waveform amplitude \mathcal{A} equal to this upper bound yields an rms angle-averaged waveform $h = (0.4/\sqrt{4\pi})(M/r) = 0.1(M/r)$ at the beginning of ringdown. From Eq. (3.24), the corresponding radiated energy is

$$E_{\text{ringdown}} \approx \frac{1}{8} \mathcal{A}^2 M^2 f_{\text{qnr}} Q \approx 0.03M. \quad (3.26)$$

As mentioned in the Introduction, comparable ringdown radiation efficiencies $\sim 3\%$ have been seen in numerical simulations of the evolution of distorted, spinning black holes [63].

To summarize, our assumed parameter values for the black hole dimensionless spin parameter a and for the dimensionless amplitude parameter \mathcal{A} for equal-mass BBHs are

$$\begin{aligned} a &= 0.98 \\ \mathcal{A} &= 0.4. \end{aligned} \quad (3.27)$$

These imply the following values for the quasi-normal ringing frequency f_{qnr} , the quality factor Q and the fraction of total mass-energy radiated during ringdown $\epsilon_{\text{ringdown}} = E_{\text{ringdown}}/M$:

$$\begin{aligned} f_{\text{qnr}} &= \frac{0.13}{M} \\ Q &\simeq 12 \\ \epsilon_{\text{ringdown}} &= 0.03. \end{aligned} \quad (3.28)$$

For non equal-mass BBHs, we assume that \mathcal{A} and $\epsilon_{\text{ringdown}}$ are reduced by the factor (3.8).

E. Number of independent frequency bins for the merger phase

In Sec. II A we showed that for any burst of gravitational waves, the band-pass filtering SNR is smaller than the optimal filtering SNR by a factor of approximately

$$\sqrt{\mathcal{N}_{\text{bins}}} = \sqrt{2T\Delta f}. \quad (3.29)$$

Here T is the duration of the merger and Δf is the band-pass filter's bandwidth, which should be approximately the largest expected signal bandwidth. The product $\mathcal{N}_{\text{bins}}$, which is roughly the number of independent frequency bins (or Fourier coefficients) needed to describe the signal, also determines how well matched filtering searches perform compared to noise-monitoring searches, as explained in Sec. II B. In this section, we obtain a rough estimate of the parameter $\mathcal{N}_{\text{bins}}$ for the merger gravitational waves.

First consider the bandwidth Δf . Our assumed bandwidth for the merger signal is $\Delta f = f_{\text{qnr}} - f_{\text{merge}} \approx f_{\text{qnr}}$ [since $f_{\text{merge}} \ll f_{\text{qnr}}$; cf. Eqs. (3.4) and (3.5)]. We cannot, however, be completely confident that all signal power in the merger will lie at frequencies below f_{qnr} , so a more appropriate choice might be $\Delta f \sim 2f_{\text{qnr}}$. Also the quasinormal ringing frequency f_{qnr} depends on the dimensionless spin parameter a of the final black hole as given by Eq. (3.23). Choosing the highest possible value, $f_{\text{qnr}} = 1/(2\pi M)$, yields

$$\Delta f \sim \frac{1}{\pi M}. \quad (3.30)$$

Turn, now, to the effective duration T of the signal, which is defined by Eq. (2.13). Clearly this parameter will vary considerably from event to event and its value is highly uncertain. To get a feeling for the range of possible values, let us consider the type of coalescence discussed in Sec. III B, where both inspiraling black holes are nearly maximally spinning, with their spins and the orbital angular momentum of the binary all aligned. In this favorable case, as argued in Sec. III B, at the end of inspiral near $r \sim 6M$ the binary has an excess $\sim 0.4M^2$ of total angular momentum that it needs to shed before it can settle down to its final Kerr state. Thus it seems reasonable to suppose that the two black holes will be somewhat centrifugally hung up and continue to orbit for several cycles before their event horizons merge. In other words, the orbital dynamical instability may be suppressed by the aligned spins, so that what we call merger (for data-analysis and computational purposes) may dynamically resemble the inspiral. The duration of the merger in this case may therefore be long. By contrast, for inspiraling non-spinning black holes, there is probably no excess angular momentum that needs to be radiated after the orbital dynamical instability is reached, and so it is plausible that the two black holes merge rather quickly. In such a case, most of the emitted energy could come out

in the ringdown waves rather than in merger waves, as has typically been seen in numerical simulations.

To estimate the duration T for the first type of scenario, we assume that the gravitational-wave luminosity dE/dt during the merger phase is roughly the same as the luminosity at the start of the ringdown, $2\epsilon_r M/\tau$. (Here, $\epsilon_r = 0.03$ is the ringdown radiation efficiency, and τ is the damping time of the QNR mode). Combining this with a total energy radiated during the merger of $\epsilon_m M$ (with $\epsilon_m = 0.1$) yields the estimate

$$T = \frac{1}{2} \frac{\epsilon_m}{\epsilon_r} \tau. \quad (3.31)$$

Clearly this estimate will become invalid for high values of τ ; in that limit, the high quality factor of the QNR mode causes a low quasi-normal ringing luminosity, whereas there is no reason for the merger luminosity to be comparably low. Nevertheless, we insert our assumed value of τ , which corresponds to a quality factor of $Q = 12$ [Eqs. (3.23) and (3.27)] into Eq. (3.31) to obtain $T \sim 50M$. Combining this with Eqs. (2.14) and (3.30) yields the estimate

$$\sqrt{\mathcal{N}_{\text{bins}}} \sim \sqrt{30} \sim 5. \quad (3.32)$$

For inspiraling Schwarzschild black holes, on the other hand, T may not be much larger than $\tau = 10M$ (assuming $a = 0.5$ say), giving $\sqrt{\mathcal{N}_{\text{bins}}} \sim \sqrt{6}$.

The factor $\sqrt{\mathcal{N}_{\text{bins}}}$ is thus likely to lie in the range $2 \lesssim \sqrt{\mathcal{N}_{\text{bins}}} \lesssim 5$. We adopt the estimate $\sqrt{\mathcal{N}_{\text{bins}}} = 4$ in Sec. VI B below to estimate the reduction in SNR resulting from using band-pass filters instead of optimal templates. We use the conservative, large value $\mathcal{N}_{\text{bins}} = 60$ in Sec. VI B to estimate detection thresholds for noise-monitoring searches for signals.

IV. INTERFEROMETER NOISE CURVES

In this section we describe our approximate, piecewise power law, analytic model for the noise curves for the initial LIGO interferometers, for the advanced LIGO interferometers, and for the LISA interferometer. We express our model in terms of the dimensionless quantity $h_{\text{rms}}(f) \equiv \sqrt{f S_h(f)}$, where $S_h(f)$ is the one sided power spectral density of the interferometer noise [56]. The quantity $h_{\text{rms}}(f)$ is the rms fluctuation in the noise at frequency f in a bandwidth $\Delta f = f$ [1]. Our approximate model for the noise spectrum is

$$h_{\text{rms}}(f) = \begin{cases} \infty & f < f_s, \\ h_m (\alpha f / f_m)^{-3/2} & f_s \leq f < f_m / \alpha \\ h_m & f_m / \alpha \leq f < \alpha f_m \\ h_m [f / (\alpha f_m)]^{3/2} & \alpha f_m < f. \end{cases} \quad (4.1)$$

This noise curve scales like $f^{3/2}$ at high frequencies and like $f^{-3/2}$ at low frequencies, and has a flat portion at intermediate frequencies. The noise curve depends on four

parameters: (i) A lower shutoff frequency f_s below which the interferometer noise rapidly becomes very large and can be approximated to be infinite. For the ground based interferometers, this low-frequency shutoff is due to seismic noise, while for LISA it is due to accelerometer noise (Ref. [7], p. 23). (ii) A frequency f_m , which is the location of the center of the flat portion of the spectrum. (iii) A dimensionless parameter h_m , which is the minimum value of $h_{\text{rms}}(f)$. (iv) A dimensionless parameter α which determines the width in frequency of the flat portion of the noise curve. We approximate the noise curves by piecewise power laws in this way for calculational convenience.

For the initial and advanced LIGO interferometers, we determined best-fit values of the parameters f_s , f_m , h_m and α by fitting to the noise curves given in Ref. [3]. (Note that Fig. 7 of Ref. [3] is a factor of 3 too small from ~ 10 Hz to ~ 70 Hz. This error does not appear in Fig. 10 of that reference [91].) The resulting parameter values are:

$$\left. \begin{aligned} f_s &= 40 \text{ Hz} \\ f_m &= 160 \text{ Hz} \\ \alpha &= 1.4 \\ h_m &= 3.1 \times 10^{-22} \end{aligned} \right\} \begin{array}{l} \text{INITIAL LIGO} \\ \text{INTERFEROMETER,} \end{array} \quad (4.2)$$

and

$$\left. \begin{aligned} f_s &= 10 \text{ Hz} \\ f_m &= 68 \text{ Hz} \\ \alpha &= 1.6 \\ h_m &= 1.4 \times 10^{-23} \end{aligned} \right\} \begin{array}{l} \text{ADVANCED LIGO} \\ \text{INTERFEROMETER.} \end{array} \quad (4.3)$$

For ground-based interferometers, the $f^{-3/2}$ portion of our approximate formula (4.1) is the thermal suspension noise and the $f^{3/2}$ portion models the laser shot noise. The intermediate portion smoothes the transition between these two pieces of the spectrum [94].

For the space-based LISA interferometer, we determined best-fit values of the parameters f_m , h_m and α by fitting to the noise curve given in Ref. [10], and obtained the lower cutoff frequency f_s from Ref. [7]. The resulting parameter values are:

$$\left. \begin{aligned} f_s &= 10^{-4} \text{ Hz} \\ f_m &= 3.7 \times 10^{-3} \text{ Hz} \\ \alpha &= 5.5 \\ h_m &= 5.8 \times 10^{-22} \end{aligned} \right\} \begin{array}{l} \text{LISA} \\ \text{INTERFEROMETER.} \end{array} \quad (4.4)$$

Our piecewise power-law model fits the true noise curve less accurately for LISA than for the LIGO interferometers, but it is still a fairly good approximation.

The sensitivity of LISA at the lower end of its frequency window may be degraded somewhat by a background of gravitational waves from white dwarf binaries [7]. We neglect this issue here as this white dwarf noise level is fairly uncertain.

V. SIGNAL-TO-NOISE RATIOS

In this section we calculate the angle-averaged SNRs for the three different stages of the coalescence (inspiral, merger, and ringdown) for initial LIGO interferometers, for advanced LIGO interferometers, and for LISA. We do so for black hole binaries at various distances and of various masses. These SNR values are obtained by substituting the energy spectra (3.20), (3.14) and (3.25) estimated in Sec. III, together with the interferometer noise curves (4.2), (4.3) and (4.4), into the SNR formula (2.34) derived in Sec. II C. The analytic calculations are carried out in Appendix A; in this section we summarize the results in three graphs (Figs. 4, 5 and 6), and discuss their implications.

We start in subsection V A by graphing the waves' energy spectra and the interferometers' noise spectra for several different examples of black hole binaries, in order to illustrate the factors determining the SNR values. The general results are presented in subsection V B.

A. Specific examples

We start by rewriting the general formula (2.34) for the SNR in a more useful form. If we define the characteristic gravitational-wave amplitude

$$h_{\text{char}}(f)^2 \equiv \frac{2(1+z)^2}{\pi^2 D(z)^2} \frac{dE}{df} [(1+z)f], \quad (5.1)$$

then from Sec. II C it can be seen that the SNR squared for an optimally oriented source is

$$\rho_{\text{optimal orientation}}^2 = \int d(\ln f) \frac{h_{\text{char}}(f)^2}{h_{\text{rms}}(f)^2}, \quad (5.2)$$

where $h_{\text{rms}}(f) = \sqrt{f S_h(f)}$. However, Eq. (2.34) shows that the angle-averaged SNR squared is a factor of 5 smaller than the optimal value (5.2), so we can rewrite Eq. (2.34) as

$$\langle \rho^2 \rangle = \int d(\ln f) \frac{h_{\text{char}}(f)^2}{h_n(f)^2}, \quad (5.3)$$

where $h_n(f) \equiv \sqrt{5} h_{\text{rms}}(f)$. We interpret the quantity h_n as the rms noise appropriate for waves from random directions with random orientations [96]. The usefulness of the quantities $h_{\text{char}}(f)$ and $h_n(f)$ is that plotting $h_{\text{char}}(f)$ and $h_n(f)$ for various sources illustrates [from Eq. (5.3)] the possible SNR values and the distribution of SNR squared with frequency (see, *e.g.*, Ref. [1]).

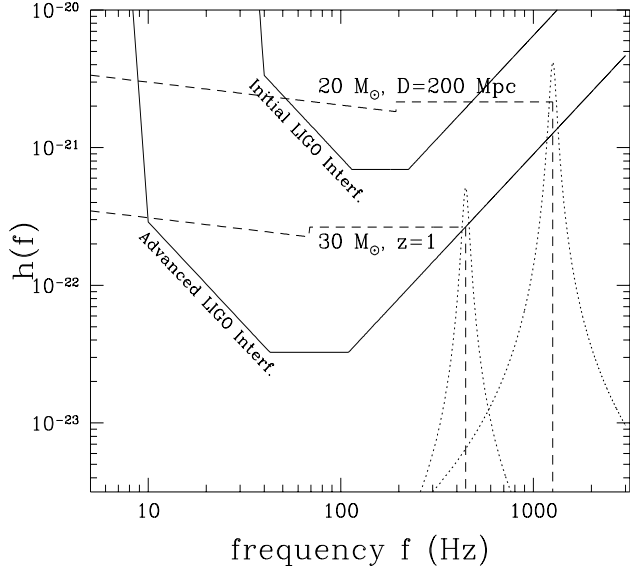


FIG. 1. An illustration of the relative magnitudes of our estimates of the *inspiral*, *merger* and *ringdown* energy spectra in two different cases. The solid lines are the rms noise amplitudes $h_n(f) \equiv \sqrt{5fS_h(f)}$ for our assumed model (4.1) of the LIGO initial and advanced interferometer noise spectra. The dashed and dotted lines show the characteristic amplitude $h_{\text{char}}(f) \propto \sqrt{dE/df}$ of the waves, defined by Eq. (5.1). The definition of h_{char} is such that the signal-to-noise ratio squared for a randomly oriented source is given by $(S/N)^2 = \int d(\ln f) [h_{\text{char}}(f)/h_n(f)]^2$. The upper dashed and dotted lines correspond to a binary of two $10M_\odot$ black holes, coalescing at a distance of $D = 200$ Mpc. The sloped portion of the dashed line is the inspiral part of the energy spectrum, which gives an SNR for the initial (advanced) interferometer noise curve of 2.6 (84). The flat portion is our crude model of the merger part of the energy spectrum, which gives an SNR of 2.1 (16). The dotted line is our estimate of the energy spectrum from the ringdown, which gives an SNR of 0.1 (0.86). An event rate of very roughly 3 yr^{-1} is expected for mergers inside this distance [17,18]. The lower dashed and dotted lines correspond to a binary of two $15M_\odot$ black holes at a redshift of $z = 1$ (or at a luminosity distance of $D = 4.6$ Gpc; the cosmological parameters $\Omega_0 = 1$ and $H_0 = 75 \text{ km s}^{-1} \text{ Mpc}^{-1}$ were assumed). In this case the inspiral, merger and ringdown SNR values for the initial (advanced) interferometers are 0.08, 0.42, and 0.07 (6.6, 7.2 and 0.5) respectively. Black hole binaries with constituents this massive will be visible to great distances, making them a possible important source, depending on the very uncertain event rate. The signal-to-noise ratio from the merger phase is enhanced for these massive distant sources, in part because the combination of cosmological redshift plus lower intrinsic frequency (due to higher mass) brings the merger part of the energy spectrum down to lower frequencies at which the interferometer noise is smaller.

In Fig. 1, we show the rms noise amplitude $h_n(f)$ for

our model (4.1) of the initial and advanced LIGO interferometer noise curves, together with the characteristic amplitude $h_{\text{char}}(f)$ for two different examples of BBH coalescences, namely a coalescence of total mass $20 M_\odot$ at a distance of $D = 200$ Mpc, and a $30 M_\odot$ coalescence at a redshift of $z = 1$. (We assume that the cosmological parameters are $\Omega_0 = 1$ and $H_0 = 75 \text{ km s}^{-1} \text{ Mpc}^{-1}$.) In each case, the sloped portion of the dashed h_{char} line is the inspiral signal, the flat portion is our crude model of the merger, and the separate dotted portion is the ringdown. Note that the ringdown and merger overlap in the frequency domain since (as we have defined them) they are disjoint in the time domain. By contrast, the inspiral and merger are approximately disjoint in both the frequency and time domains, since the adiabatic approximation is just breaking down at the end of the inspiral [73].

Notice that in both cases, $20 M_\odot$ and $30 M_\odot$, the waves' characteristic amplitude $h_{\text{char}}(f)$ is rather larger than $h_n(f)$ for most of the merger spectrum for the advanced interferometers, indicating the detectability of the merger waveform when optimal filtering can be used. In particular, note that the waves should be quite visible to the advanced interferometers for the $30 M_\odot$ binary even though it is at a cosmological distance. Even if such binaries are rare, they are visible to such great distances that measurements can be made of a huge volume of the Universe, making them a potentially very important and interesting source. Cosmological binaries have an enhanced SNR in part because the cosmological redshift moves their frequency spectrum down closer to LIGO's optimal band; this redshift enhancement effect can sometimes be so strong that for two identical mergers at different distances, the more distant merger can have the larger SNR.

Figure 1 also shows that, of these two example BBH coalescences, only the nearby one at a distance of $D = 200$ Mpc would be detectable by the initial interferometers. Such coalescences may yield an interesting event rate for the initial interferometers—as discussed in the Introduction, a coalescence rate of very roughly 3 yr^{-1} is expected for BBH coalescences in this mass range ($M \lesssim 30M_\odot$) inside 200 Mpc [17,18], although there is considerable uncertainty in this estimate.

A qualitatively different, possibly important type of source for the initial LIGO interferometers (and also for the advanced interferometers) is the coalescence of black hole binaries with masses of order $M \sim 100 M_\odot$, as we have discussed in the Introduction. (We call such binaries intermediate mass BBHs, as distinct from solar mass or supermassive binaries.) In Fig. 2 we show the characteristic amplitude $h_{\text{char}}(f)$ for a hypothetical BBH coalescence of total mass $100 M_\odot$ at a redshift of $z = 0.5$, corresponding to a luminosity distance of $D = 2.2$ Gpc. Note in particular that the initial LIGO interferometer noise curve has best sensitivity at ~ 200 Hz just where the (redshifted) ringdown frequency is located. We discuss further in Sec. VI the range and possible detection

rates for the initial LIGO interferometers for this type of source.

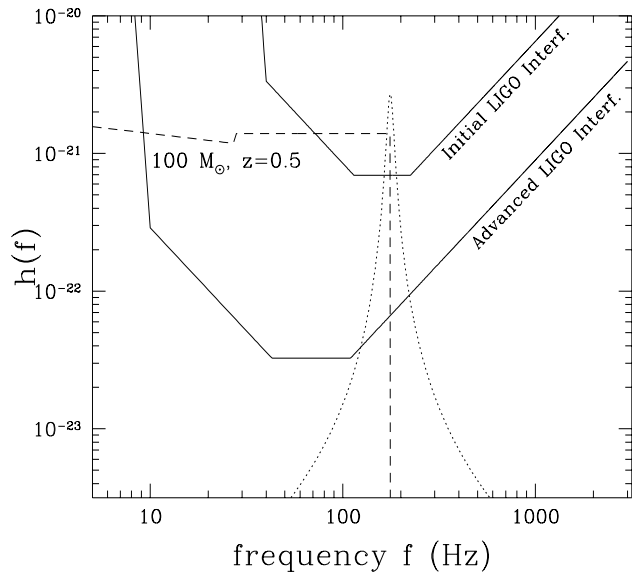


FIG. 2. A merger of a binary consisting of two $50 M_{\odot}$ black holes at a redshift of $z = 0.5$, together with the rms noise amplitudes $h_n(f)$ for both the initial and advanced interferometer noise curves for LIGO (see caption of Fig. 1). The signal to noise ratios for the inspiral, merger, and ringdown stages are about 0, 1.7 and 1.0 respectively for the initial interferometer noise level, and about 11, 52 and 11 respectively for advanced interferometers.

Turn, now, to the detection of supermassive BBH signals by the possible future space-based detector LISA [5,6]. LISA can study BBH mergers with far higher accuracy and resolution than the ground based interferometers, because the SNR values are typically much higher ($\gtrsim 10^3$). Our calculation of the inspiral SNR values for LISA differs from the other SNR calculations in the following way. In the frequency integral of Eq. (2.34), if one were to integrate over the whole frequency domain allowed by the noise curve (as is done for the LIGO initial and advanced interferometers), one would in some cases obtain the SNR for a measurement which lasts several hundred years, which is unrealistic. Thus, it is necessary when calculating inspiral SNRs for LISA to restrict the integral over frequency in Eq. (2.34) to the domain that corresponds to, say, one year of observation; see Appendix A.

Figure 3 shows our approximate model [Eqs. (4.1) and (4.4)] of LISA's projected noise spectrum, together with the gravitational-wave amplitude $h_{\text{char}}(f)$ for the inspiral, merger and ringdown stages of two different BBH coalescences: a BBH of total mass $10^6 M_{\odot}$ at a redshift of $z = 5$, and a BBH of total mass $5 \times 10^4 M_{\odot}$ at a redshift of $z = 1$. The $10^6 M_{\odot}$ BBH enters the LISA waveband at $f = f_s \simeq 10^{-4}$ Hz roughly one week before the final

merger. The SNRs obtained in this case from the inspiral, merger and ringdown signals are approximately 1800, 4600 and 1700 respectively. The $5 \times 10^4 M_{\odot}$ BBH enters the LISA waveband about twenty years before the final merger. The SNR obtained from the last year of the inspiral signal, from $f \simeq 1.6 \times 10^{-4}$ Hz to $f \simeq 4 \times 10^{-2}$ Hz is approximately 900, while the merger and ringdown SNRs are about 70 and 4 respectively.

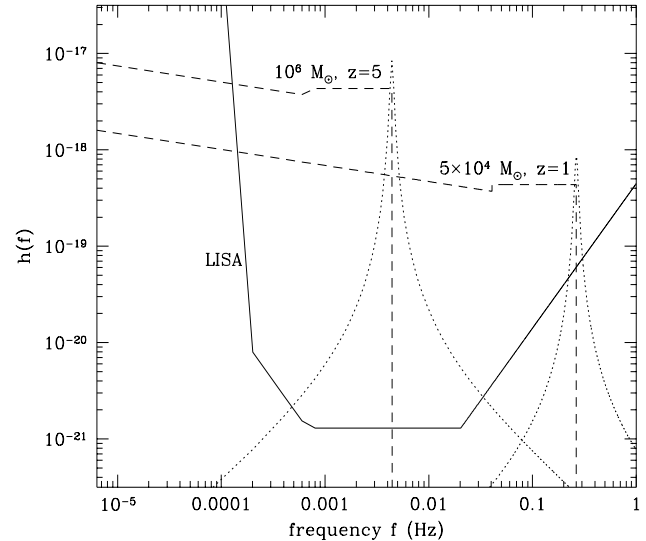


FIG. 3. The noise spectrum $h_n(f)$ of the possible future space-based detector LISA (Laser Interferometer Space Antenna), together with the characteristic amplitude h_{char} for the various stages of two different equal-mass binary black hole coalescences (see caption of Fig. 1). The first coalescence is that of a binary of total mass $10^6 M_{\odot}$ at a redshift of $z = 5$. The inspiral signal of this binary enters the LISA waveband at $f \simeq 10^{-4}$ Hz about one week before the final merger, and the signal-to-noise ratios from the inspiral, merger and ringdown are about 1800, 4600 and 1700 respectively. The second coalescence is that of a binary of total mass $5 \times 10^4 M_{\odot}$ at a redshift of $z = 1$, which enters the LISA waveband about twenty years before the final merger. In this case a signal-to-noise ratio of approximately 900 would be obtained for the last year of inspiral (from $f \simeq 1.6 \times 10^{-4}$ Hz to $f \simeq 4 \times 10^{-2}$ Hz). The signal-to-noise ratios from the merger and ringdown in this case would be about 70 and 4.

B. The general signal-to-noise ratio results

We now turn from these specific examples to the dependence of the SNR values on the mass of and distance to the binary in general. In Appendix A we obtain analytic formulae for the SNR values for the three phases of BBH coalescences, and for the various interferometers. In this section we plot the results for equal-mass BBHs, which are shown in Figs. 4, 5 and 6. The in-

spiral and merger curves in these figures (except for the LISA inspiral curves; see Appendix A) are obtained from Eqs. (A4) and (A10) of Appendix A, while the ringdown curves are obtained by numerically integrating Eq. (3.24) in Eq. (2.34).

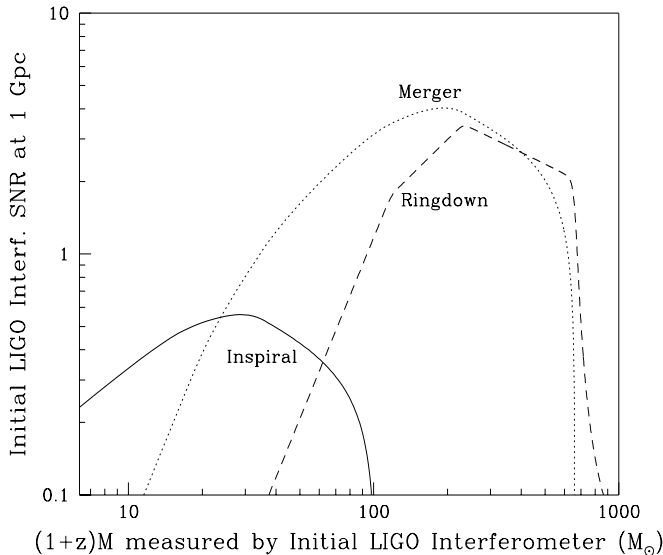


FIG. 4. The signal to noise ratio (SNR) for equal-mass black hole-black hole coalescences detected by LIGO initial interferometers, assuming Wiener optimal filtering, as a function of the redshifted mass $(1+z)M$ of the final black hole, at a luminosity distance of 1 Gpc. For fixed redshifted mass, the SNR values are inversely proportional to luminosity distance. The solid, dotted, and dashed curves are the SNR values from the inspiral, merger and ringdown portions of the signal respectively. For non equal-mass binaries, the inspiral SNRs will be reduced by the factor $\sim \sqrt{4\mu/M}$, while the merger and ringdown SNRs will be reduced by $\sim 4\mu/M$; thus the inspiral signal will be enhanced relative to the merger and ringdown signals. This plot indicates that it is possible that an important source for the initial LIGO interferometers may be the coalescences of binary black holes where the black holes have masses in the range of several hundred solar masses, which would be visible out to almost 1 Gpc. For such sources, the inspiral portion of the signal would not be detectable, and the waves would have to be detected using either the ringdown or merger portions.

The SNR values for the initial LIGO interferometers are shown in Fig. 4. This figure shows that it is possible that an important source for the initial LIGO interferometers may be the coalescences of binary black holes where the black holes have masses in the range of several hundred solar masses, which would be visible out to almost 1 Gpc. For such sources, the inspiral portion of the signal would not be detectable, and one would need to search for the ringdown or merger portions of the signal in order to detect the waves. See Sec. VI for further dis-

cussion. The event rate for such high mass BBHs is very uncertain; see Ref. [24] for a possible formation scenario.

Intermediate mass BBHs with $\mu \ll M$ (e.g., $m_1 \sim 10 M_\odot$, $m_2 \sim 500 M_\odot$) are presumably much more common in the Universe than the intermediate mass BBHs with $\mu \sim M$ discussed above. The SNRs for such mixed binaries will be much lower, however. As seen in Appendix A, the merger and ringdown SNR's scale as $(\mu/M)^2$, while the inspiral ringdown scales as μ/M . The difference in scaling occurs because the duration of the merger and ringdown signals are approximately independent of μ , but the duration of the inspiral signal scales as $1/\mu$.

For BBH coalescences of total mass less than or of order $20 M_\odot$, the results of Fig. 4 can be summarized by the following approximate formulae for the initial LIGO interferometers [c.f. Eqs. (A4), (A10), and (A16) of Appendix A]:

$$\begin{aligned} \left(\frac{S}{N}\right)_{\text{inspiral}} &\sim 2.8 \left(\frac{200 \text{ Mpc}}{D(z)}\right) \left(\frac{(1+z)M}{18 M_\odot}\right)^{5/6} \\ \left(\frac{S}{N}\right)_{\text{merger}} &\sim 1.5 \left(\frac{\epsilon_m}{0.1}\right)^{1/2} \left(\frac{200 \text{ Mpc}}{D(z)}\right) \left(\frac{(1+z)M}{18 M_\odot}\right)^{5/2} \\ \left(\frac{S}{N}\right)_{\text{ringdown}} &\sim 0.1 \left(\frac{\epsilon_r}{0.03}\right)^{1/2} \left(\frac{200 \text{ Mpc}}{D(z)}\right) \left(\frac{(1+z)M}{18 M_\odot}\right)^{5/2}, \end{aligned} \quad (5.4)$$

where ϵ_m is the fraction of the total mass-energy radiated in the merger signal and ϵ_r is the corresponding fraction for the ringdown signal.

Figure 4 also shows that the inspiral signals from low mass BBH mergers with $M \lesssim 30 M_\odot$ should be visible to ~ 200 Mpc (the SNR detection threshold is ~ 5 [40]). The ground-based interferometers will, over a period of years, gradually be improved from the initial sensitivity levels to the advanced sensitivity levels [3]. Roughly half way between the initial and advanced interferometers, the range of the detector system for $M \lesssim 30 M_\odot$ BBHs will be ~ 1 Gpc. As explained in the Introduction, it is thought to be plausible that most BBH progenitor systems do not disrupt during the stellar collapses that produce the black holes, so that their coalescence rate could be about the same as the birth rate for their progenitors, about 1/100,000 years in our Galaxy, or several per year within a distance of 200 Mpc [17,18,19,20,21]. If this is the case, BBHs should be detected early in the gradual process of interferometer improvement.

It is also conceivable that BBHs could be seen closer than 200 Mpc. High mass stars may have been much more numerous among population III stars due to the lower metallicity at high redshift, so there could be a large population of BBHs that are remnants of population III stars living in galactic halos. Galactic nuclei could also produce a larger population of BBHs than normal stellar evolution in non-nuclear regions [24]. Either

of these scenarios could increase event detection rate and hasten the first detections of BBHs.

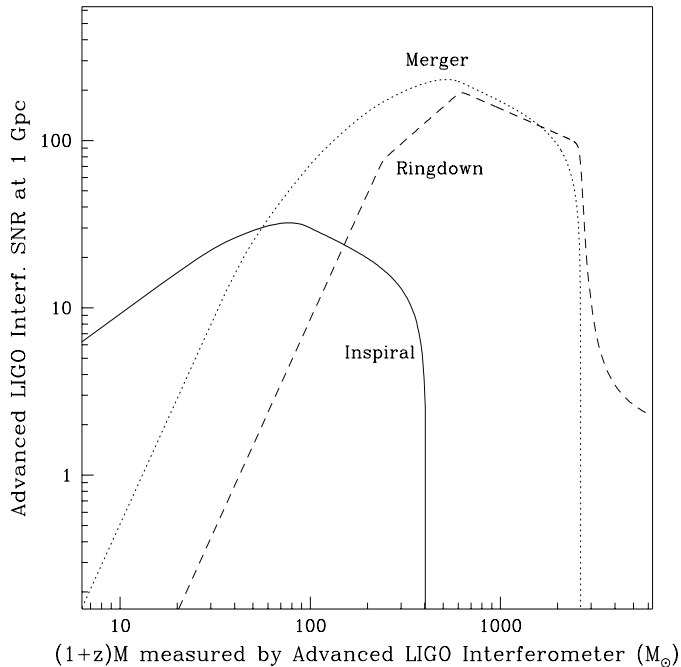


FIG. 5. The SNR values for advanced LIGO interferometers for the inspiral (solid line), merger (dotted line) and ringdown (dashed line) phases of equal-mass BBH coalescences; see caption of Fig. 4. For fixed redshifted mass, the SNR values are inversely proportional to luminosity distance. For values of the redshifted final mass lower than $\sim 60 M_\odot$ the inspiral SNR is largest, while for larger BBH systems the merger and/or ringdown portions of the signal dominate.

Figure 5 shows the SNR values for the advanced LIGO interferometers. For BBH coalescences of total mass less than or on the order of a few tens of solar masses, the results in Fig. 5 can be summarized by the following approximate formulae for the advanced LIGO interferometers [c.f. Eqs. (A4), (A10) and (A16) of Appendix A]:

$$\begin{aligned}
 \left(\frac{S}{N}\right)_{\text{inspiral}} &\sim 27 \left(\frac{1 \text{ Gpc}}{D(z)}\right) \left(\frac{(1+z)M}{37 M_\odot}\right)^{5/6} \\
 \left(\frac{S}{N}\right)_{\text{merger}} &\sim 13 \left(\frac{\epsilon_m}{0.1}\right)^{1/2} \left(\frac{1 \text{ Gpc}}{D(z)}\right) \left(\frac{(1+z)M}{37 M_\odot}\right)^{5/2} \\
 \left(\frac{S}{N}\right)_{\text{ringdown}} &\sim 0.7 \left(\frac{\epsilon_r}{0.03}\right)^{1/2} \left(\frac{1 \text{ Gpc}}{D(z)}\right) \left(\frac{(1+z)M}{37 M_\odot}\right)^{5/2}.
 \end{aligned} \tag{5.5}$$

Our estimate (5.5) for the ringdown SNR is roughly consistent with previous estimates by Finn [16].

From Fig. 5 it can be seen that for advanced LIGO interferometers, equal-mass BBH inspirals will be visible out to $z \sim 1/2$ for the entire range of masses

$10M_\odot \lesssim (1+z)M \lesssim 300M_\odot$. Thus, there is likely to be an interesting event rate. Indeed, the SNRs will be high enough even for rather large distances that it should be possible to extract each binary's parameters with reasonable accuracy [10]. By contrast, the ringdown SNR is fairly small except for the largest mass systems. For very massive binaries or binaries that are closer than 1 Gpc, advanced interferometers may measure some fairly good ringdown SNRs, which would allow fairly good estimates of the mass and spin of the final black hole [15,16].

Figure 6 shows the SNR values obtainable from the three phases of BBH coalescences by LISA: the last year of inspiral, the merger and the ringdown. We also show the SNR value obtainable from one year of integration of the inspiral signal one hundred years before the merger, and a similar curve for one thousand years before the merger. This figure shows that LISA will be able to perform very high accuracy measurements of BBH mergers (SNR values $\gtrsim 10^3$) essentially throughout the observable Universe ($z \lesssim 10$) in the mass range $10^6 M_\odot \lesssim M \lesssim 10^9 M_\odot$. As discussed in the Introduction, there is likely to be an interesting event detection rate. The SNR curves in Fig. 6 for measurements one hundred and one thousand years before merger show that many inspiraling BBHs that are far from merger should be detectable by LISA as well. If the merger rate of SMBH binaries turns out to be about one per year throughout the observable Universe, then at any given time one would expect roughly one thousand SMBH binaries to be a thousand years or less away from merger. LISA will be able to monitor the inspiral of such binaries (if they are of sufficiently low mass) with moderate to large SNR [10].

Finally, it should be noted that the relative magnitude of the merger and ringdown SNR values is somewhat uncertain. As we have discussed in Sec. III, we have assumed a total radiated energy of $0.1M$ in the merger portion of the signal, and $0.03M$ in the ringdown portion, a ratio of 3 : 1. In reality, it may turn out that in individual cases the ratio is as high as 10 or as low as $\lesssim 1$. It may even turn out to be the case that for most coalescences, the ringdown portion of the waveform carries most of the radiated energy of the combined merger/ringdown regime (depending possibly on the distribution of initial spins). Thus, the SNR values shown in Figs. 4, 5 and 6 should merely be taken as illustrative.

We now turn to a discussion of the implications of the above signal-to-noise ratios for the required search strategies for the various types of signals, and for the distances to which these types of signals can be detected.

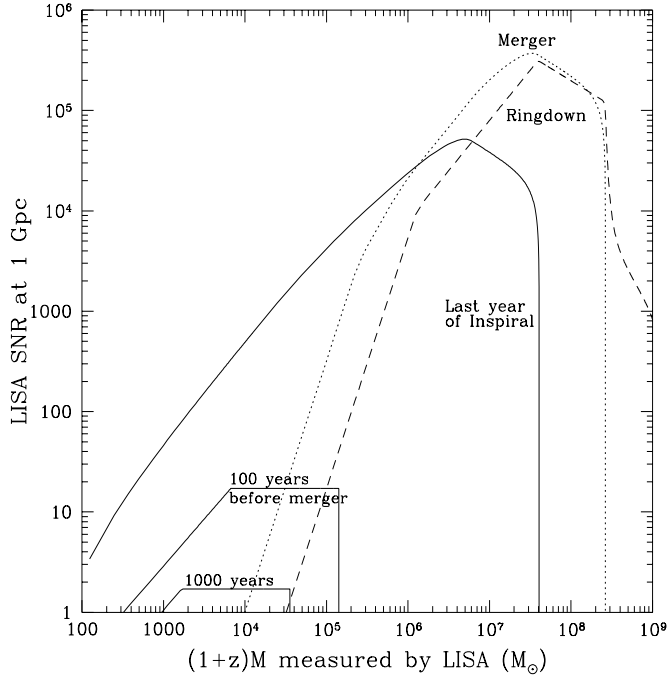


FIG. 6. The signal to noise ratio (SNR) for equal-mass black hole-black hole coalescences detected by LISA, assuming Wiener optimal filtering, as a function of the redshifted mass $(1+z)M$ of the final black hole, at a luminosity distance of 1 Gpc. For fixed redshifted mass, the SNR values are inversely proportional to luminosity distance. The dotted and dashed curves are the SNR values from the merger and ringdown portions of the signal, respectively. The upper solid curve is the SNR value that would be obtained from measuring the last year of the inspiral signal. For values of the redshifted final mass lower than about $10^6 M_\odot$, the last-year-inspiral SNR is largest, while for larger BBH systems the merger and/or ringdown portions of the signal dominate. Also shown (lower solid curves) are the SNRs that would be obtained from one year of integration of the inspiral signal at one hundred and one thousand years before the final merger. If the rate of SMBH coalescences within $z \lesssim$ (a few) is roughly one per year, then one would expect roughly one thousand SMBH binaries to be a thousand years or less away from merger. This plot shows that LISA will be able to measure the inspiral of such binaries (provided they are of sufficiently low mass) with moderate to large SNR [10].

VI. IMPLICATIONS FOR DETECTABILITY OF THE GRAVITATIONAL-WAVE SIGNAL

One of the reasons that coalescences of compact objects are such good sources for gravitational-wave detectors is that the inspiral portion of the signal is very predictable, so that optimal filtering may be used in searching for the waves [1]. As we have discussed, optimal filtering enhances the achievable SNR values by a factor of roughly $\sqrt{\mathcal{N}_{\text{cyc}}}$, where \mathcal{N}_{cyc} is the number of cycles

in the waveform in the frequency band of the detectors. For neutron star-neutron star (NS-NS) coalescences, \mathcal{N}_{cyc} will be on the order of several thousand, while for BBH coalescences it will be on the order of several hundred [40]. Thus, for NS-NS coalescences, and also for BBH coalescences with total mass a few tens of solar masses or less, the inspiral portion of the gravitational-wave signal will be used to *detect* the entire waveform. In these cases, it is not necessary to *search* for the merger and ringdown portions of the waveform, since it will be known roughly where in the interferometer data stream they are expected to lie. However, there is no guarantee in these cases that the merger and ringdown portions will be visible in the noisy data stream. A key issue is how visible these portions are and how much information can be extracted from them. We discuss this issue in detail in paper II [36].

For larger mass black hole systems, however, our signal to noise ratio calculations show that the merger and ringdown SNR values can be larger than the inspiral SNR values. For equal-mass BBHs, this will occur whenever $(1+z)M \gtrsim 30M_\odot$ for the initial LIGO interferometers, and whenever $(1+z)M \gtrsim 60M_\odot$ for the advanced LIGO interferometers. Moreover, the inspiral SNR completely shuts off for large enough $(1+z)M$, as can be seen from Figs. 4 and 5. The reason for this shutoff is that at large enough values of $(1+z)M$, the entire inspiral energy spectrum lies at frequencies below the “seismic wall” shutoff in the interferometer noise curve. The mass cutoff occurs at $(1+z)M \sim 100M_\odot$ for the initial interferometers, and at $(1+z)M \sim 400M_\odot$ for the advanced interferometers. Admittedly, BBH binaries of total mass $\gg 20M_\odot$ may well be very much more rare than BBH binaries of $\sim 20M_\odot$; however, they will be visible to such great distances that there may be an interesting event rate. Moreover, for the initial LIGO interferometers, the mass scale $\sim 30M_\odot$ at which the inspiral SNR becomes much smaller than the merger/ringdown SNRs is not terribly high.

In such high mass cases for which the merger and inspiral SNRs exceed the inspiral SNR, it will be necessary to perform a search for the merger and/or ringdown portions of the signal, independently of any searches for inspiral signals, in order that all possible events be detected. If one seeks to detect the waves merely by optimal filtering for the inspiral waveform, some fraction of the events will be missed which otherwise might have been detectable. In fact, it may very well turn out that merger signals from BBH coalescences could be the dominant source for the initial LIGO interferometers.

Therefore a search in real time should be performed in the data stream for ringdown and merger signals from high mass, BBH mergers. One might imagine that the gravitational waves would generally be easier to detect by searching for the merger signal, since we have estimated that the SNR values for the merger phase are typically a factor of a few larger than those for the ringdown (*cf.* Figs. 4 and 5). There are several factors that com-

licate this conclusion, however. On the one hand, the ringdown's waveform shape is better understood, which makes it easier to produce search templates and hence easier to detect the signal. On the other hand, the ratio between the merger and ringdown SNRs is really quite uncertain, as discussed in Sec. VB, and so it is plausible that the merger SNR will be larger than we have indicated relative to the ringdown SNR. In any case, the ratio between merger and ringdown SNRs will presumably vary a lot from event to event. Thus, it would seem that searches will be necessary for *both* types of signal in the data stream, at least for the mass range in which the ringdown SNR is expected to exceed the inspiral SNR. [From Sec. V we estimate this mass range to be $(1+z)M \gtrsim 200 M_\odot$ for the advanced interferometers, and $(1+z)M \gtrsim 60 M_\odot$ for the initial interferometers.]

We summarize the discussion of this section by displaying the optimum search strategies for various mass ranges for the three different interferometers. In each case below, the mass range marked merger refers to matched filtering searches for merger signals. If merger templates are available, then in the indicated mass ranges merger searches will probably be more successful than inspiral or ringdown searches; the question mark is a reminder that templates for the merger may not be available, and that consequently such searches might not be possible.

$$\left. \begin{array}{l} \text{INSPIRAL} \quad : 1M_\odot \lesssim M \lesssim 60M_\odot \\ \text{RINGDOWN} \quad : 60M_\odot \lesssim M \lesssim 1000M_\odot \\ \text{MERGER (?) } \quad : 30M_\odot \lesssim M \lesssim 1000M_\odot \end{array} \right\} \begin{array}{l} \text{LIGO} \\ \text{INITIAL} \\ \text{INTERF.} \end{array} \quad (6.1)$$

$$\left. \begin{array}{l} \text{INSPIRAL} \quad : 1M_\odot \lesssim M \lesssim 200M_\odot \\ \text{RINGDOWN} \quad : 200M_\odot \lesssim M \lesssim 3000M_\odot \\ \text{MERGER (?) } \quad : 80M_\odot \lesssim M \lesssim 3000M_\odot \end{array} \right\} \begin{array}{l} \text{LIGO} \\ \text{ADVANCED} \\ \text{INTERF.} \end{array} \quad (6.2)$$

$$\left. \begin{array}{l} \text{INSPIRAL} \quad : 10^3M_\odot \lesssim M \lesssim 10^7M_\odot \\ \text{RINGDOWN} \quad : 10^7M_\odot \lesssim M \lesssim 10^9M_\odot \\ \text{MERGER (?) } \quad : 2 \times 10^6M_\odot \lesssim M \lesssim 10^9M_\odot \end{array} \right\} \begin{array}{l} \text{LISA} \\ \text{INTERF.} \end{array} \quad (6.3)$$

A. The detectability of high mass black-hole coalescences via the ringdown signal

Consider first the search for ringdown signals. In this case, since the shape of the signal is known up to several unknown parameters, it will be feasible to implement a search based on the method of matched filters, analogous to what is being planned for detecting mergers of NS-NS and low mass NS-BH and BBH binaries using the inspiral waveform [40,44,86,97]. In other words, a bank of templates of the form (3.21), for different values of the

ringdown frequency and damping time, can be integrated against the (suitably pre-filtered) interferometer output. This will be feasible for both the initial and advanced LIGO interferometers, and also for LISA.

The number $\mathcal{N}_{\text{templates}}$ of required templates [57] can be estimated by combining the formalism developed by Owen [86] and the results of Echeverria and Finn on the expected accuracy of measurement of the ringdown frequency and damping time [15,16]. Using Eqs. (4.15) of Ref. [16] and Eqs. (2.23) and (2.28) of Ref. [86] we find that the metric defined by Owen on the space of parameters is given by [98]

$$ds^2 = \frac{1}{8Q^2} dQ^2 + \frac{Q^2}{2f_{\text{qnr}}^2} df_{\text{qnr}}^2, \quad (6.4)$$

where Q is the quality factor. The formula (6.4) for the Owen metric is valid only in the high Q limit; it has corrections of order $1/Q^2$. Moreover, the formula is also only valid when the noise spectrum $S_h(f)$ does not vary significantly within the resonance bandwidth $\Delta f \sim f_{\text{qnr}}/Q$. Therefore estimates obtained from Eq. (6.4) for the number of template shapes required for ringdown searches will only be accurate to within factors of a few, but this is adequate for our purposes.

Using Eq. (2.16) of Ref. [86] we find that the number of required templates is approximately

$$\mathcal{N}_{\text{templates}} \approx \frac{1}{8} Q_{\text{max}} (1 - MM)^{-1} \ln \left[\frac{M_{\text{max}}}{M_{\text{min}}} \right], \quad (6.5)$$

where Q_{max} , M_{min} and M_{max} are the extremal values of the quality factor and of the black hole mass that define the range of signal searches. The quantity MM in the formula (6.5) is the *minimal match* parameter introduced by Owen; its meaning is that the event detection rate obtainable by a lattice of templates that have a certain minimal match MM is smaller than the ideal event detection rate (obtainable from an infinitely dense lattice of templates) by the factor $(MM)^3$ [86]. We assume $MM = 0.97$ as in Ref. [86], which corresponds to a 10% loss in event rate due to the coarse gridding of the template space, and take $Q_{\text{max}} = 100$ [which by Eq. (3.23) corresponds to $1-a \simeq 10^{-4}$]. For the initial and advanced LIGO interferometers, the mass range to be searched corresponds to roughly $M_{\text{min}} \simeq 1M_\odot$ and $M_{\text{max}} = 5000M_\odot$; this yields from Eq. (6.5)

$$\mathcal{N}_{\text{templates}} \lesssim 4000. \quad (6.6)$$

This is a rather small number of template shapes compared to the number expected to be necessary for inspiral searches [86], and therefore the ringdown search should be fairly easy to implement. A similarly small number of required template shapes ($\mathcal{N}_{\text{templates}} \lesssim 6000$) is obtained for LISA assuming $M_{\text{min}} \sim 10^3 M_\odot$ and $M_{\text{max}} \sim 10^9 M_\odot$.

We next discuss the distance to which BBH mergers should be detectable via their ringdown signals. As explained in Sec. II B, a rough estimate of the appropriate

signal-to-noise ratio threshold for detection using one interferometer is [99]

$$\rho_{\text{threshold}} \sim \sqrt{2 \ln[\mathcal{N}_{\text{templates}} T / (\epsilon \Delta t)]} \quad (6.7)$$

where T is the observation time, Δt is the sampling time and $\epsilon = 10^{-3}$ is as defined in Section II B. In fact coinciding between the 4 different interferometers in the LIGO/VIRGO network will be carried out, in order to increase detection reliability and combat non-Gaussian noise (see Sec. II A). If the noise were exactly Gaussian, the appropriate detection criterion would be to demand that

$$\sum_j \rho_j^2 \geq \rho_{\text{threshold}}^2, \quad (6.8)$$

where the sum is over the different SNRs obtained in each interferometer. In order to combat non-Gaussian noise, the detection criterion will be modified to require approximately equal SNRs in each interferometer:

$$\rho_j \geq \rho_{\text{threshold}} / \sqrt{2} \text{ for all } j. \quad (6.9)$$

We have chosen a factor of $\sqrt{2}$ here to be conservative; it corresponds to combining the outputs of just two interferometers (say, the two LIGO 4km interferometers) instead of four interferometers.

Taking $T = 10^7$ s and $\Delta t = 1$ ms yields the estimate $\rho_{\text{threshold}} / \sqrt{2} \approx 6.0$ for the initial and advanced LIGO interferometers. Therefore, from Fig. 4, we see that the initial LIGO interferometers should be able to see ringdowns from equal-mass BBHs in the mass range $100 M_{\odot} \lesssim M \lesssim 700 M_{\odot}$ out to ~ 200 Mpc, if the radiation efficiency ϵ_r is as large as we have estimated. The advanced LIGO interferometers, by contrast, should see ringdowns in the mass range $200 M_{\odot} \lesssim (1+z)M \lesssim 3000 M_{\odot}$ out to $z \sim 1$ (from Fig. 5). For non equal-mass BBHs, these distances are reduced by the factor $\sim (4\mu/M)$.

For LISA, the detection threshold is given by Eq. (6.7). Although LISA does incorporate several partially independent interferometers, we have used the noise spectrum (4.4) which is the effective noise spectrum that applies to the LISA detector as a whole [7]. Thus it is consistent to treat LISA as one interferometer. Taking $T = 10^7$ s and $\Delta t = 1$ s, and using the value $\mathcal{N}_{\text{shapes}} = 6000$ estimated above yields $\rho_{\text{threshold}} \approx 7.5$. Hence, from Fig. 6, LISA should see ringdowns in the mass range $10^6 M_{\odot} \lesssim (1+z)M \lesssim 3 \times 10^8 M_{\odot}$ out to $z \gtrsim 100$.

B. The detectability of high mass black hole coalescences via the merger signal

We next discuss the feasibility of searches for the merger signal. As we have explained, this will be most necessary when the merger SNR is larger than both the inspiral and ringdown SNRs by factors of a few (since the

fractional loss in event detection rate, if searches for the merger signal are not carried out, is the cube of the ratio of the SNR values).

Consider first the ideal situation in which theoretical template waveforms are available, so that matched filtering can be used in searches. From Figs. 4 and 5 it can be seen that the merger SNR values are larger than the inspiral/ringdown values by a factor of up to ~ 4 , in the mass ranges $30 M_{\odot} \lesssim M \lesssim 200 M_{\odot}$ for initial LIGO interferometers and $100 M_{\odot} \lesssim M \lesssim 400 M_{\odot}$ for advanced LIGO interferometers. More precisely, in this mass range,

$$\frac{\left(\frac{S}{N}\right)_{\text{merger}}}{\max\left[\left(\frac{S}{N}\right)_{\text{inspiral}}, \left(\frac{S}{N}\right)_{\text{ringdown}}\right]} \lesssim 4 \left(\frac{\epsilon_m}{0.1}\right)^{1/2} \left(\frac{\epsilon_r}{0.03}\right)^{-1/2}. \quad (6.10)$$

The detection threshold for merger searches should be approximately the same as that for inspiral and merger searches, if the number of template shapes $\mathcal{N}_{\text{shapes}}$ is not too large (see further discussion below). Therefore, the gain in event rate over inspiral/ringdown searches, due to searching for merger waves, should vary between 1 and about $4^3 = 64$, depending on the mass of the system, if our estimates of ϵ_m and ϵ_r are approximately correct. Clearly, the large possible gain in event rate shows the importance of searching for merger waves [100]. Moreover, the ratio of ϵ_m/ϵ_r of energies radiated in the merger and ringdown stages, which we have estimated to be roughly 3, is quite uncertain; we think that in some cases it could be rather larger than this (notwithstanding the fact that there has been at least one wagered bottle of wine in the community that $\epsilon_m/\epsilon_r \lesssim 1$ generically [101]). In such cases the benefit of searching for the merger waves would be even greater.

It is not clear, however, how feasible it will be to produce a set of numerically generated templates that is complete enough to be used to successfully implement an optimal filtering search. There may be a very large number of distinct waveform shapes, each of which will require extensive numerical computations. If both black holes are spinning rapidly, the waveforms could depend in significant and nontrivial ways on 6 distinct angular parameters, suggesting that the number of distinct shapes could be very large.

Turn next to the situation where templates are unavailable. Consider first band-pass filtering searches. From the estimate $\sqrt{\mathcal{N}_{\text{bins}}} = 4$ of Sec. III E, combined with Eq. (2.14), we obtain the relation

$$\left(\frac{S}{N}\right)_{\text{merger, band-pass search}} \simeq \frac{1}{4} \left(\frac{S}{N}\right)_{\text{merger, optimal}}. \quad (6.11)$$

Therefore, from Eq. (6.10) it is apparent that the maximum achievable band-pass filtering SNR for the merger is likely to be essentially no larger than the SNRs obtained from the inspiral/ringdown signals.

However, as explained in Secs. ID and IIB, noise monitoring searches will be more efficient than band-pass filtering searches, and will be almost as efficient as matched filtering searches in most cases, when searching for merger waves. [For the inspiral waves, by contrast, noise-monitoring searches perform considerably worse than matched filtering searches, since the parameter $\mathcal{N}_{\text{bins}}$ is much larger for inspiral waves ($\gtrsim 1000$) than it is for merger waves ($\lesssim 60$)]. The event-detection rate from noise-monitoring is a factor

$$\mathcal{R} = \left(\frac{\rho_*}{\rho_{\text{threshold}}} \right)^3 \quad (6.12)$$

lower than the event rate from matched filtering. Here ρ_* is the noise-monitoring detection threshold, given by Eqs. (2.30) and (2.31) as a function of the parameters ϵ , $\mathcal{N}_{\text{start-times}}$ and $\mathcal{N}_{\text{bins}}$, and $\rho_{\text{threshold}}$ is the matched filtering threshold, given by Eq. (2.15) as a function of the parameters $\mathcal{N}_{\text{shapes}}$ and $\mathcal{N}_{\text{start-times}}$.

Equation (6.12) is based on the assumption that the statistical properties of the noise are Gaussian. In reality the noise in the individual interferometers will have significant non-Gaussian components. Coinciding between several interferometers is expected to reduce the effect of these non-Gaussian components, and the efficiency of this reduction may be higher for matched filtering than for noise-monitoring for the reason discussed in Sec. IIB. Hence, if coinciding does not completely efface non-Gaussian effects, the loss factor in event rate \mathcal{R} may be somewhat higher than the estimate (6.12).

We now estimate the loss factor in event rate \mathcal{R} . To obtain the most pessimistic estimate possible of the loss in event rate, we use the following assumptions: (i) The number of template shapes in the matched filtering search is $\mathcal{N}_{\text{shapes}} = 1$; a more realistic larger number would yield a smaller \mathcal{R} . (ii) The number of frequency bins is $\mathcal{N}_{\text{bins}} = 60$, twice the upper limit estimated in Sec. III E. (iii) The number of starting times in the data stream is $\mathcal{N}_{\text{start-times}} = 10^8$, corresponding to a sampling time of 0.1 s in a data set of one third of a year. Such a large sampling time would only be appropriate for the largest mass black holes; more realistic sampling times will be smaller. Larger values of $\mathcal{N}_{\text{start-times}}$ give smaller values of \mathcal{R} . (iv) The parameter ϵ in Eqs. (2.30) and (2.15) is $\epsilon = 10^{-3}$. With these assumptions we obtain $\rho_{\text{threshold}} = 6.8$, $\rho_* = 10.3$ and the resulting loss in event rate factor is

$$\mathcal{R} = 3.5.$$

Hence, the availability of templates could increase the event detection rate by a factor of at most 4, and more typically only 2 over noise-monitoring searches.

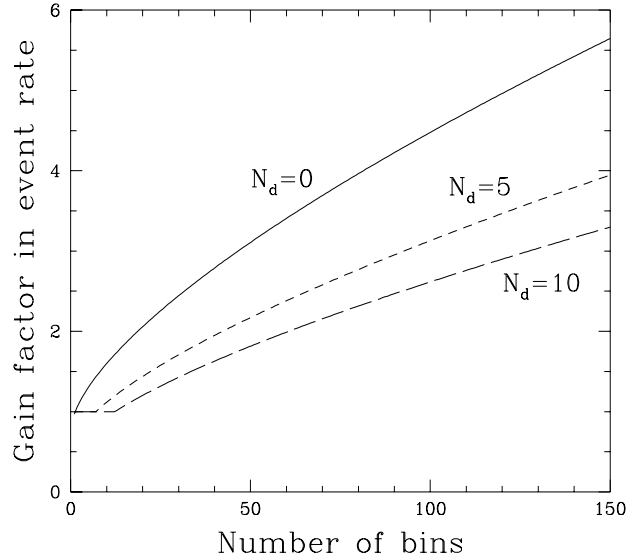


FIG. 7. This plot shows that factor by which the event detection rate is increased when a matched filtering search using theoretical template waveforms is carried out, for gravitational waves from the merger phase of binary black hole coalescences. It is assumed that in the absence of theoretical templates, a search is carried out using the noise-monitoring, nonlinear filtering method described in the text. Plotted on the horizontal axis is the number $\mathcal{N}_{\text{bins}} = 2T\Delta f$ of independent frequency bins characterizing the space of signals that one searches for; T is the maximum expected signal duration and Δf is the frequency bandwidth. The gain factor \mathcal{R} in event rate, which is plotted on the vertical axis, depends on the number of statistically independent waveform shapes in the set of signals one is searching for, which is currently unknown. This number of waveform shapes can be characterized by the effective dimension \mathcal{N}_d of the manifold of signals, as explained in the text. The upper, solid line shows the gain factor in the limit when the number of template shapes is small ($\mathcal{N}_d = 0$), and is an upper limit on the gain factor obtainable from matched filtering. The lower two dashed lines show the gain factor when $\mathcal{N}_d = 5$ and $\mathcal{N}_d = 10$. Our best-guess estimate of the number of frequency bins is $\mathcal{N}_{\text{bins}} = 30$, corresponding to $T = 50M$ and $\Delta f = 1/(\pi M)$, and $\mathcal{N}_{\text{bins}}$ is unlikely to be much larger than 100 (Sec. III E). This plot can be generated by combining Eqs. (2.30), (2.31), (2.15) and (6.13) of the text, with the assumed parameter values $\mathcal{N}_{\text{start-times}} = 10^8$ and $\epsilon = 10^{-3}$.

This discussion assumed that the number of waveform shapes $\mathcal{N}_{\text{shapes}}$ is small. As this number increases, the performance of matched filtering searches gradually worsens until at $\mathcal{N}_{\text{shapes}} \sim \mathcal{N}_{\text{shapes,max}}$, matched filtering performs about as well as noise monitoring (see Sec. IIB). From Eqs. (2.33) and (2.30), the critical value of the number of shapes is $\sim 10^{13}$ for $\mathcal{N}_{\text{bins}} = 60$, and $\sim 10^7$ for $\mathcal{N}_{\text{bins}} = 20$, assuming $\mathcal{N}_{\text{start-times}} = 10^8$. The number of shapes will vary with the signal-to-noise level ρ . We

can define an effective dimension N_d of the manifold of signals by the equation

$$\ln [\mathcal{N}_{\text{shapes}}(\rho)] = \frac{1}{2} N_d(\rho) \ln [1 + \rho^2 / N_d(\rho)]. \quad (6.13)$$

From Eq. (2.33), we see that $N_d(\rho)$ is the dimension of the equivalent linear space of signals that has the same number of distinguishable waveform shapes with $\text{SNR} \leq \rho$ as the true (nonlinear and curved) manifold of merger signals. In Fig. 7 we show the gain factor \mathcal{R} in event rate as a function of $\mathcal{N}_{\text{bins}}$, for the values $N_d = 0, 5$ and 10 . The true value of N_d is quite uncertain and will vary to some extent with ρ ; at high signal-to-noise levels it could conceivably be as large as ~ 10 .

By combining the gain factor of 64 discussed above with the loss factor \mathcal{R} , it follows that noise-monitoring searches for merger waves should increase the number of discovered BBHs by a factor of up to ~ 10 over those found from inspiral and ringdown searches.

For LISA, the expected SNRs are so high that the availability of merger templates will likely have no impact on event detection rates. However, for LISA, as well as for ground-based interferometers, accurate merger templates will be vitally important for interpreting the detected waveforms, for extracting all the available information, and for testing general relativity [36].

VII. CONCLUSIONS

It seems quite likely that the gravitational waves from merging BBH systems will be detected by the ground-based interferometers that are now under construction. The initial LIGO interferometers will be able to detect low mass ($\lesssim 30M_\odot$) coalescences of equal-mass BBHs out to about 200 Mpc via their inspiral waves, and higher mass ($100M_\odot \lesssim M \lesssim 700M_\odot$) systems out to about 200 Mpc via their ringdown waves. The advanced LIGO interferometers will be able to detect equal-mass BBH coalescences in the mass range $10M_\odot \lesssim M \lesssim 300M_\odot$ to $z \sim 1/2$ via their inspiral waves, and higher mass ($200M_\odot \lesssim M \lesssim 3000M_\odot$) systems to $z \sim 1$ via their ringdown waves. For non-equal mass BBHs, these distances will be reduced by a factor of $\sim \sqrt{4\mu/M}$ for inspiral signals and $\sim 4\mu/M$ for ringdown signals.

Searches for massive BBHs ($M \gtrsim 50M_\odot$ for LIGO/VIRGO) based on merger waves could increase the range of the interferometers by an additional factor of ~ 2 , without requiring detailed knowledge of the waveform shapes. It seems likely that BBH coalescences will be detected early in the gradual process of improvement from the first interferometers to the advanced interferometers, rather than later, and there is a strong possibility that they will be the first sources of gravitational radiation to be detected.

Theoretical template waveforms obtained from numerical relativity supercomputer simulations will be crucial

for analyzing the measured merger waves. A match of the detected waveform with a predicted waveform would be a triumph for the theory of general relativity and an absolutely unambiguous signature of the existence of black holes. A complete set of such theoretical templates would also aid the search for BBHs, but not by a large amount.

The space-based interferometer LISA will be an extremely high precision instrument for studying the coalescences of supermassive BBHs. Coalescences with masses in the range $10^6 M_\odot \lesssim (1+z)M \lesssim 10^9 M_\odot$ should be detectable out to $z \sim 10$ with very large SNRs ($\gtrsim 10^3$), via their merger and ringdown waves. Additionally, systems in the mass range $10^4 M_\odot \lesssim (1+z)M \lesssim 3 \times 10^7 M_\odot$ should be detected to similar distances and with SNRs $\gtrsim 10^2$ via their inspiral waves.

ACKNOWLEDGMENTS

We thank Kip Thorne for suggesting this project to us, for being a constant source of ideas and encouragement along the way, and for detailed comments on the paper's content and presentation. We also thank Patrick Brady and David Chernoff for some helpful conversations. This research was supported by NSF Grants PHY-9220644, PHY-9408378, PHY-9424337, and PHY-9514726, and by NASA grant NAGW-4268. S.A.H. gratefully acknowledges the support of a National Science Foundation Graduate Fellowship, and É.F. likewise acknowledges the support of an Enrico Fermi fellowship.

APPENDIX A: SIGNAL TO NOISE RATIO FORMULAE

In this appendix, we give the details of our calculations of the signal-to-noise ratios. The results of this appendix were used to make Figs. 4, 5 and 6 in the text, and also the approximate SNR formulae (5.4) and (5.5) given in Sec. V. The following three subsections give the calculations for the inspiral waves, the merger waves and the ringdown waves respectively.

Note that throughout this appendix we use “ MM_\odot ” (Mega solar-mass) as shorthand for $10^6 M_\odot$.

1. Inspiral

To calculate the angle-averaged SNR squared for the inspiral, we insert the inspiral energy spectrum (3.20) and our parameterized model (4.1) of an interferometer’s noise spectrum into Eq. (2.34), and integrate from $f = f_s$ to $f = f_{\text{merge}}$. The result is

$$\langle \rho^2 \rangle = \begin{cases} \mathcal{F}_i(M, z, D) v^3 \left[9\alpha^{1/3} - \frac{36}{5}\alpha^{-1/3} - \frac{4}{5}\alpha^{-1/3} v^{10/3} - \alpha^3 \left(\frac{f_s}{f_m} \right)^{8/3} \right] & \alpha f_m \leq f_{\text{merge}}/(1+z) \\ \mathcal{F}_i(M, z, D) \left[9\alpha^{1/3} - 8 \left(\frac{v}{\alpha} \right)^{1/3} - \alpha^3 \left(\frac{f_s}{f_m} \right)^{8/3} \right] & f_m/\alpha \leq f_{\text{merge}}/(1+z) < \alpha f_m \\ \mathcal{F}_i(M, z, D) \left[\alpha^{1/3} \left(\frac{\alpha^2}{v} \right) - \alpha^3 \left(\frac{f_s}{f_m} \right)^{8/3} \right] & f_s \leq f_{\text{merge}}/(1+z) < f_m/\alpha \\ 0 & f_{\text{merge}}/(1+z) < f_s, \end{cases} \quad (\text{A1})$$

where

$$v \equiv \frac{(1+z)\alpha f_m}{f_{\text{merge}}} \quad (\text{A2})$$

and

$$\mathcal{F}_i(M, z, D) = \frac{[(1+z)M]^{5/3} [4\mu/M]}{80\pi^{4/3} D(z)^2 h_m^2 f_m^{1/3}}. \quad (\text{A3})$$

Here $D(z)$ is the luminosity distance to the source, f_s , α , f_m and h_m are parameters characterizing the detector noise spectrum (4.1), and f_{merge} is given by Eq. (3.4).

Inserting the values of the noise spectrum parameters from Eq. (4.2) for initial LIGO interferometers, we obtain the following numerical values for the SNR in the equal-mass case $\mu = M/4$:

$$\left(\frac{S}{N} \right)_{\text{initial}} = \begin{cases} 2.8 \left(\frac{200 \text{ Mpc}}{D(z)} \right) \left(\frac{(1+z)M}{18 M_\odot} \right)^{5/6} \left[1 - 0.20 \left(\frac{(1+z)M}{18 M_\odot} \right)^{10/3} \right]^{1/2} & (1+z)M \leq 18 M_\odot \\ 4.7 \left(\frac{200 \text{ Mpc}}{D(z)} \right) \left(\frac{(1+z)M}{18 M_\odot} \right)^{5/6} \left[1 - 0.71 \left(\frac{(1+z)M}{18 M_\odot} \right)^{1/3} \right]^{1/2} & 18 M_\odot < (1+z)M \leq 36 M_\odot \\ 2.7 \left(\frac{200 \text{ Mpc}}{D(z)} \right) \left(\frac{(1+z)M}{36 M_\odot} \right)^{-1/2} \left[1 - 0.06 \left(\frac{(1+z)M}{36 M_\odot} \right)^{8/3} \right]^{1/2} & 36 M_\odot < (1+z)M \leq 102 M_\odot \\ 0 & 102 M_\odot < (1+z)M. \end{cases} \quad (\text{A4})$$

For the noise curve parameters (4.3) appropriate for advanced LIGO interferometers we obtain

$$\left(\frac{S}{N} \right)_{\text{advanced}} = \begin{cases} 27 \left(\frac{1 \text{ Gpc}}{D(z)} \right) \left(\frac{(1+z)M}{37 M_\odot} \right)^{5/6} \left[1 - 0.16 \left(\frac{(1+z)M}{37 M_\odot} \right)^{10/3} \right]^{1/2} & (1+z)M \leq 37 M_\odot \\ 43 \left(\frac{1 \text{ Gpc}}{D(z)} \right) \left(\frac{(1+z)M}{37 M_\odot} \right)^{5/6} \left[1 - 0.65 \left(\frac{(1+z)M}{37 M_\odot} \right)^{1/3} \right]^{1/2} & 37 M_\odot < (1+z)M \leq 95 M_\odot \\ 31 \left(\frac{1 \text{ Gpc}}{D(z)} \right) \left(\frac{(1+z)M}{95 M_\odot} \right)^{-1/2} \left[1 - .021 \left(\frac{(1+z)M}{95 M_\odot} \right)^{8/3} \right]^{1/2} & 95 M_\odot < (1+z)M \leq 410 M_\odot \\ 0 & 410 M_\odot < (1+z)M. \end{cases} \quad (\text{A5})$$

As explained in Sec. V A, the calculation of the inspiral SNR for LISA differs from the other SNR calculations in the following way. If one were to integrate over the whole frequency domain in the interferometer waveband up to

$f = f_{\text{merge}}$ (as is done for the initial and advanced interferometers in LIGO), in some cases one would obtain the SNR for a measurement of several hundred years duration, which is obviously irrelevant. Thus, it is necessary to restrict the integral over frequency in Eq. (2.34) to the domain that corresponds to, say, one year of observation when calculating inspiral LISA SNRs. Using the Newtonian relationship for the rate of frequency sweep, we obtain for the frequency at time T before merger in the equal-mass case

$$f_{\text{insp}}(T) = \left[f_{\text{merge}}^{-8/3} + \frac{64}{5} \pi^{8/3} M^{5/3} (1+z)^{5/3} T \right]^{-3/8}. \quad (\text{A6})$$

Binaries of redshifted total mass $(1+z)M$ larger than about $5 \times 10^5 M_\odot$ enter the LISA waveband at $f = f_s = 10^{-4}$ Hz less than one year before merger, while binaries of smaller redshifted mass spend more than one year in the LISA waveband. To calculate the SNR, we insert Eq. (3.20) into Eq. (2.34) and integrate numerically from the larger of f_s and $f_{\text{insp}}(1 \text{ yr})$ to f_{merge} . The resulting SNR values are shown in Fig. 6. We also show in Fig. 6 the SNR obtained from one year of observation one hundred years before the final merger, obtained by integrating from $f_{\text{insp}}(100 \text{ yr})$ to $f_{\text{insp}}(99 \text{ yr})$, as well as a similar curve for one thousand years prior to merger.

Equation (A1) applies to LISA only for $(1+z)M \gtrsim 5 \times 10^5 M_\odot$. By combining Eqs. (A1) and (4.4) for $(1+z)M \gtrsim 5 \times 10^5 M_\odot$ together with an approximate fit to Fig. 6 for $(1+z)M \lesssim 10^5 M_\odot$ we obtain for the SNR from the last year of inspiral in the equal-mass case

$$\left(\frac{S}{N} \right)_{\text{LISA}} \approx \begin{cases} 1.5 \times 10^4 \left(\frac{1 \text{ Gpc}}{D(z)} \right) \left(\frac{(1+z)M}{0.5 \text{ MM}_\odot} \right) & 100 M_\odot \lesssim (1+z)M \lesssim 0.5 \text{ MM}_\odot \\ 1.9 \times 10^4 \left(\frac{1 \text{ Gpc}}{D(z)} \right) \left(\frac{(1+z)M}{0.5 \text{ MM}_\odot} \right)^{5/6} \left[1 - 0.38 \left(\frac{(1+z)M}{0.5 \text{ MM}_\odot} \right)^{1/3} \right]^{1/2} & 0.5 \text{ MM}_\odot < (1+z)M \leq 6.0 \text{ MM}_\odot \\ 5.0 \times 10^4 \left(\frac{1 \text{ Gpc}}{D(z)} \right) \left(\frac{(1+z)M}{6 \text{ MM}_\odot} \right)^{-1/2} \left[1 - 0.006 \left(\frac{(1+z)M}{6 \text{ MM}_\odot} \right)^{8/3} \right]^{1/2} & 6.0 \text{ MM}_\odot < (1+z)M \leq 41 \text{ MM}_\odot \\ 0 & 41 \text{ MM}_\odot < (1+z)M. \end{cases} \quad (\text{A7})$$

2. Merger

To calculate the merger SNR we use the energy spectrum (3.14) and follow the same procedure as above. The result is

$$\langle \rho^2 \rangle = \begin{cases} \mathcal{F}_m(\epsilon_m, M, z, D) v^3 \left[\frac{\kappa^3 - 1}{\kappa^3} \right] & f_{\text{merge}}/(1+z) \geq \alpha f_m \\ \mathcal{F}_m(\epsilon_m, M, z, D) \left[3 \ln v - \frac{v^3 - \kappa^3}{\kappa^3} \right] & f_m/\alpha \leq f_{\text{merge}}/(1+z) < \alpha f_m \leq f_{\text{qnr}}/(1+z) \\ {}^{\text{LA}} \mathcal{F}_m(\epsilon_m, M, z, D) \left[2 - \frac{\alpha^6}{v^3} - \frac{v^3}{\kappa^3} + 6 \ln \alpha \right] & f_{\text{merge}}/(1+z) \leq f_m/\alpha < \alpha f_m \leq f_{\text{qnr}}/(1+z) \\ {}^{\text{L}} \mathcal{F}_m(\epsilon_m, M, z, D) [3 \ln \kappa] & f_m/\alpha \leq f_{\text{merge}}/(1+z) < f_{\text{qnr}}/(1+z) \leq \alpha f_m \\ {}^{\text{I}} \mathcal{F}_m(\epsilon_m, M, z, D) \left[2 - \left(\frac{\alpha f_s}{f_m} \right)^3 - \frac{v^3}{\kappa^3} + 6 \ln \alpha \right] & f_{\text{merge}}/(1+z) \leq f_s < f_m/\alpha < \alpha f_m \leq f_{\text{qnr}}/(1+z) \\ {}^{\text{A,L}} \mathcal{F}_m(\epsilon_m, M, z, D) \left[1 + 3 \ln \left(\frac{\kappa \alpha^2}{v} \right) - \frac{\alpha^6}{v^3} \right] & f_s \leq f_{\text{merge}}/(1+z) < f_m/\alpha \leq f_{\text{qnr}}/(1+z) \\ {}^{\text{LA}} \mathcal{F}_m(\epsilon_m, M, z, D) \left[1 - \left(\frac{\alpha f_s}{f_m} \right)^3 + 3 \ln \left(\frac{\kappa \alpha^2}{v} \right) \right] & f_{\text{merge}}/(1+z) \leq f_s < f_m/\alpha \leq f_{\text{qnr}}/(1+z) \\ {}^{\text{L}} \mathcal{F}_m(\epsilon_m, M, z, D) [\alpha^6 v^{-3} (\kappa^3 - 1)] & f_s \leq f_{\text{merge}}/(1+z) < f_{\text{qnr}}/(1+z) \\ \mathcal{F}_m(\epsilon_m, M, z, D) \left[\left(\frac{\kappa \alpha^2}{v} \right)^3 - \left(\frac{\alpha f_s}{f_m} \right)^3 \right] & f_{\text{merge}}/(1+z) \leq f_s < f_{\text{qnr}}/(1+z) \leq f_m/\alpha \\ 0 & f_{\text{qnr}}/(1+z) < f_s. \end{cases} \quad (\text{A8})$$

Here v is given by Eq. (A2), ϵ_m is the fraction of total mass energy radiated during the merger (which we have also denoted by ϵ_{merger} in the body of the paper), $\kappa \equiv f_{\text{qnr}}/f_{\text{merge}}$, and

$$\mathcal{F}_m(\epsilon_m, M, z, D) = \frac{2\epsilon_m M (1+z)^2 [4\mu/M]^2}{15\pi^2 D(z)^2 h_m^2 f_{\text{merge}} (\kappa - 1)}. \quad (\text{A9})$$

Lines marked with the superscript ‘‘I’’ turn out to hold for the initial LIGO interferometer parameters; those with ‘‘A’’ hold for advanced LIGO interferometer parameters; and those with ‘‘L’’ hold for LISA.

Using the numerical values of the noise curve parameters (4.2) for initial LIGO interferometers, and Eqs. (3.4), (3.5), (A2), and (A8) we find for the initial LIGO interferometers in the equal-mass case

$$\left(\frac{S}{N}\right)_{\text{initial}} = \begin{cases} 1.5 \left(\frac{\epsilon_m}{0.1}\right)^{1/2} \left(\frac{200 \text{ Mpc}}{D(z)}\right) \left(\frac{(1+z)M}{18 M_\odot}\right)^{5/2} & (1+z)M \leq 18 M_\odot \\ 1.5 \left(\frac{\epsilon_m}{0.1}\right)^{1/2} \left(\frac{200 \text{ Mpc}}{D(z)}\right) \left(\frac{(1+z)M}{18 M_\odot}\right) \\ \quad \times \left[1 + 3 \ln\left(\frac{(1+z)M}{18 M_\odot}\right) - 3.6 \times 10^{-3} \left(\frac{(1+z)M}{18 M_\odot}\right)^3\right]^{1/2} & 18 M_\odot < (1+z)M \leq 36 M_\odot \\ 6.1 \left(\frac{\epsilon_m}{0.1}\right)^{1/2} \left(\frac{200 \text{ Mpc}}{D(z)}\right) \left(\frac{(1+z)M}{36 M_\odot}\right) \\ \quad \times \left[1 + .23 \left(\frac{(1+z)M}{36 M_\odot}\right)^{-3} - 0.007 \left(\frac{(1+z)M}{36 M_\odot}\right)^3\right]^{1/2} & 36 M_\odot < (1+z)M \leq 102 M_\odot \\ 17.3 \left(\frac{\epsilon_m}{0.1}\right)^{1/2} \left(\frac{200 \text{ Mpc}}{D(z)}\right) \left(\frac{(1+z)M}{102 M_\odot}\right) \\ \quad \times \left[1 - .17 \left(\frac{(1+z)M}{102 M_\odot}\right)^3\right]^{1/2} & 102 M_\odot < (1+z)M \leq 118 M_\odot \\ 9.9 \left(\frac{\epsilon_m}{0.1}\right)^{1/2} \left(\frac{200 \text{ Mpc}}{D(z)}\right) \left(\frac{(1+z)M}{118 M_\odot}\right) \left[1 - 3.1 \ln\left(\frac{(1+z)M}{230 M_\odot}\right)\right]^{1/2} & 118 M_\odot < (1+z)M \leq 230 M_\odot \\ 20 \left(\frac{\epsilon_m}{0.1}\right)^{1/2} \left(\frac{200 \text{ Mpc}}{D(z)}\right) \left(\frac{(1+z)M}{230 M_\odot}\right)^{-1/2} \left[1 - 0.04 \left(\frac{(1+z)M}{230 M_\odot}\right)^3\right]^{1/2} & 230 M_\odot < (1+z)M \leq 660 M_\odot \\ 0 & 660 M_\odot < (1+z)M. \end{cases} \quad (\text{A10})$$

Similarly using Eq. (4.3) we find for advanced LIGO interferometers

$$\left(\frac{S}{N}\right)_{\text{advanced}} = \begin{cases} 13 \left(\frac{\epsilon_m}{0.1}\right)^{1/2} \left(\frac{1 \text{ Gpc}}{D(z)}\right) \left(\frac{(1+z)M}{37 M_\odot}\right)^{5/2} & (1+z)M \leq 37 M_\odot \\ 13 \left(\frac{\epsilon_m}{0.1}\right)^{1/2} \left(\frac{1 \text{ Gpc}}{D(z)}\right) \left(\frac{(1+z)M}{37 M_\odot}\right) \\ \quad \times \left[1 + 3 \ln\left(\frac{(1+z)M}{37 M_\odot}\right) - 3.6 \times 10^{-3} \left(\frac{(1+z)M}{37 M_\odot}\right)^3\right]^{1/2} & 37 M_\odot < (1+z)M \leq 95 M_\odot \\ 76 \left(\frac{\epsilon_m}{0.1}\right)^{1/2} \left(\frac{1 \text{ Gpc}}{D(z)}\right) \left(\frac{(1+z)M}{95 M_\odot}\right) \\ \quad \times \left[1 - 0.21 \left(\frac{(1+z)M}{95 M_\odot}\right)^{-3} - 0.013 \left(\frac{(1+z)M}{95 M_\odot}\right)^3\right]^{1/2} & 95 M_\odot < (1+z)M \leq 240 M_\odot \\ 88 \left(\frac{\epsilon_m}{0.1}\right)^{1/2} \left(\frac{1 \text{ Gpc}}{D(z)}\right) \left(\frac{(1+z)M}{240 M_\odot}\right) \\ \quad \times \left[1 - 3 \ln\left(\frac{(1+z)M}{620 M_\odot}\right) - 0.061 \left(\frac{(1+z)M}{240 M_\odot}\right)^{-3}\right]^{1/2} & 240 M_\odot < (1+z)M \leq 410 M_\odot \\ 150 \left(\frac{\epsilon_m}{0.1}\right)^{1/2} \left(\frac{1 \text{ Gpc}}{D(z)}\right) \left(\frac{(1+z)M}{410 M_\odot}\right) \left[1 - 3.0 \ln\left(\frac{(1+z)M}{620 M_\odot}\right)\right]^{1/2} & 410 M_\odot < (1+z)M \leq 620 M_\odot \\ 220 \left(\frac{\epsilon_m}{0.1}\right)^{1/2} \left(\frac{1 \text{ Gpc}}{D(z)}\right) \left(\frac{(1+z)M}{620 M_\odot}\right)^{-1/2} \left[1 - 0.013 \left(\frac{(1+z)M}{620 M_\odot}\right)^3\right]^{1/2} & 620 M_\odot < (1+z)M \leq 2600 M_\odot \\ 0 & 2600 M_\odot < (1+z)M. \end{cases} \quad (\text{A11})$$

Finally, using the parameters (4.4) appropriate for LISA, we obtain

$$\left(\frac{S}{N}\right)_{\text{LISA}} = \begin{cases} 1.9 \times 10^3 \left(\frac{\epsilon_m}{0.1}\right)^{1/2} \left(\frac{1 \text{ Gpc}}{D(z)}\right) \left(\frac{(1+z)M}{2.0 \times 10^5 M_\odot}\right)^{5/2} & (1+z)M \leq 2.0 \times 10^5 M_\odot \\ 1.9 \times 10^3 \left(\frac{\epsilon_m}{0.1}\right)^{1/2} \left(\frac{1 \text{ Gpc}}{D(z)}\right) \left(\frac{(1+z)M}{2.0 \times 10^5 M_\odot}\right) \\ \quad \times \left[1 + 3 \ln\left(\frac{(1+z)M}{2.0 \times 10^5 M_\odot}\right) - 3.6 \times 10^{-3} \left(\frac{(1+z)M}{2.0 \times 10^5 M_\odot}\right)^3\right]^{1/2} & 2.0 \times 10^5 M_\odot < (1+z)M \leq 1.3 \text{ MM}_\odot \\ 2.8 \times 10^4 \left(\frac{\epsilon_m}{0.1}\right)^{1/2} \left(\frac{1 \text{ Gpc}}{D(z)}\right) \left(\frac{(1+z)M}{1.3 \text{ MM}_\odot}\right) & 1.3 \text{ MM}_\odot < (1+z)M \leq 6.0 \text{ MM}_\odot \\ 3.4 \times 10^4 \left(\frac{\epsilon_m}{0.1}\right)^{1/2} \left(\frac{1 \text{ Gpc}}{D(z)}\right) \left(\frac{(1+z)M}{6.0 \text{ MM}_\odot}\right) \\ \quad \times \left[1 - 3 \ln\left(\frac{(1+z)M}{39 \text{ MM}_\odot}\right) - \left(\frac{(1+z)M}{6.0 \text{ MM}_\odot}\right)^{-3}\right]^{1/2} & 6.0 \text{ MM}_\odot < (1+z)M \leq 39 \text{ MM}_\odot \\ 3.6 \times 10^5 \left(\frac{\epsilon_m}{0.1}\right)^{1/2} \left(\frac{1 \text{ Gpc}}{D(z)}\right) \left(\frac{(1+z)M}{39 \text{ MM}_\odot}\right)^{-1/2} & 39 \text{ MM}_\odot < (1+z)M \leq 41 \text{ MM}_\odot \\ 3.4 \times 10^5 \left(\frac{\epsilon_m}{0.1}\right)^{1/2} \left(\frac{1 \text{ Gpc}}{D(z)}\right) \\ \quad \times \left(\frac{(1+z)M}{41 \text{ MM}_\odot}\right)^{-1/2} \left[1 - 3.8 \times 10^{-3} \left(\frac{(1+z)M}{41 \text{ MM}_\odot}\right)^3\right]^{1/2} & 41 \text{ MM}_\odot < (1+z)M \leq 260 \text{ MM}_\odot \\ 0 & 260 \text{ MM}_\odot < (1+z)M. \end{cases} \quad (\text{A12})$$

3. Ringdown

The ringdown SNRs are calculated a little differently from the inspiral and merger SNRs. First, we use the effective energy spectrum (3.24) which yields an estimate of the true SNR obtainable from the model waveform (3.21) that is accurate to within a few tens of percent (see Appendix B). Second, the integral over frequency in the SNR formula (2.34) with the noise spectrum (4.1) and the energy spectrum (3.24) cannot easily be evaluated analytically. Hence, we calculated this integral numerically to produce the plots of ringdown SNR versus BBH mass shown in Figs. 4, 5 and 6.

In the remainder of this appendix we derive approximate formulae for the ringdown SNR as a function of mass, by approximating the ringdown energy spectrum as a delta function at the ringdown frequency [*cf.* Eq. (3.25)]. This approximation yields (see Appendix B and Ref. [103])

$$\langle \rho^2 \rangle = \frac{(1+z)^3 M^2 \mathcal{A}^2 Q [4\mu/M]^2}{20\pi^2 D(z)^2 f_{\text{qnr}} S_h[f_{\text{qnr}}/(1+z)]}. \quad (\text{A13})$$

Using Eq. (3.23) and the relation (3.28) between the dimensionless coefficient \mathcal{A} and the radiated energy we can rewrite formula (A13) as

$$\langle \rho^2 \rangle = \frac{8}{5} \frac{1}{F(a)^2} \epsilon_r \frac{(1+z)M}{S_h[f_{\text{qnr}}/(1+z)]} \left[\frac{(1+z)M}{D(z)}\right]^2 \left[\frac{4\mu}{M}\right]^2, \quad (\text{A14})$$

where ϵ_r is the fraction of the total mass energy radiated in the ringdown, and

$$F(a) = 1 - \frac{63}{100}(1-a)^{3/10}. \quad (\text{A15})$$

An equivalent formula was previously obtained by Finn [102].

We find the following numerical result when we insert our assumed values $\epsilon_r = 0.03$ and $a = 0.98$ for the ringdown signal together with the parameters for the initial LIGO interferometer noise curve in the equal-mass case:

$$\left(\frac{S}{N}\right)_{\text{initial}} = \begin{cases} 0.08 \left(\frac{\epsilon_r}{0.03}\right)^{1/2} \left(\frac{200 \text{ Mpc}}{D(z)}\right) \left(\frac{(1+z)M}{18 M_\odot}\right)^{5/2} & (1+z)M \leq 118 M_\odot \\ 8.8 \left(\frac{\epsilon_r}{0.03}\right)^{1/2} \left(\frac{200 \text{ Mpc}}{D(z)}\right) \left(\frac{(1+z)M}{118 M_\odot}\right) & 118 M_\odot < (1+z)M \leq 230 M_\odot \\ 17 \left(\frac{\epsilon_r}{0.03}\right)^{1/2} \left(\frac{200 \text{ Mpc}}{D(z)}\right) \left(\frac{(1+z)M}{230 M_\odot}\right)^{-1/2} & 230 M_\odot < (1+z)M \leq 660 M_\odot \\ 0 & 660 M_\odot < (1+z)M. \end{cases} \quad (\text{A16})$$

The corresponding formulae for advanced LIGO interferometers are

$$\left(\frac{S}{N}\right)_{\text{advanced}} = \begin{cases} 0.71 \left(\frac{\epsilon_r}{0.03}\right)^{1/2} \left(\frac{1 \text{ Gpc}}{D(z)}\right) \left(\frac{(1+z)M}{37 M_\odot}\right)^{5/2} & (1+z)M \leq 240 M_\odot \\ 77 \left(\frac{\epsilon_r}{0.03}\right)^{1/2} \left(\frac{1 \text{ Gpc}}{D(z)}\right) \left(\frac{(1+z)M}{240 M_\odot}\right) & 240 M_\odot < (1+z)M \leq 620 M_\odot \\ 200 \left(\frac{\epsilon_r}{0.03}\right)^{1/2} \left(\frac{1 \text{ Gpc}}{D(z)}\right) \left(\frac{(1+z)M}{620 M_\odot}\right)^{-1/2} & 620 M_\odot < (1+z)M \leq 2600 M_\odot \\ 0 & 2600 M_\odot < (1+z)M. \end{cases} \quad (\text{A17})$$

Finally, the corresponding formulae for LISA are

$$\left(\frac{S}{N}\right)_{\text{LISA}} = \begin{cases} 96 \left(\frac{\epsilon_r}{0.03}\right)^{1/2} \left(\frac{1 \text{ Gpc}}{D(z)}\right) \left(\frac{(1+z)M}{0.2 \text{ MM}_\odot}\right)^{5/2} & (1+z)M \leq 1.3 \text{ MM}_\odot \\ 1.0 \times 10^4 \left(\frac{\epsilon_r}{0.03}\right)^{1/2} \left(\frac{1 \text{ Gpc}}{D(z)}\right) \left(\frac{(1+z)M}{1.3 \text{ MM}_\odot}\right) & 1.3 \text{ MM}_\odot < (1+z)M \leq 39 \text{ MM}_\odot \\ 3.1 \times 10^5 \left(\frac{\epsilon_r}{0.03}\right)^{1/2} \left(\frac{1 \text{ Gpc}}{D(z)}\right) \left(\frac{(1+z)M}{39 \text{ MM}_\odot}\right)^{-1/2} & 39 \text{ MM}_\odot < (1+z)M \leq 260 \text{ MM}_\odot \\ 0 & 260 \text{ MM}_\odot < (1+z)M. \end{cases} \quad (\text{A18})$$

By comparing Eqs. (A16) – (A18) with Figs. 4 – 6 it can be seen that the delta-function energy spectrum approximation is fairly good except for $M \gtrsim 3000 M_\odot$ for advanced LIGO interferometers and $M \gtrsim 3 \times 10^8 M_\odot$ for LISA. The approximation fails to capture the high mass tails of the SNR curves.

APPENDIX B: ENERGY SPECTRUM FOR RINGDOWN WAVES

There is a subtlety in calculating the SNR for the ringdown waves, related to the fact that the SNR squared does not accumulate locally in the time domain. In order to explain this subtlety, let us focus not on the angle-averaged SNR squared which was our main concern in the body of the paper, but rather on the SNR squared obtained in one interferometer from a specific source with specific relative angular orientations. In this case the waveform $h(t)$ seen in the interferometer, for $t > 0$, is of the form

$$h(t) = h_0 \cos(2\pi f_{\text{qnr}} t + \psi_0) e^{-t/\tau} \quad (\text{B1})$$

for some constants h_0 and ψ_0 , while $h(t)$ is the (unknown) merger waveform for $t < 0$.

Let us also focus first on the simple, idealized case of white noise, $S_h(f) = S_h = \text{const}$. Then, the SNR squared (2.7) accumulates locally in time:

$$\rho^2 = \frac{2}{S_h} \int_{-\infty}^{\infty} dt h(t)^2. \quad (\text{B2})$$

Hence, for white noise, the SNR squared from the ringdown is clearly unambiguously given by

$$\begin{aligned} \rho_{\text{ringdown}}^2 &= \frac{2}{S_h} \int_0^{\infty} h_0^2 \cos^2(2\pi f_{\text{qnr}} t + \psi_0)^2 e^{-2t/\tau} dt \\ &= \frac{h_0^2 \tau}{2S_h} \left[1 + \frac{\cos(2\psi_0) - Q \sin(2\psi_0)}{1 + Q^2} \right] \\ &\approx \frac{h_0^2 \tau}{2S_h} [1 + O(1/Q)], \end{aligned} \quad (\text{B3})$$

where $Q = \pi f_{\text{qnr}} \tau$. Now consider the case when the noise is not exactly white. Naively, we expect that in the Fourier domain the energy spectrum of the ringdown signal will be a resonance curve that peaks at $f = f_{\text{qnr}}$ with width $\sim f_{\text{qnr}}/Q$. Thus, for large Q we would expect that most of the SNR squared will be accumulated near $f = f_{\text{qnr}}$, unless the noise spectrum varies very strongly with frequency. Moreover, if the noise spectrum $S_h(f)$ does not vary much over the bandwidth $\sim f_{\text{qnr}}/Q$ of the resonance peak, then we would expect the formula (B3) to be valid to a good approximation, with S_h replaced by $S_h(f_{\text{qnr}})$. We show below that this is indeed the case: under such circumstances, Eq. (B3) is fairly accurate, and the resulting approximate ringdown SNR is embodied in our approximate delta-function energy spectrum (3.25) and in Eqs. (A13) - (A17) of Appendix A [103].

In many cases of interest, it will indeed be true that most of the SNR squared for ringdown waves will be accumulated in the vicinity of the resonance peak, so that the SNR will approximately be given by Eq. (B3). However, this will not always be the case. For instance, suppose that we were lucky enough that two $10^5 M_\odot$ black holes were to merge at the center of our own galaxy. Would

such an event be detectable by advanced LIGO interferometers? Clearly, most of the power in the ringdown waves in this case would be far below the LIGO/VIRGO waveband. However, given that the merger is only at ~ 10 kpc, one might hope to be able to detect the tail of the ringdown waves that extends upwards in frequency into the LIGO/VIRGO waveband. Or, consider the detectability of a ringdown of a nearby $10^3 M_\odot$ black hole by LISA. In this case most of the ringdown power is concentrated at frequencies above LISA's optimum waveband, and the detectability of the signal is determined by the amount of power in the low frequency tail of the ringdown. In such cases, it is clearly necessary to understand the power carried in the ringdown waves at frequencies far from the resonant frequency.

Normally, such an understanding is obtained simply by taking a Fourier transform of the waveform $h(t)$. In the case of ringdown waves from BBH mergers, however, the waveform for $t < 0$ is the unknown, merger waveform. In order to obtain the SNR squared from the ringdown signal alone, one might guess that the appropriate thing to do is to take $h(t) = 0$ for $t < 0$, and insert this together with Eq. (B1) into the standard formula (2.7) for the signal to noise squared. However, the resulting energy spectrum has unrealistic high frequency behavior due to a discontinuity in $h(t)$ at $t = 0$ (or a discontinuity in $h'(t)$ at $t = 0$ in the case $\psi_0 = \pi/2$), and the resulting SNRs can in some cases differ from the correct values (see below) by factors $\gtrsim 10$. Other choices for $h(t)$ for $t < 0$ [for instance $h(t) = h(0)$] get around this problem but instead have unrealistic low frequency behavior. In any case, it is clear that these choices are somewhat *ad hoc* and that there should be some more fundamental, unique way to calculate the SNR.

We now explain the correct method to calculate the SNR. The question that effectively is being asked is: What is the probability that there is a ringdown waveform present in the data stream, starting at (say) $t = 0$? This probability is to be calculated given only the data from $t > 0$, without using the measured data from $t < 0$ which is contaminated by the unknown merger waveform. To do this one must effectively integrate over all possible realizations of the noise for $t < 0$. The necessity for such an integration is illustrated by the following simple analogy. Suppose that one is measuring two real variables, h_+ ("waveform for positive t ") and h_- ("waveform for negative t "), and that the measured values of these variables are \bar{h}_+ and \bar{h}_- . Suppose that because of the noise in the measurement process, the probability distribution for the true values of these parameters given their measured values is

$$p(h_+, h_-) = \frac{1}{2\pi\sigma^2} \exp \left\{ -\frac{1}{2\sigma^2} [(h_+ - \bar{h}_+)^2 + (h_- - \bar{h}_-)^2 + 2\varepsilon(h_+ - \bar{h}_+)(h_- - \bar{h}_-)] \right\}. \quad (\text{B4})$$

Thus, h_+ and h_- are Gaussian distributed about their

means \bar{h}_+ and \bar{h}_- , and they are correlated. If we assume that $h_- = 0$ [analogous to assuming $h(t) = 0$ for $t < 0$], we obtain for the probability distribution for h_+

$$p(h_+ | h_- = 0) = \frac{1}{\sqrt{2\pi}\sigma} e^{-(h_+ - \bar{h}_+)^2 / (2\sigma)^2}, \quad (\text{B5})$$

where $\bar{h}'_+ = \bar{h}_+ - \varepsilon \bar{h}_-$. By contrast, if we instead calculate the probability distribution for h_+ alone by integrating over h_- we find

$$p(h_+) = \frac{1}{\sqrt{2\pi}\sigma^*} e^{-(h_+ - \bar{h}_+)^2 / (2\sigma^*)^2}, \quad (\text{B6})$$

where $\sigma^* = \sigma / \sqrt{1 - \varepsilon^2}$. It is clear in this simple example that one should use the reduced distribution (B6) rather than the distribution (B5). Note also that the widths of the probability distributions (B5) and (B6) are different, and that the correct distribution (B6) could not have been obtained from the joint distribution (B4) for any assumed choice of h_- .

Turn now to the analogous situation for random processes. If $n(t)$ is the interferometer noise, let $C_n(\Delta t) \equiv \langle n(t)n(t + \Delta t) \rangle$ denote the autocorrelation function. Define the inner product

$$\langle h_1 | h_2 \rangle \equiv \int_0^\infty dt \int_0^\infty dt' K(t, t') h_1(t) h_2(t') \quad (\text{B7})$$

on the space of functions $h(t)$ for $t > 0$, where the kernel $K(t, t')$ is determined from

$$\int_0^\infty dt'' K(t, t'') C_n(t'' - t) = \delta(t - t') \quad (\text{B8})$$

for $t, t' \geq 0$. The quantity $K(t, t')$ is analogous to the modified width σ^* in Eq. (B6) above. Using the inner product (B7), the usual theory of optimal filtering [54,55] can be applied to random processes on the half line $t > 0$. Thus, if $s(t)$ is the interferometer output and $h(t)$ is the waveform (B1), the detection statistic is $Y = \langle s | h \rangle$, and the SNR squared for the measurement is

$$\begin{aligned} \rho^2 &\equiv \frac{E[Y]^2}{E[Y^2] - E[Y]^2} \\ &= \langle h | h \rangle \\ &= \int_0^\infty dt \int_0^\infty dt' K(t, t') h(t) h(t'), \end{aligned} \quad (\text{B9})$$

where $E[\dots]$ means expectation value. If we define

$$G(f, f') = \int_0^\infty dt \int_0^\infty dt' e^{2\pi i f t} e^{-2\pi i f' t'} K(t, t') \quad (\text{B10})$$

and

$$\tilde{h}(f) = \int_0^\infty e^{2\pi i f t} h(t) dt, \quad (\text{B11})$$

the SNR squared can be rewritten as

$$\rho^2 = \int_{-\infty}^\infty df \int_{-\infty}^\infty df' \tilde{h}(f)^* G(f, f') \tilde{h}(f'). \quad (\text{B12})$$

Note that the Fourier transform $G(f, f')$ of $K(t, t')$ is not proportional to $\delta(f - f') / S_n(f)$ but instead is in general *non-diagonal* in frequency.

The formula (B12) resolves the ambiguities discussed above in the method of calculating the ringdown SNR; the result does not require a choice of the waveform $h(t)$ for $t < 0$. Unfortunately, the final answer (B12) is complicated in the sense that it cannot be expressed in the form (2.34) for any effective energy spectrum dE/df . This is somewhat inconvenient for the purposes of this paper: the wave's energy spectrum is a useful and key tool for visualizing and understanding the SNRs. Clearly, an approximate, effective energy spectrum (to the extent that one exists) would be very useful. We now turn to a derivation of such an approximate, effective energy spectrum, namely the spectrum (3.24) which is used throughout the body of this paper.

We start our derivation by describing an alternative method of calculating the exact ringdown SNR given by Eqs. (B1) and (B9). It is straightforward to show that the quantity (B9) can be obtained by (i) choosing *any* waveform $h(t)$ for $t < 0$, (ii) calculating the SNR from the usual formula (2.7), and (iii) minimizing over all choices of the function $h(t)$ on the negative real axis. We have experimented with several choices of $h(-t)$ for $t > 0$, namely $h(-t) = 0$, $h(-t) = h(0)$, $h(-t) = h(t)$. We found that the SNR obtained by minimizing over these choices is always (for the entire black hole mass ranges discussed in Sec. V) within a few tens of percent of the SNR obtained from the following prescription: (i) Assume that $h(t)$ for negative t is identical to the waveform for positive t except for the sign of t/τ ; *i.e.*, that

$$h(t) = h_0 \cos(2\pi f_{\text{qnr}} t + \psi_0) e^{-|t|/\tau} \quad (\text{B13})$$

for positive and negative t . (ii) Calculate the total SNR using the standard formula (2.7). (iii) Divide by a correction factor of $\sqrt{2}$ in amplitude to compensate for the doubling up. This prescription gives the correct, exact result (B9) for white noise. For more realistic noise curves, the errors of a few tens of percent resulting from this prescription are unimportant compared to the uncertainty in the overall amplitude \mathcal{A} of the ringdown signal. Moreover, the resulting SNR values multiplied by $\sqrt{2}$ are an upper bound for the true SNR (since if our *ad hoc* choice of $h(t)$ for $t < 0$ happened to be exactly right, then the prescription would underestimate the SNR by $\sqrt{2}$).

We now explain how to obtain the energy spectrum (3.24) from the above approximate prescription. From Eqs. (2.35) and (3.21) it can be seen that the waveform as seen in one interferometer, before angle averaging, is given by Eq. (B1) with

$$h_0 e^{i\psi_0} = \frac{\mathcal{A}M}{r} [F_+(\theta, \varphi, \psi) + iF_-(\theta, \varphi, \psi)] {}_2S_2^2(\iota, \beta, a) e^{i\varphi_0}. \quad (\text{B14})$$

Here the angles θ , φ , ψ , ι and β have the meanings explained in Sec. II C. Let us now insert the waveform (B1) into the formula (B9) for the exact SNR, and then average over the angles θ , φ , ψ , ι and β using Eqs. (2.38) and (3.22). This yields for the angle-averaged, exact SNR squared

$$\langle \rho_{\text{exact}}[h(t)]^2 \rangle = \frac{1}{20\pi} [\rho_{\text{exact}}[h_{+,0}(t)]^2 + \rho_{\text{exact}}[h_{\times,0}(t)]^2], \quad (\text{B15})$$

where $\rho_{\text{exact}}[h(t)]$ denotes the exact SNR functional (B9) and

$$\begin{aligned} h_{+,0}(t) &= \frac{\mathcal{A}M}{r} \cos(2\pi f_{\text{qnr}}t) e^{-t/\tau} \\ h_{\times,0}(t) &= \frac{\mathcal{A}M}{r} \sin(2\pi f_{\text{qnr}}t) e^{-t/\tau}, \end{aligned} \quad (\text{B16})$$

for $t > 0$. Now, for each of the two terms on the right hand side of Eq. (B15), we make the approximation discussed above consisting of using Eqs. (2.7) and (B13) and dividing by 2. This yields

$$\langle \rho_{\text{exact}}[h(t)]^2 \rangle \approx \frac{1}{10\pi} \int_0^\infty df \frac{[|\tilde{h}_{+,0}(f)|^2 + |\tilde{h}_{\times,0}(f)|^2]}{S_h(f)}, \quad (\text{B17})$$

where it is understood that $h_{+,0}$ and $h_{\times,0}$ have been extended to negative t in the manner of Eq. (B13). Finally, evaluating the Fourier transforms yields an angle averaged SNR squared of the form (2.34), with energy spectrum given by Eq. (3.24).

[1] K. S. Thorne, in *300 Years of Gravitation*, ed. S. W. Hawking and W. Israel (Cambridge University Press, Cambridge, 1987), pp. 330-458.

[2] B. F. Schutz, *Sources of Gravitational Waves*, in NASA, Relativistic Gravitational Experiments in Space pp. 7-13 (1989).

[3] A. Abramovici, W. E. Althouse, R. W. P. Drever, Y. Gürsel, S. Kawamura, F. J. Raab, D. Shoemaker, L. Sievers, R. E. Spero, K. S. Thorne, R. E. Vogt, R. Weiss, S. E. Whitcomb, and M. E. Zucker, *LIGO: The Laser Interferometer Gravitational-wave Observatory*, *Science* **256**, 325 (1992).

[4] C. Bradaschia *et al.*, *Nucl. Instrum. & Methods* **A289**, 518 (1990); also in *Gravitation: A Banff Summer Institute*, ed. R. Mann and P. Wesson (World Scientific, Singapore, 1991).

[5] P. Bender, A. Brilliet, I. Ciufolini, K. Danzmann, R. Hellings, J. Hough, A. Lobo, M. Sandford, B. Schutz, and P. Touboul. *LISA, Laser interferometer space antenna for gravitational wave measurements: ESA Assessment Study Report*. R. Reinhard, ESTEC, 1994.

[6] Hough, J. *et al.*, in *Gravitational Wave Experiments* (proceedings of the Edoardo Amaldi Conference, World Scientific, 1995), p.50.

[7] P. Bender, I. Ciufolini, K. Danzmann, W. Folkner, J. Hough, D. Robertson, A. Rüdiger, M. Sandford, R. Schilling, B. Schutz, R. Stebbins, T. Summer, P. Touboul, S. Vitale, H. Ward, and W. Winkler, *LISA: Laser Interferometer Space Antenna for the detection and observation of gravitational waves*, Pre-Phase A Report, December 1995 (unpublished).

[8] L. E. Kidder, C. M. Will, and A. G. Wiseman, *Phys. Rev. D* **47**, 3281 (1993); *Class. Quant. Grav.* **9** L125 (1992).

[9] G. B. Cook, *Phys. Rev. D* **50**, 5025 (1994). See especially Fig. 3.

[10] K. S. Thorne, in *Proceedings of the Snowmass 95 Summer Study on Particle and Nuclear Astrophysics*, eds. E.W. Kolb and R. Peccei (World Scientific, Singapore, 1995) (gr-qc/9506086).

[11] A. Ori and K. S. Thorne, in preparation.

[12] D. Lai and A. G. Wiseman, "Innermost Stable Circular Orbit of Inspiring Neutron-Star Binaries: Tidal Effects, Post-Newtonian Effects and the Neutron-Star Equation of State", gr-qc/9609014.

[13] S. A. Teukolsky and W. H. Press, *Astrophys. J.* **193**, 443 (1974).

[14] S. Chandrasekhar and S. L. Detweiler, *Proc. R. Soc. London* **A344**, 441 (1975).

[15] F. Echeverria, *Phys. Rev. D* **40**, 3194 (1988).

[16] L. S. Finn, *Phys. Rev. D* **46**, 5236 (1992). See also F. Echeverria, unpublished PhD thesis, California Institute of Technology, addendum to Ch. 2 (1993). This is an addendum to Ref. [15] which shows that the methods used to calculate measurement errors in Refs. [15] and [16] are equivalent.

[17] R. Narayan, T. Piran, and A. Shemi, *Astrophys. J.* **379**, L17 (1991)

[18] E. S. Phinney, *Astrophys. J.* **380**, L17 (1991).

[19] E. P. J. Van den Heuvel and D. R. Lorimer, *Mon. Not. R. Astron. Soc.* **283**, L37-L39 (1996).

[20] A. V. Tutukov and L. R. Yungelson, *Mon. Not. Roy. Astron. Soc.* **260** 675, 1993.

[21] H. Yamaoka, T. Shigeyama, and K. Nomoto, *Astron. Astrophys.* **267**, 433, 1993.

[22] K. A. Postnov, M. E. Prokhorov and N. I. Shakura, In *NAS-NRC High Energy Astrophysics. American and Soviet Perspectives*, p 316-321.

[23] B. W. Murphy, H. N. Cohn, P. M. Lugger and J. D. Dull, *Bull. Am. Astron. Soc.* **185** (1994); K. Gephardt *et al.*, *Fabry-Perot Observations of Globular Clusters III: M15*, preprint 1996 (astro-ph/9612116).

[24] G. D. Quinlan and S. L. Shapiro, *Astrophys. J.* **343**, 725 (1989) (especially Fig. 12); *ibid* **356**, 483 (1990).

[25] R. D. Blandford, in *Active Galactic Nuclei: Saas-Fee Adv Course 20*, ed. T. Courvoisier & M. Mayor (Springer-Verlag, Berlin, 1990); M. J. Rees, *Science* **247**, 817 (1990).

[26] M. Begelman and M. Rees, *Gravity's fatal attraction: Black Holes in the Universe*, W.H. Freeman and Co., Basingstoke, England (1995); and references therein.

[27] D. Hils and P. L. Bender, *Astrophys. J.* **445**, L7 (1995).

[28] E. Poisson, *Measuring black-hole parameters and testing*

general relativity using gravitational wave data from space-based interferometers, preprint 1996, gr-qc/9606024.

- [29] M. C. Begelman, R. D. Blandford, M. J. Rees, *Nature* **287**, 307 (1980).
- [30] H. D. Wahlquist, *Detecting gravity waves from binary black holes*, In NASA, Relativistic Gravitational Experiments in Space p 14-17 (SEE N90-19940 12-90) (1989).
- [31] M. G. Haehnelt, *Mon. Not. Roy. Astron. Soc.* **269** 199 (1994); astro-ph/9405032.
- [32] N. Roos, J.S. Kaastra, C.A. Hummel, *Astrophys. J.* **409**, 130 (1993).
- [33] A. Sillanpaa *et al*, *Astrophys. J.* **325**, 628 (1988).
- [34] C.M. Gaskell, *Astrophys. J.* **464**, L107 (1996); C.M. Gaskell, in *Jets from Stars and Galaxies*, ed. W. Kundt (Springer, Berlin) pp. 165-196 (1996).
- [35] B.F. Schutz, in *The detection of gravitational radiation* Ed. D. Blair, (Cambridge University Press, Cambridge, England, 1989).
- [36] É. E. Flanagan and S. A. Hughes, *Measuring gravitational waves from binary black hole coalescence: II. The waves' information and its extraction, with and without merger templates*, in preparation.
- [37] L. Blanchet, *Phys. Rev. D* **54**, 1417 (1996) (gr-qc/9603048).
- [38] L. Blanchet, private communication.
- [39] By post- n -Newtonian order, we mean $O[(v/c)^{2n}]$ in secular terms and $O[(v/c)^{5+2n}]$ in dissipative, radiation reaction terms ($2n$ orders beyond the leading quadrupole radiation reaction term). This is the standard counting method for post-Newtonian waveforms.
- [40] C. Cutler, T. A. Apostolatos, L. Bildsten, L. S. Finn, É. E. Flanagan, D. Kennefick, D. M. Marković, A. Ori, E. Poisson, G. J. Sussman, and K. S. Thorne, *Phys. Rev. Lett.* **70**, 2984 (1993).
- [41] E. Poisson, *Phys. Rev. D* **52**, 5719 (1995). (gr-qc/9505030).
- [42] R. Balasubramanian and S. V. Dhurandhar, *Phys. Rev. D* **50**, 6080 (1994) (gr-qc/9404009).
- [43] C. Cutler and É. E. Flanagan, in preparation.
- [44] Families of template waveforms optimized for signal searches are in the early stages of development; see B. S. Sathyaprakash, *Phys. Rev. D* **40**, R7111 (1994); B. S. Sathyaprakash and S. V. Dhurandhar, *Phys. Rev. D* **44**, 3819 (1991); **49**, 1707 (1994); A. Królak, K. D. Kokkotas, and G. Schäfer, *Proceedings of the 17th Texas Symposium on Relativistic Astrophysics*, *Ann. N. Y. Acad. Sci.*, 1995; T. A. Apostolatos, *Phys. Rev. D* **52**, 605 (1995).
- [45] K.S. Thorne, presentation at *Intermediate Binary Black Hole* workshop, Caltech, July 1996. The location of the post-Newtonian breakdown can be seen from Fig. 1 of Ref. [41].
- [46] A workshop focusing on this issue was held at Caltech in July, 1996.
- [47] Even if such methods are not found, post-Newtonian templates should be adequate for searching for inspiral waves even in the IBBH regime; IBBH templates will likely be needed only as a foundation for extracting the waves' information. We also note that the method of Padé approximants has recently been found to improve significantly the convergence of the post-Newtonian series [48]; the implications of this for the IBBH regime are not yet clear.
- [48] B. S. Sathyaprakash, in preparation.
- [49] One can convince oneself of the likelihood of this cleanliness by considering various possible sources of perturbations to the gravitational-wave signal. Accretion disks will have masses much smaller than the black hole masses (for the equal mass coalescences that we are considering); and moreover for solar mass BBHs any accretion disks from previous phases in the binary's evolution will be long gone before the black holes coalesce. However, one case where a possible perturbing effect on the gravitational-wave signal may be observable is the stochastic influence of a surrounding stellar cluster on the orbits of members of a SMBH binary during the early stages of the inspiral. While strictly speaking this could make our assumption of the applicability of Wiener optimal filtering invalid for some SMBH inspirals, such inapplicability is not a cause for concern: the SNRs are typically so high anyway that it should be possible to easily detect both the coherent portions of the inspiral radiation and any isolated changes in phase due to close-encounter perturbations.
- [50] The Grand Challenge Alliance is an NSF funded collaboration among physicists and computer scientists at eight institutions: University of Texas, Austin; NCSA/University of Illinois; University of North Carolina, Chapel Hill; Cornell University; Syracuse University NPAC; University of Pittsburgh; Northwestern University; and Penn State University. The P.I. is Richard Matzner. More information about the Grand Challenge Alliance and their efforts to solve the binary black hole problem can be found at the WWW address <http://jean-luc.ncsa.uiuc.edu/GC/GC.html>; see also Ref. [51] for a review.
- [51] L. S. Finn, *A numerical approach to binary black hole coalescence*, to appear in the conference proceedings of GR14, gr-qc/9603004.
- [52] S. Chandrasekhar, *The Mathematical Theory of Black Holes*, Oxford University Press, New York, 1983; p. 528.
- [53] C. W. Helstrom, *Statistical Theory of Signal Detection*, (Pergamon, Oxford, 1968).
- [54] L. A. Wainstein and V. D. Zubakov, *Extraction of Signals from Noise*, (Prentice-Hall, Englewood Cliffs, 1962).
- [55] C. Cutler and É. E. Flanagan, *Phys. Rev. D* **49**, 2658 (1994).
- [56] Our convention for the normalization of the spectral noise density $S_h(f)$ is such that

$$\langle n(t)^2 \rangle = \int_0^\infty S_h(f) df,$$

where $n(t)$ is the detector noise ("One-sided spectral noise density"). This determines the constant 4 appearing in Eq. (2.7). Note that the alternative convention used in Refs. [53,54] results in a factor 2 instead of 4 in Eq. (2.7). In Eq. (29) of Ref. [1], the spectral noise density that is used is the one-sided spectral noise density (as in this paper), and thus the overall factor in front of the integral should be 4, not 2.

- [57] Note that we distinguish between the number of statistically independent waveform shapes $\mathcal{N}_{\text{shapes}}$ in the manifold of waveforms that one is trying to detect using the

matched filtering process, and the actual number of templates $\mathcal{N}_{\text{templates}}$ used in the computations. The number $\mathcal{N}_{\text{shapes}}$ is the volume of the subset of the manifold of signals with $\text{SNR} \leq \rho$, in the natural metric induced by the statistical properties of the noise; thus $\mathcal{N}_{\text{shapes}}$ depends on ρ . The number $\mathcal{N}_{\text{templates}}$ is defined in Sec. VIA. In general $\mathcal{N}_{\text{templates}} < \mathcal{N}_{\text{shapes}}$ since the optimum computational method will have less than one template per statistically independent waveform shape. For the purposes of calculating SNR thresholds, $\ln(\mathcal{N}_{\text{templates}}) \approx \ln(\mathcal{N}_{\text{shapes}})$ to a good approximation.

- [58] É. É. Flanagan, in preparation.
- [59] S. L. Shapiro and S. A. Teukolsky, *Black Holes, White Dwarfs, and Neutron Stars: The Physics of Compact Objects* (Wiley, New York, 1983).
- [60] For instance, if the post-Newtonian expansion is taken to order 3/2, we would find in the equal mass case (see, e.g., Ref. [61])
- $$\frac{dE}{df} = \frac{1}{12} \pi^{2/3} M^{5/3} f^{-1/3} \left[1 - \frac{1}{6} \left(9 + \frac{1}{4} \right) (\pi M f)^{2/3} \right].$$
- The correction to the Newtonian formula is ~ 0.24 at $f = f_{\text{merge}}$; when taken to higher order, there will be additional corrections. For the purposes of our discussion, these corrections are not important – an estimate of the SNR that is accurate to a few tens of percent is adequate. Also, the loss in SNR due the phase lag between the approximate, post-Newtonian templates and the true, general-relativistic signal will be small [43,44].
- [61] C. M. Will. In M. Sasaki, editor, *Relativistic Cosmology*, page 83. Universal Academy Press, 1994.
- [62] This is the value predicted by the numerical initial data sets of Ref. [9] at $f = f_{\text{merge}} = 0.02/M$; see also the arguments concerning angular momentum in Sec. IIIB.
- [63] S. R. Brandt and E. Seidel, Phys. Rev. D **52**, 870 (1995) (gr-qc/9412073); the run labeled r3 of a distorted Kerr black hole with $a \sim 0.35$ yields an energy radiated in ringdown waves of $\sim 3\%$ (from Table IV, and also from Fig. 18 which shows that most of the radiated energy can be ascribed to the ringdown waves).
- [64] L. L. Smarr, Ph.D. dissertation, University of Texas at Austin, unpublished (1975).
- [65] S. Detweiler, in *Sources of Gravitational Radiation*, ed. L. L. Smarr (Cambridge University Press, Cambridge, 1979).
- [66] See, e.g., J. Baker, A. Abrahams, P. Anninos, S. Brandt, R. Price, J. Pullin, E. Seidel, *The collision of boosted black holes*, preprint, 1996 (gr-qc/9608064).
- [67] When we say that a source is visible out to a distance D , we mean that the rate of detection of events is the roughly the same as the rate of occurrence of events within a sphere of radius D . Note that some events within this sphere will be missed, and some outside this sphere will be detected, due to the beaming and orientation effects discussed in Sec. IIC. Rare, optimally oriented sources will be visible out to several times D .
- [68] V. M. Lipunov, K. A. Postnov and M. E. Prokhorov, Sternberg Astronomical Institute preprint (1996); astro-ph/9610016
- [69] It would be quite simple to improve on this filter. For example, one could divide it by the noise spectral density

in order to weight the filter according to the instrumental noise characteristics, i.e., pre-whiten the data stream. The main result of our analysis, the formula (2.11), would also approximately apply to such an improved filtering method.

- [70] P. R. Brady, T. Creighton, C. Cutler, B. F. Schutz, *Searching for period sources with LIGO*, Phys. Rev. D, to appear (gr-qc/9702050).
- [71] D. Marković, Phys. Rev. D **48**, 4738 (1993); E.W. Kolb and M.S. Turner, *The Early Universe*, Addison-Wesley, Redwood, CA. (1990) p. 44.
- [72] K. S. Thorne, in *Gravitational Radiation*, ed. N. Deruelle and T. Piran, North-Holland Publishing Co., 1983.
- [73] During the inspiral phase, the timescale over which the frequency of the waves changes is much longer than the instantaneous period, so it makes sense to talk about the frequency of the waves at a certain time. In particular, we can (roughly) talk either about the time or the frequency at which the inspiral ends — the notion of instantaneous frequency is just beginning to break down then.
- [74] L. L. Smarr, in *Sources of Gravitational Radiation*, ed. L. L. Smarr (Cambridge University Press, Cambridge, 1979).
- [75] P. Anninos, D. Hobill, E. Seidel, L. Smarr, W.-M. Suen, Phys. Rev. Lett. **71**, 2851 (1993); Phys. Rev. D **52**, 2044 (1995).
- [76] S.L. Detweiler, Proc. R. Soc. London **A352**, 381 (1977).
- [77] D. Christodoulou, Phys. Rev. Lett. **67**, 1486 (1991); K. S. Thorne, Phys. Rev. D **45**, 520 (1992); A. G. Wiseman and C. M. Will, Phys. Rev. D **44**, R2945 (1991).
- [78] D. Kennefick, Phys. Rev. D **50** 3587 (1994).
- [79] Since ϵ is a scalar quantity, it can only depend on scalar products of \mathbf{S}_1 , \mathbf{S}_2 and $\hat{\mathbf{L}}$ and not on these vectorial quantities themselves. Therefore the number of independent variables that ϵ depends on is six.
- [80] J. K. Blackburn and S. Detweiler, Phys. Rev. D **46**, 2318 (1992); the geometry at which $S = 7.5 m_1$ in their notation.
- [81] D. M. Eardley, in *Gravitational Radiation*, ed. N. Deruelle and T. Piran, North-Holland Publishing Co., 1983.
- [82] See, for example, K. S. Thorne, Rev. Mod. Phys. **52**, 299 (1980), Eqs. (4.16') and (4.23').
- [83] The inequality $|\mathbf{S}_{\text{final}}| \leq M^2$ used in deriving Eq. (3.10) should really be $|\mathbf{S}_{\text{final}}| \leq (M - E_{\text{rad}})^2$, since it is the mass of the final black hole and not the initial total mass of the system that is relevant. An argument parallel to that leading to Eq. (3.12) then yields the inequality $\epsilon_{\text{rad}} \gtrsim [1.4 - (1 - \epsilon_{\text{rad}})^2]/4$ or $\epsilon_{\text{rad}} \gtrsim 0.18$, where $\epsilon_{\text{rad}} = E_{\text{rad}}/M$. Hence, even if only $\sim 50\%$ of the emitted radiation is quadrupolar, the estimate $\epsilon_{\text{rad}} \sim 0.1$ used in Sec. IIIB is probably still fairly realistic.
- [84] D. M. Eardley and E. W. Hirschmann, *Comment on "Instabilities in Close Neutron Star Binaries"*, ITP Santa Barbara preprint NSF-ITP-95-165 (gr-qc/9601019).
- [85] C. W. Misner et al., *Gravitation* (Freeman, New York, 1973), Sec. 36.6.
- [86] B. J. Owen, Phys. Rev. D **53**, 6749 (1996).
- [87] E. W. Leaver, Proc. R. Soc. Lond. A **402**, 285 (1985). Leaver's data on the $l = m = 2$ mode, which was used by Echeverria, is unpublished.

- [88] K. S. Thorne, *Ap. J.* **191**, 507 (1974).
- [89] Actually the QNR metric perturbation will vanish at the event horizon; one could instead use the boundary of the ergo-region. Also the ratio \mathcal{R} of the circumferences will actually be gauge dependent. However, if we expand \mathcal{R} as $\mathcal{R} = 1 + \alpha\mathcal{A} + O(\mathcal{A}^2)$, then the coefficient α will be gauge invariant and we could take $\mathcal{A}_2 = 1/\alpha$.
- [90] More specifically, an ellipsoidal solid body of mass M of uniform density whose axes are given by $l^2, l^2(1 \pm (3/5)\sin(\omega t))$ gives rise to a luminosity $L = 9M^2 l^4 \omega^6 / 5^5$; comparing this to the luminosity $\mathcal{A}^2 M^2 \omega_{\text{qnr}}^2 / (16\pi)$ for the waveform (3.21) at $t = 0$, and identifying $\omega = \omega_{\text{qnr}} = 2\pi \cdot 0.13/M$ and taking $l = r_+ = M + \sqrt{M^2 - a^2}$ for $a = 0.97M$ say yields $\mathcal{A} = 0.4$. This crude estimation method clearly does not take into account the potential barrier through which the radiation must propagate (among other things). We imagine that a more precise calculation will find a somewhat smaller value of \mathcal{A} .
- [91] This error can be seen by inserting the parameter values $m = 1000$ kg, $f_0 = 1$ Hz, and $Q_0 = 10^9$ given in Ref. [3] into the standard equation for suspension thermal noise due to viscous damping, as given in, *e.g.*, Eq. (4.3) of Ref. [92]. The resulting noise level is 3 times larger than the noise level shown in Fig. 7 of Ref. [3] for $10\text{ Hz} \lesssim f \lesssim 70\text{ Hz}$. This error was not made in the corresponding figure V.4 of the 1989 LIGO proposal [93]. [K. S. Thorne, private communication]
- [92] L. S. Finn and D. F. Chernoff, *Phys. Rev. D* **47**, 2198 (1993).
- [93] R.E. Vogt et. al., "Proposal to the National Science Foundation for the Construction, Operation, and Supporting Research and Development of a Laser Interferometer Gravitational-Wave Observatory", (California Institute of Technology, 1989), unpublished.
- [94] The $h_{\text{rms}}(f) = \text{const}$ piece in the noise curve happens to have the same frequency dependence that the test masses' thermal noise would have if this noise were due to structural damping [95]. We emphasize that it is *not* our aim to alter the standard LIGO advanced interferometer noise spectrum by assuming that structural internal thermal noise is dominant between 40 Hz and 110 Hz; rather, the $h_{\text{rms}}(f) = \text{const}$ region is just a way to smooth the transition between the suspension thermal noise dominated and laser shot noise dominated pieces of the noise spectrum.
- [95] A. Gillespie and F. Raab, *Phys. Lett. A*, **190**, 213 (1994).
- [96] See Eq. (32) of Ref. [1]. Note also that our $h_n(f)$ is similar to the quantity $h_{3/\text{yr}}$ defined in Ref. [1], which is the same as the quantity denoted $h_{\text{SB}}(f)$ in Refs. [3,10]. These quantities differ from $h_n(f)$ by the factor $\sqrt{\ln \mathcal{N}} \sim 5$, where \mathcal{N} is the number of independent starting times per third of a year that must be tried in the optimal filtering search process; see Eq. (34) of Ref. [1]. We omit this factor in our definition of h_n since in paper II [36] we will be discussing SNRs in situations when the waves have already been detected and where the factor $\sqrt{\ln \mathcal{N}}$ is not relevant. The factor instead appears in our SNR thresholds discussed in Sec. VI. Note also that our signal-to-noise ratios differ from those in Refs. [3,10] by an overall factor of $\sqrt{3/2}$, as discussed after Eq. (2.34) above.
- [97] K. D. Kokkotas, A. Królak, and G. Tsegas, *Class. Quant. Grav.* **11**, 1901 (1994).
- [98] We obtained the metric (6.4) in the following way: (i) We took the large Q limit of the matrix $\mathcal{C}'_{ij}{}^{-1}$ of Ref. [16], which was calculated assuming white noise, (ii) We inverted this matrix, took a 2×2 sub-block and re-inverted, thus eliminating (effectively integrating out) the variables V and T . This procedure for eliminating the time-of-arrival variable T is equivalent to the procedure embodied in Eq. (2.28) of Ref. [86]. (iii) We divided by 2 in order to accord with the definition (2.12) of Ref. [86].
- [99] This is Eq. (2.16) with $\ln(\mathcal{N}_{\text{shapes}})$ replaced by $\ln(\mathcal{N}_{\text{shapes}})$, *cf.* Ref. [57] above.
- [100] In the situation where merger templates are available, the optimum search method would in fact be a combination of inspiral, merger and ringdown searches, in which the entire inspiral–merger–ringdown signal as a whole is searched for using matched filtering.
- [101] K. S. Thorne and R. H. Price, private communication. This bet was posed at the *Astrophysical Sources of Gravitational Waves* workshop held at Penn State in July 1995.
- [102] The small z , equal-mass limit of Eq. (A14) agrees with the large Q limit of Eq. (4.7) of Ref. [16] when that equation is multiplied by a correction factor of 2.
- [103] To see that angle-averaging the approximate formula (B3) yields the formula (A13) for the ringdown SNR, corresponding to the approximate delta function energy spectrum (3.25), proceed as follows. Starting from Eq. (B14), average over the angles $\theta, \varphi, \psi, \iota$ and β using Eqs. (2.38) and (3.22). This yields

$$\langle h_0(\theta, \varphi, \psi, \iota, \beta)^2 \rangle = \frac{1}{10\pi} \frac{\mathcal{A}^2 M^2}{r^2}.$$

Substitute this into Eq. (B3), make the replacement $S_h \rightarrow S_h(f_{\text{qnr}})$, and make the appropriate substitutions to account for cosmological effects as explained in Sec. IIC to obtain Eq. (A13).